COMPUTER AIDED DESIGN OF WAVEGUIDE FILTERS USING THE MODE MATCHING METHOD

A Thesis

Submitted to the College of Graduate Studies and Research

in Partial Fulfillment of the Requirements

for the Degree of

Master of Science

in the Department of Electrical Engineering

University of Saskatchewan

Saskatoon

by

Raju Balasubramanian

June 1997

Permission To Use

In presenting this thesis in partial fulfillment of the requirements for a Postgraduate degree from the University of Saskatchewan, I agree that the Libraries of this University may make it freely available for inspection. I further agree that permission for copying of this thesis in any manner, in whole or in part, for scholarly purposes may be granted by the professor or professors who supervised my thesis work or, in their absence, by the Head of the Department or the Dean of the College in which my thesis work was done. It is understood that any copying or publication or use of this thesis or parts thereof for financial gain shall not be allowed without my written permission. It is also understood that due recognition shall be given to me and to the University of Saskatchewan in any scholarly use which may be made of any material in my thesis.

Request for permission to copy or to make other use of material in this thesis in whole or part should be addressed to:

Head of the Department of Electrical Engineering
University of Saskatchewan
57 Campus Drive
Saskatoon, Saskatchewan, Canada
S7N 5A9

Abstract

Modern satellite and terrestrial telecommunication systems usually employ a large number of waveguide filters, operating at microwave frequencies. Traditionally, waveguide filters are designed empirically using approximate discontinuity models and extensive bread-boarding. Over the last two decades, the demand for accurate analysis and design techniques has generated a tremendous output of numerical methods for microwave applications. The mode matching method, based on a combined field theory and modern network theory approach, is a powerful technique for solving waveguide discontinuity problems which are inherently present in waveguide filter structures. With the advent of powerful computers and workstations, field theory based models became desirable tools for computer aided design of waveguide filters. In this thesis, complete computer aided design methods for waveguide bandpass and low-pass filters are developed. Several existing filter structures are designed and new filter structures with better performance characteristics are proposed. The results obtained are verified using experimental and published results. With the computer aided design method developed in this thesis, waveguide low-pass and bandpass filters at microwave frequencies can be designed accurately without bread-boarding and post-production tuning of the designed filters. The design process in mass production of the microwave waveguide filters can be greatly simplified with the use of the computer aided design method developed.

Acknowledgements

The author is indebted to Dr. Protap Pramanick for his supervision, constant encouragement and financial support during the course of this work. Thanks are due to the Department of Electrical Engineering, University of Saskatchewan, Saskatoon for providing the facilities to pursue this research and for providing some financial support.

It is a pleasure to acknowledge Microwaves Development Company, North Andover, MA, USA for providing the experimental results. The author also wishes to express his sincere gratitude to the Electrical Engineering Department and Institute for Systems Research, University of Maryland, College Park, USA for granting the permission to use the optimization code.

The author is indebted to many friends for invaluable suggestions and advice. Particular thanks are due to D. A. Cargill, R. Tanha and F. R. Djoemadi. The author wishes to thank his family and relatives in India for their guidance and encouragement.

Dedication

This thesis is dedicated to the author's mother for her love, care, patience, dedication and constant support.

Table Of Contents

List of Tables

List of Figures

List of Symbols

a	broad dimension of rectangular waveguide
b	narrow dimension of rectangular waveguide
c	speed of light; broad dimension of rectangular waveguide
d	narrow dimension of rectangular waveguide
B,B_a,B_b	Normalized susceptance
f	frequency
$f_{c,mn}$	waveguide cutoff frequency for mode m,n
f_o	bandpass filter center frequency
ϵ_o	permittivity of free space
μ_o	permeability of free space
ω	angular frequency
λ	wavelength
λ_g	guide wavelength
λ_o	free space wavelength
$\lambda_{c,mn}$	cutoff wavelength for mode m,n
$k_{c,mn}$	wave number for mode m,n
Z_w	wave impedance in a waveguide
E	electric field
H	magnetic field; coupling matrix
E_t	tangential electrical field
H_t	tangential magnetic field
η	impedance of free space
Z_o	characteristic impedance
V	potential difference
P	Power
IL	Insertion loss

RL	Return loss
t	thickness of the iris
V^+	incident voltage wave
V^-	reflected voltage wave
$[S]$	S matrix
$[U]$, I	unitary matrix
$[S]^t$	transpose of S matrix
$[S]^*$	conjugate of S matrix
a_1, a_2	incident voltage waves
b_1, b_2	reflected voltage waves
L	length of transmission line; Inductance
Z_N	~~reference~~ impedance
γ	propagation constant; isolation bandwidth factor
P, Q, N, M	integers; number of modes in the waveguide
p, q, n, m	integers; waveguide mode number
$[Y]$	admittance
ϕ	modal functions; reference plane locations
j	$\sqrt{-1}$
i, j	integers; indices
δ_{ij}	Kronecker delta
C	Capacitance
D	diagonal matrix
ϵ	passband ripple
L_A	Isolation
BW	Bandwidth
f_L	lower cutoff frequency of bandpass filter
f_H	upper cutoff frequency of bandpass filter
K	impedance inverter

X	reactance
Z_{in}	input impedance
l	length of waveguide resonator section
w	iris opening
λ_{g0}	midband guide wavelength
λ_{gL}	guide wavelength in the resonator section at f_L
λ_{gH}	guide wavelength in the resonator section at f_H
α	scaling parameter
N, n	integer; number of resonators
f_c	low-pass filter cutoff frequency
w_g	fractional bandwidth
θ_o	electrical length corresponding to the cutoff frequency f_c
L_s	minimum stopband attenuation level
L_p	maximum passband attenuation level
N_s	integer; number of frequency sampling points in the stopband
N_p	integer; number of frequency sampling points in the passband
VSWR	Voltage standing wave ratio
TE	Transverse Electric
TM	Transverse Magnetic
TEM	Transverse Electric and Magnetic

$K_{n,n+1}$ = Normalized K-inverter value

K' = K-inverter value

Chapter 1

Introduction

Microwaves are electromagnetic waves with wavelengths ranging from slightly less than 30 cm down to 0.03 mm, corresponding to frequencies ranging from 10^9 to 10^{13} Hz. Microwaves possess several useful characteristics. One of the most important characteristics of microwaves is that the size of the structure is comparable to the wavelength of the wave guided by the structure. The short wavelengths and wide frequency spectrum of microwaves are the obvious advantages for the application of microwaves. The high frequencies of microwaves can be used to achieve very large bandwidths in communication links. Microwaves have the property of directly passing through the ionosphere which reflects lower frequency waves. All these special and unique properties of microwaves led to the wide use of microwaves in modern communication systems like radar and satellite communication systems. Due to the rapid developments in the modern communication field, an extensive amount of research in microwave engineering is in progress since it began two decades ago.

1.1 Rectangular Waveguide

In microwave circuits, microwaves are transmitted by structures commonly known as transmission lines and waveguides. Waveguides can be of rectangular or circular cross-section. Rectangular waveguides are the more common and widely used. The nature of propagation of waves in the transmission lines can be categorized as either

Transverse Electro-Magnetic waves (TEM) or non-TEM waves. In TEM waves, both the electric and magnetic fields are entirely transverse to the direction of propagation. In non-TEM waves electric field (E) or magnetic field (H) are present in the direction of propagation. If the waves supported by the structure have purely magnetic field (H) in the direction of propagation, then the waves are known as transverse electric (TE) waves. Similarly, if there exists purely electric field (E) in the direction of propagation, then the waves are known as transverse magnetic (TM) waves. There are some situations with inhomogeneous dielectric filling or anisotropic material filling in the waveguide where the waveguide modes have both longitudinal electric and magnetic fields. These are known as hybrid modes.

A rectangular waveguide of width a and height b, throughout this thesis width and height are represented as a and b, respectively and (a > b) as illustrated in Figure 1.1 is an example of a guiding structure, that cannot support a TEM wave but can propagate waves of type TE and TM waves. The waveguide transmits electromagnetic waves through its interior by multiple reflections from its metallic walls, which provide excellent shielding between the exterior and the interior.

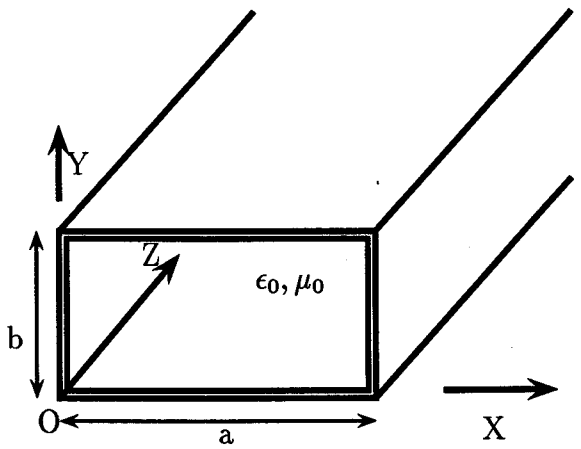

Figure 1.1: Rectangular Waveguide

In Figure 1.1, perfectly conducting walls are at x = 0, a and y = 0, b. The waveguide may be filled with a dielectric of permittivity ϵ_r. However, in practice, the waveguide interior is more likely to be air-filled (ϵ_r=1).

The rectangular waveguide Ref. [1] is the basic building block of many microwave components including directional couplers, power dividers, multiplexers, phase shifters, filters, isolators etc. In this thesis, rectangular waveguide filter design and analysis problems are considered.

1.1.1 Mode Nomenclature

The essential properties of air-filled loss-free guides are that there is a double infinity of possible solutions for both TE and TM waves. These waves, or modes, are identified by two integer subscripts m and n, for example, TE_{mn}. The integers m and n pertain to the number of standing wave interference maxima occurring in the field solutions that describe the variation of the fields along the two transverse coordinates (X and Y). Each mode has a characteristic cutoff frequency $f_{c,mn}$, which is dependent on the waveguide cross-section, below which the mode does not propagate in the waveguide.

Propagation of the wave in the longitudinal or the Z direction is governed by the function $e^{\pm j\beta_{mn}z}$. The propagation factor β_{mn} is given by,

$$\beta_{mn} = \sqrt{(k_0^2 - k_{c,mn}^2)}, \tag{1.1}$$

where,

$$k_0 = \omega\sqrt{\mu_0\epsilon_0}, \quad k_{c,mn} = 2\pi f_{c,mn}\sqrt{\mu_0\epsilon_0}, \tag{1.2}$$

ϵ_0 and μ_0 are the permittivity and permeability of free space respectively, $\omega = 2\pi f$,

where f is the operating frequency. The cutoff frequency $f_{c,mn}$ is given by,

$$f_{c,mn} = \frac{c}{2\pi}\sqrt{(\frac{m\pi}{a})^2 + (\frac{n\pi}{b})^2}, \tag{1.3}$$

where c is the velocity of light ($c = 1/\sqrt{\mu_o \epsilon_o}$). The guide wavelength is given by,

$$\lambda_g = \frac{\lambda_0}{\sqrt{(1 - \lambda_0^2/\lambda_{c,mn}^2)}} \tag{1.4}$$

where λ_0 is the free-space wavelength of plane waves and the cutoff wavelength is given by,

$$\lambda_{c,mn} = \frac{2\pi}{k_{c,mn}}. \tag{1.5}$$

1.1.2 TE_{10}-mode

The TE_{10} mode, the mode for which the cutoff frequency is minimum when (a>b), is called the *dominant mode* of a rectangular waveguide. In this thesis, the dominant mode is considered to be the incident wave on the waveguide filter unless specified otherwise. The cutoff wavelength for the dominant mode is given by $\lambda_{c,10} = 2a$.

1.1.3 Waveguide Impedance

The wave impedance in waveguide is defined as,

$$Z_w = \frac{E_t}{H_t} \tag{1.6}$$

where the subscript t is used to denote the components of the field perpendicular to the direction of propagation.

For TM-modes,

$$Z_w = \frac{\beta}{\omega\epsilon} = \eta\frac{\lambda_0}{\lambda_g} \tag{1.7}$$

For TE-modes,

$$Z_w = \frac{\omega\mu}{\beta} = \eta\frac{\lambda_g}{\lambda_o} \tag{1.8}$$

where the impedance of free space η is given by,

$$\eta = \sqrt{\frac{\mu_o}{\epsilon_o}} \approx 120\,\pi\ \Omega \tag{1.9}$$

For TM or TE modes in a waveguide, the wave impedance is a constant for any mode irrespective of the position in the cross-section of the waveguide at which E_t or H_t are taken. The characteristic impedance of the dominant TE_{10} mode can be defined in three different ways, namely the voltage-current, the power-voltage and the power-current definition. In this thesis, power-voltage definition is used. For the dominant mode it is comparatively easy to determine the voltage. The voltage is the integral across the height of the waveguide of the electric field intensity at the centre of the broad face of the waveguide, i.e. the maximum value of E_y. The characteristic impedance is given by,

$$Z_0 = \frac{V^2}{P} = \frac{2\omega\mu b}{\beta a} = Z_w\frac{2b}{a} \tag{1.10}$$

which is equal to the wave impedance when a = 2b.

1.2 Filters

Filters are devices which allow a certain range of desired frequencies to pass through with minimum attenuation while attenuating the undesired frequencies Ref. [2]. Filters are classified as low-pass, bandpass, bandstop and high-pass. In Figure 1.2, the frequency responses of these basic types of filters are shown.

Figure 1.3 shows the general representation of a filter in a microwave network. At the input plane of the filter, the power is divided into three components:

- P_{in}, the incident power from the generator

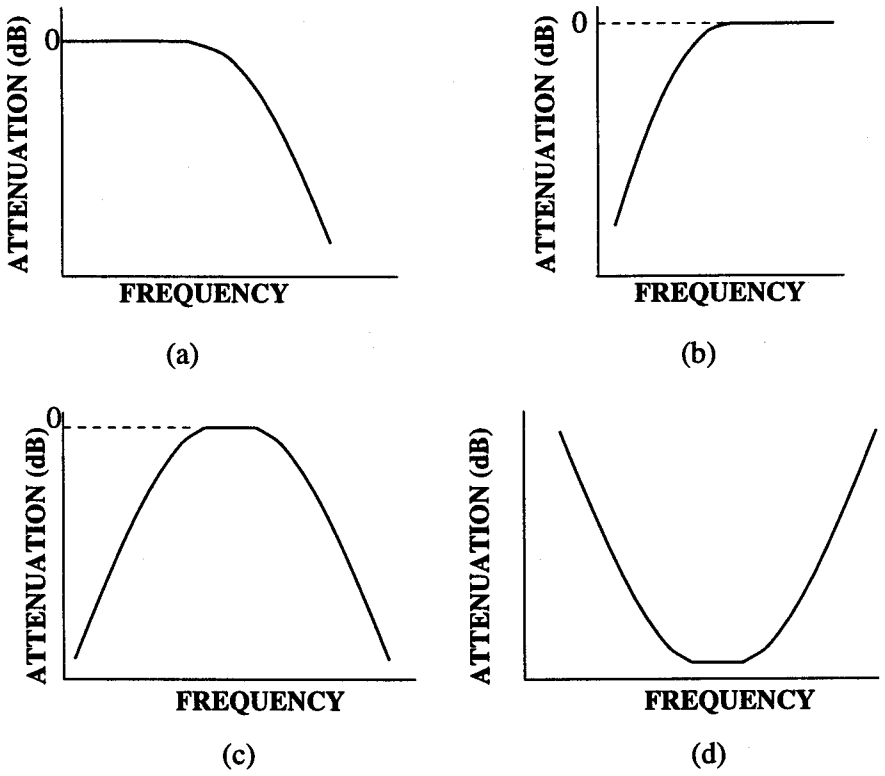

Figure 1.2: Basic types of filters. (a) Low Pass (b) High Pass (c) Bandpass (d) Bandstop

- P_R, the power reflected towards the generator
- P_A, the power absorbed by the filter

and P_L, is the power transmitted to the load in the network.

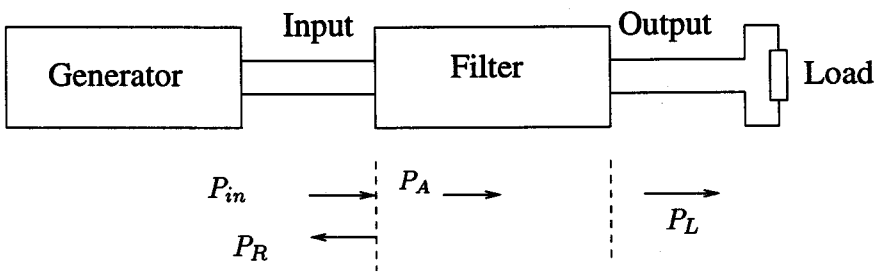

Figure 1.3: General representation of a filter network

By conservation of energy,

$$P_{in} = P_R + P_A, \qquad P_L \leq P_A \tag{1.11}$$

If $P_L = P_A$, the filter is lossless and $P_L = P_{in}$ implies that there are no reflections and the filter is lossless. The insertion loss (IL) and return loss (RL) at a particular frequency is defined as,

$$IL = -10log\frac{P_L}{P_{in}}, \qquad RL = -10log\frac{P_R}{P_{in}}. \tag{1.12}$$

The units for both IL and RL are decibels (dB). Ideally, the passband insertion loss should be 0 dB and the stopband insertion loss should be infinity. However, filters in practice have a frequency response deviating from the ideal filter response.

Filters can be classified into *Buttterworth, Chebyshev* and *Elliptic* type of filters based on their frequency response characteristics as shown in Figure 1.4.

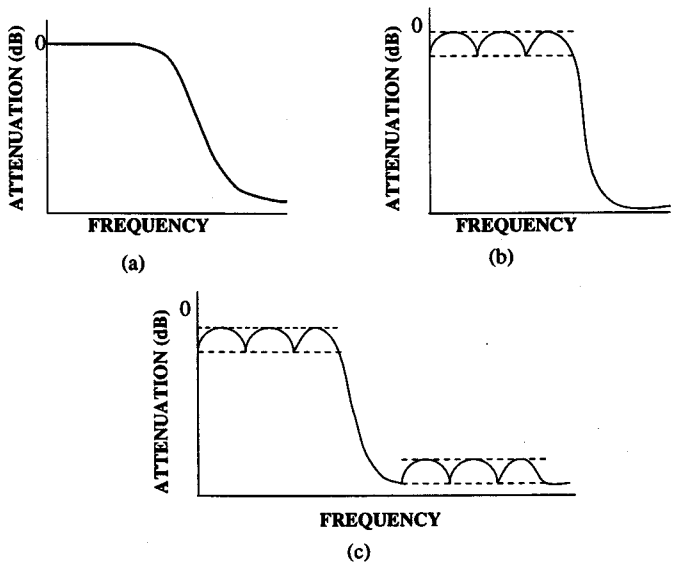

Figure 1.4: Different types of frequency response (a) Butterworth (b) Chebyshev (c) Elliptic

Butterworth filters have a flat passband response, Chebyshev filters have an equal-ripple characteristics in the passband and elliptic filters exhibit equal-ripple characteristics in both the passband and stopband. Chebyshev filters have a sharp cutoff and are often preferred over Butterworth filters. Elliptic filters have even sharper cutoff but are very difficult to design precisely for use at microwave frequencies.

1.2.1 Microwave Filters

The difference between conventional and microwave filters can be better explained by classifying the lumped and distributed elements according to network theory. In lumped elements, the phase variation of the signal over the largest physical dimension of the element is negligible while in distributed elements it is not negligible. At low frequencies, lumped elements (capacitors and inductors) can be used to realize filters. It is possible to accurately synthesize the lumped element filter from the required filter response by following procedures based on network theory. Filters at microwave frequencies are realized using distributed elements (transmission lines, waveguides) or a combination of lumped and distributed elements. Electric and magnetic fields have to be considered in the design of filters using distributed elements, rather than the voltage and current as in the case of lumped elements. Designing filters using distributed elements is more complicated and the synthesis involves complicated procedures requiring empirical adjustments to experimental filters for obtaining a filter with satisfactory frequency response.

There are two methods which are well known for the design of microwave filters, the image-parameter method and the insertion loss method. These methods are discussed in detail in Ref. [3, 4] and in article Ref. [5]. Both these methods use a trial and error based approach for the design of the filter. As a result, these methods are very cumbersome and laborious. In addition, time consuming experimental post-production tuning is required to get the required performance because of the approximate procedures in these design methods.

1.3 Thesis Objectives

1.3.1 Computer Aided Design: A Motivation

Computers are powerful tools that can be employed to perform arduous, error-prone and iterative calculations faster, cheaper and more accurately than ever before; thanks to the new computational technologies like parallel processors and reduced instruction set computer (RISC) processors Ref. [6]. The considerable growth in the computational technology over the last few decades has added a new dimension for microwave engineers in designing microwave products at or beyond the state-of-the-art. With the ever increasing demand for accurate design of microwave components, accurate full-wave analysis using the field theory approach became a necessity. The superiority of the field-theory based approach over the equivalent circuit models attracted microwave engineers for extensive research on several numerical methods for the design of microwave passive and active structures.

Waveguide filters are an inherent part of modern communication systems, such as radar and satellite communications. The rapid growth in modern communication systems entails accurate design and analysis of waveguide filters. By efficient combination of modern network theory, field theory and CAD (Computer Aided Design) tools, fast, accurate and compact design of waveguide filters is possible.

Traditionally, waveguide filters have been tuned by adding tuning screws. By trial and error based approach the desired frequency response for the filter was achieved. The design was based on empirical models for the discontinuities and extensive breadboarding. The presence of tuning screws in the filter structures causes reflections and loss in the signal. Moreover, at high frequencies the tuning screws vibrate and this affects the performance characteristics of the filter.

The main objectives of this thesis are:

1. To develop efficient computer aided design and analysis methods for the design of a large variety of existing waveguide filters without requiring post-production tuning

2. To use the developed methods to design new efficient and compact waveguide filter structures

The mode matching method is a numerical method applied to structures with well defined boundary conditions (eg. waveguides), for the accurate characterization of the discontinuities in the structures. The developed computer aided synthesis techniques utilizes the mode matching method for the characterization of the discontinuities in the waveguide filter.

The waveguide filters thus designed should possibly eliminate the need for tuning screws in comparison with the traditionally designed filters for the same frequency response characteristics. The elimination of bread-boarding and post-tuning of the filter would alleviate the problems involved in the mass production of filters. In addition, the filters designed are superior in performance because of the absence of tuning screws which introduces many problems as mentioned previously.

1.4 Thesis Overview

The thesis is divided into six chapters. Chapter 2 develops the modern network theory including the S parameters and $ABCD$ parameters. Different types of waveguide discontinuities encountered in the thesis are also introduced in chapter 2. Chapter 3 is dedicated to the application of the mode matching method for the characterization of various types of waveguide discontinuities. The results from the mode matching method are furnished and compared with the results from traditional methods Ref. [7] and the advantages of the mode matching method over other numerical methods are

briefly discussed. Chapter 4 develops the computer aided synthesis method for the problem of designing waveguide low-pass and bandpass filters. The analysis method to simulate the frequency response characteristics of the designed filter is also developed along with a brief introduction to optimization of the designed waveguide filters. Chapter 5 furnishes the results obtained from the computer aided design method developed in this thesis and its comparison with experimental results from Microwaves Development Company, USA and published results. Finally, chapter 6 concludes the thesis along with a note of limitations of the design methods developed in this thesis and directions for future work.

Chapter 2

Literature review and background

2.1 Literature survey

Microwave filters are the most common passive components in any microwave network. Research on microwave filters commenced in 1937. Much of the work was done at various laboratories that were set up during World War II from 1941 to 1945. A very good historical perspective of the research done in the microwave filter design and development is given in Ref. [5]. A very concise summary of the development in the theory and design of microwave filters is given in Ref. [6]. R. Levy [8, 9], N. Marcuvitz [7] and many other well known names contributed to the development of filter design and some of their work is still unsurpassed. Much of this earlier work is based on empirical relations and models for the waveguide discontinuities obtained directly from Ref. [7].

In the past two decades the research focus shifted to numerical characterization and modeling of waveguide components. A good review of the computational methods used for the solution of electromagnetic fields along with an introduction to numerical methods is given in Ref. [10]. A number of numerical methods that are applied to the passive components is described in Ref. [11]. A specific numerical method is selected based on the type of the structure to be analysed and bearing in mind the memory requirements and processor speed of the computer. Although complete numerical 3D analysis techniques, such as the finite element or finite difference approach, have been

commercially available, the analytical mode-matching method proves to be faster and more efficient for analyzing and optimizing waveguide components having well defined boundaries.

Since transverse and longitudinal waveguide junctions form building blocks of waveguide filters, the significance of characterization of waveguide junctions led to considerable research in solving waveguide discontinuity problems. The problems of scattering from a rectangular-to-rectangular waveguide junctions were exactly solved with convergent numerical results using the mode-matching method and the principle of conservation of complex power in Ref. [12]. It was the first of its kind in characterizing waveguide discontinuities and it utilized the generalized TE-TM mode analysis. A modified TE^{x}_{mn} approach was used later on by Ref. [13] which consumed less memory and computer time without loss of accuracy when compared with the generalized TE-TM approach.

Typically, structures with multiple waveguide discontinuities are analyzed by cascading the generalized scattering matrices of individual discontinuities. But the generalized scattering matrix approach required large memory space and computer time to store and process matrices of very large size. Several improvements to the generalized scattering method were proposed and an improved modal expansion method for cascading junctions and its application to waveguide filters was developed recently in Ref. [14].

Since the field theory based approach was possible in solving waveguide filter design problems using CAD, waveguide filters were designed accurately. Variations made in the structures like tapering of the waveguide were studied. R. Levy, first proposed a synthesis technique for designing tapered corrugated waveguide low-pass filters Ref. [9]. But the synthesis technique used empirical models for waveguide discontinuities and hence was approximate. Post-production tuning was done to realize the required specifications of the filter. Post-production tuning is a highly

cumbersome, laborious and an expensive process, which slows mass production of the filters. In addition, the presence of tuning screws in the waveguide structures creates additional problems as mentioned in the previous chapter.

In this thesis a successful attempt is made to develop a computer aided method for the design of tapered corrugated waveguide low-pass and bandpass filters. By efficient combination of modern network theory and field theory the speed and memory requirements of the program developed were improved without losing the accuracy of the design. The results obtained agreed very well with the measured results, establishing confidence in the design approach and the computer aided design method developed in this thesis.

2.2 Waveguide discontinuities

In this section, a general description of the types of waveguide discontinuities and a brief introduction to some of the techniques used for characterizing these waveguide junctions are presented.

Typical waveguide discontinuities are,

- Step change in dimensions of the waveguide
- Bends (right-angle or other type of bends)
- T-junctions

It is very imperative to characterize these discontinuities for analysing microwave circuits. There have been several methods proposed for the solution of the waveguide discontinuity problems over the past 30 years. All the techniques characterized the discontinuity using formulae, which were used for calculating the solution for specific dimensions by hand calculation. These techniques, in spite of their approximations were considered indispensable at that time due to the lack of cheap powerful computers. The present revolutionary changes in the computer technology, paved the way

for more accurate solution of the discontinuities. The solution, however, is considered to be very complex and impossible for hand calculations.

2.2.1 Step Junctions

It is possible to have (i) E-plane, (ii) H-plane and (iii) EH-plane step discontinuities in a rectangular waveguide. A H-plane step is a junction of two rectangular guides of unequal widths but equal heights. An E-plane step is a junction of two rectangular guides of unequal heights but equal widths. An EH-plane step is a junction of two rectangular guides of unequal widths and heights. These structures are shown in Figure 2.1 and Figure 2.2. The discontinuities can also be classified into symmetric and asymmetric junctions. The discontinuities shown in Figure 2.1 and Figure 2.2 are symmetric.

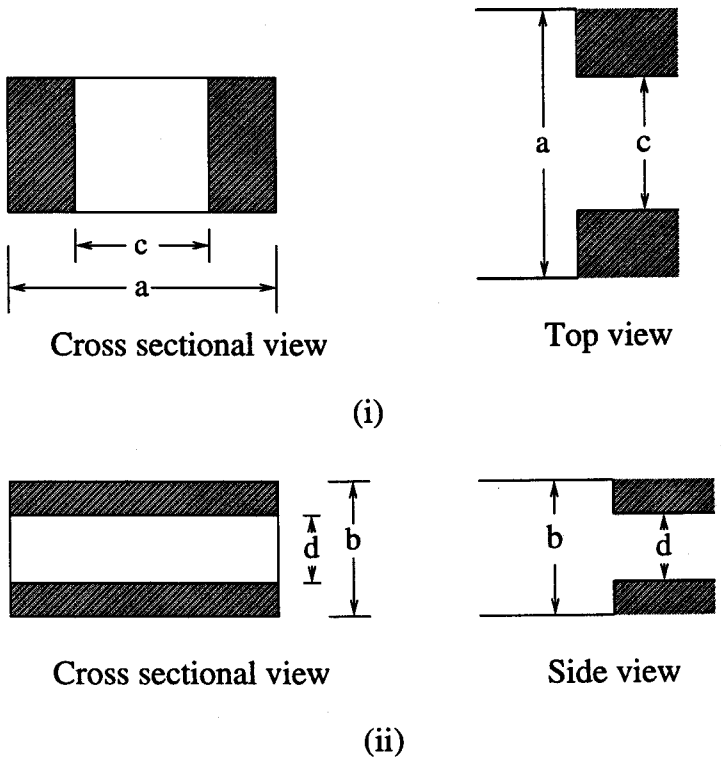

Figure 2.1: Step discontinuities in a rectangular waveguide (i) H-plane (ii) E-plane

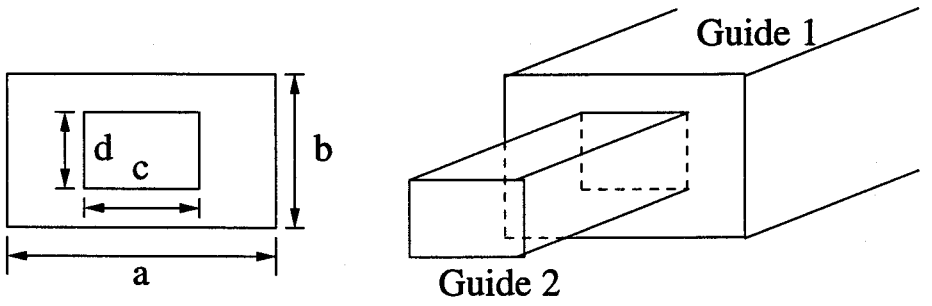

Figure 2.2: EH-plane step discontinuity in a rectangular waveguide

2.2.2 Iris

When two E-plane step junctions (A and B) are connected back to back with a small waveguide section of length t, an E-plane iris is formed as shown in Figure 2.3. In

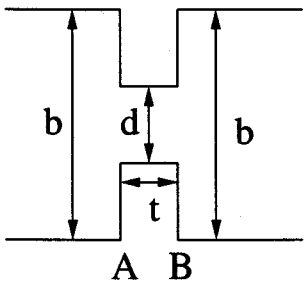

Figure 2.3: E-plane iris in a rectangular waveguide

an E-plane iris the width of the waveguide remains constant while the height of the waveguide changes. Similarly, H-plane and EH-plane step junctions can be connected back to back with a small waveguide section, to form H-plane and EH-plane irises, respectively. A complete characterization of the waveguide discontinuity involves the determination of the frequency-dependent scattering matrix coefficients associated with the discontinuity. The definition of scattering matrix is given in the next section.

2.3 Scattering Parameters

The conventional admittance and impedance parameters Ref. [1] are impractical for characterizing two-port microwave networks, since it is impossible in practice to realize proper open and short circuit terminations at microwave frequencies. Scattering parameters are defined in terms of incident and reflected waves, and they require transmission lines that are terminated in their characteristic impedances instead of a physical shorting or opening the network.

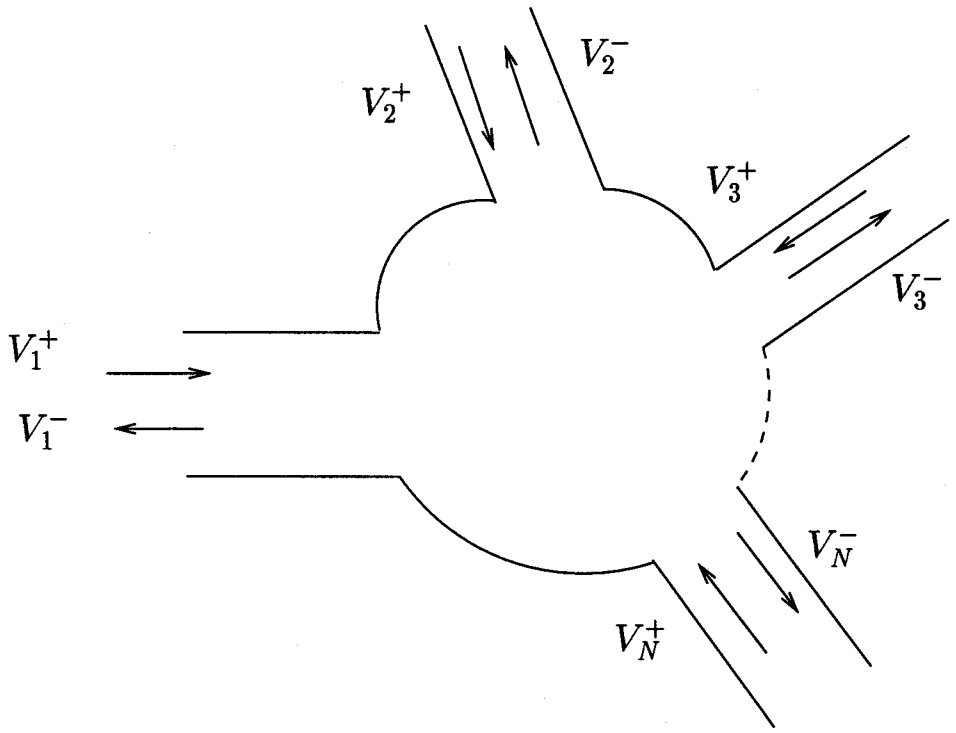

Figure 2.4: An N-port junction illustrating scattered waves

Consider the N-port junction in Figure 2.4. The incident voltage waves are denoted by the '+' superscript while the reflected waves are denoted by the '-' superscript, and the port number is denoted as the subscript of the voltage wave. For instance, V_1^+ and V_1^-, are the incident and reflected waves, respectively, at the port 1.

When V_1^+ is incident on port 1, a reflected wave $V_1^- = S_{11}V_1^+$ is produced, where S_{11} is known as the reflection or scattering coefficient at port 1. Similarly, for all the other ports, $V_i^- = S_{ii}V_i^+$ for i=2,3..N are defined. The waves, in addition to reflection, will be transmitted to other ports and will have a proportional output of the incident wave. $V_i^- = S_{i1}V_1^+$, i = 2,3..N, gives the transmission coefficient S_{i1}, which represents the wave transmitted from port 1 to the i^{th} port. Thus, when the wave is incident on all the ports simultaneously,

$$\begin{bmatrix} V_1^- \\ V_2^- \\ \vdots \\ V_N^- \end{bmatrix} = \begin{bmatrix} S_{11} & S_{12} & \cdots & S_{1N} \\ S_{21} & S_{22} & \cdots & S_{2N} \\ \vdots & \vdots & \ddots & \vdots \\ S_{N1} & S_{N2} & \cdots & S_{NN} \end{bmatrix} \begin{bmatrix} V_1^+ \\ V_2^+ \\ \vdots \\ V_N^+ \end{bmatrix} \tag{2.1}$$

or in a simplified form,

$$\left[V^-\right] = [S]\left[V^+\right]$$

where $[S]$ is called the scattering matrix of the network.

For a passive, reciprocal, lossless network,

$$[S]^t [S]^* = [U] \tag{2.2}$$

This is known as the unitary condition and the proof of this is given in Ref. [1]. The superscripts 't' and '*' are the transpose and the conjugate of the matrix. This condition is very useful for checking the conservation of power and hence the debugging of the program, but not the validity of the numerical solution itself. Since the waveguide filter considered in this thesis is a physical two port network, an elaborate discussion

of two port S parameters is done in this section. For a two port network,

$$V_1^- = S_{11}V_1^+ + S_{12}V_2^+ \tag{2.3}$$

$$V_2^- = S_{21}V_1^+ + S_{22}V_2^+ \tag{2.4}$$

From the above two equations,

$$S_{11} = \left.\frac{V_1^-}{V_1^+}\right|_{V_2^+=0} \qquad S_{12} = \left.\frac{V_1^-}{V_2^+}\right|_{V_1^+=0} \tag{2.5}$$

$$S_{21} = \left.\frac{V_2^-}{V_1^+}\right|_{V_2^+=0} \qquad S_{22} = \left.\frac{V_2^-}{V_2^+}\right|_{V_1^+=0} \tag{2.6}$$

where S_{11} is the reflection coefficient in port 1, with port 2 terminated in a matched load. S_{21} is the transmission coefficient into port 2 from port 1, with port 2 terminated in a matched load. Similar definitions apply to S_{12} and S_{22} with respect to port 2.

2.3.1 Scattering Matrix of a Transmission Line

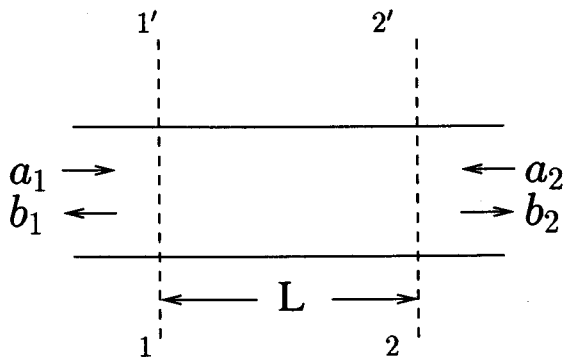

Figure 2.5: A section of lossless uniform transmission line

Consider the matrix of a section of uniform lossless transmission line of length L, as shown in Figure 2.5. A two-port junction with incident voltage waves a_1, a_2

and reflected voltage waves b_1, b_2, for ports 1 and 2, respectively are shown. The scattering matrix for the transmission line for the reference planes $1-1'$ and $2-2'$, is given by Ref. [15],

$$S = \begin{bmatrix} 0 & e^{-j\beta L} \\ e^{-j\beta L} & 0 \end{bmatrix} \tag{2.7}$$

where β is the propagation factor defined in chapter 1.

2.4 *ABCD* parameters

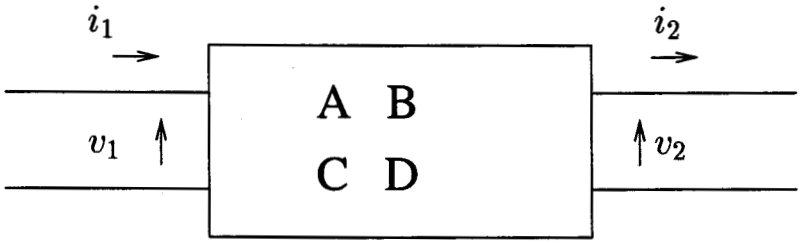

Figure 2.6: *ABCD* parameters of a two port network

The main advantage of the *ABCD* parameters lies in the fact that in a two port cascaded network, where several two terminal-pair networks are connected in cascade, the over-all or the resultant network parameters can be expressed as the product of the individual two port *ABCD* matrices arranged in the same sequence as the respective networks to which they pertain. Figure 2.6 shows a two port network with the current direction in port 2 same as port 1 in order to facilitate the multiplication of *ABCD* matrices of the individual networks when connected in cascade.

$$\begin{bmatrix} v_1 \\ i_1 \end{bmatrix} = \begin{bmatrix} A & B \\ C & D \end{bmatrix} \begin{bmatrix} v_2 \\ i_2 \end{bmatrix} \tag{2.8}$$

Figure 2.7 shows a network in which two ports are connected in cascade. The overall

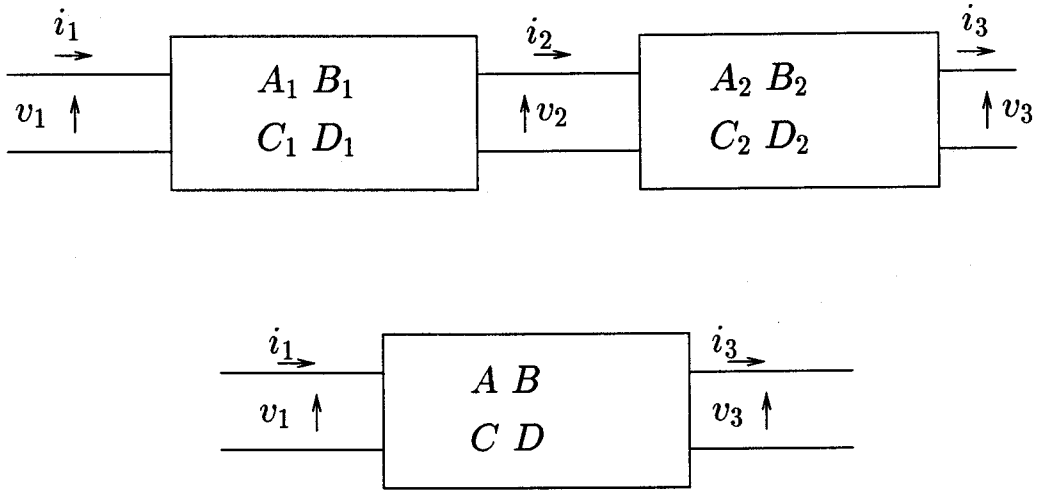

Figure 2.7: Cascading of $ABCD$ parameters

$ABCD$ matrix of the network is obtained by premultiplying the $ABCD$ matrix of the second network with the $ABCD$ matrix of the first network.

$$\begin{bmatrix} A & B \\ C & D \end{bmatrix} = \begin{bmatrix} A_1 & B_1 \\ C_1 & D_1 \end{bmatrix} \begin{bmatrix} A_2 & B_2 \\ C_2 & D_2 \end{bmatrix}$$

This method of directly multiplying matrices can be easily implemented in a computer, and hence $ABCD$ parameters plays an important role in finding a solution to a complex cascaded microwave network.

2.5 Conversion of S to $ABCD$ parameters

The conversion of S parameters to $ABCD$ parameters is done using the following conversion formulae Ref. [16],

$$A = \frac{Z_{N1}^* + Z_{N1}S_{11} - Z_{N1}^*S_{22} - Z_{N1}\Delta_s}{2S_{21}\sqrt{Re\,[Z_{N1}]\,Re\,[Z_{N2}]}} \tag{2.9}$$

$$B = \frac{Z_{N1}^* Z_{N2}^* + Z_{N1} Z_{N2}^* S_{11} + Z_{N1}^* Z_{N2} S_{22} + Z_{N1} Z_{N2} \Delta_s}{2 S_{21} \sqrt{Re\,[Z_{N1}]\, Re\,[Z_{N2}]}} \tag{2.10}$$

$$C = \frac{1 - S_{11} - S_{22} + \Delta_s}{2 S_{21} \sqrt{Re\,[Z_{N1}]\, Re\,[Z_{N2}]}} \tag{2.11}$$

$$D = \frac{Z_{N2}^* - Z_{N2}^* S_{11} + Z_{N2} S_{22} - Z_{N2} \Delta_s}{2 S_{21} \sqrt{Re\,[Z_{N1}]\, Re\,[Z_{N2}]}} \tag{2.12}$$

where Z_{N1} and Z_{N2} are the reference impedances, which may be complex, of the two ports and $\Delta_s = S_{11}S_{22} - S_{12}S_{21}$. Z_N^* is the conjugate of Z_N.

2.6 Physical and electrical port networks

The number of physical terminal-pair present in the network gives the number of physical ports present in the network. For instance, a two terminal-pair network is said to be a physical two port network. In microwave structures, consisting of waveguide components, the single incident mode scatters into infinite number of modes or waves at the discontinuity. Hence, it is possible to have several transmitted and reflected waves. Due to this reason, a two port network consisting of waveguide structures, is considered to have several electrical ports with two physical ports. Each S parameter no longer remains a single element but is represented in the form of a matrix. The scattering matrix S of the network is expressed as a matrix of matrices as shown below,

$$S = \begin{bmatrix} [S_{11}] & [S_{12}] \\ [S_{21}] & [S_{22}] \end{bmatrix}$$

For example, considering two modes for simplicity, the S matrix is given by,

$$S = \begin{bmatrix} S_{11}(0,0) & S_{11}(0,1) & S_{12}(0,0) & S_{12}(0,1) \\ S_{11}(1,0) & S_{11}(1,1) & S_{12}(1,0) & S_{12}(1,1) \\ S_{21}(0,0) & S_{21}(0,1) & S_{22}(0,0) & S_{22}(0,1) \\ S_{21}(1,0) & S_{21}(1,1) & S_{22}(1,0) & S_{22}(1,1) \end{bmatrix} \tag{2.13}$$

Considering TE_{10} mode as the incident mode and that TE_{20} mode propagates in addition to the incident mode, the matrix element $S_{11}(0,0)$ represents the reflection coefficient of the reflected TE_{10} mode in port 1 and the matrix element $S_{11}(0,1)$ represents the reflection coefficient of the reflected TE_{20} mode in port 1. Similarly, $S_{21}(1,0)$ represents the transmission coefficient of the TE_{20} mode.

Practically the fundamental mode elements (0,0) are of only interest. However, the contribution of higher order modes to the fundamental mode elements drastically affects the accurate representation of the network. Hence for accurate representation of the network, the higher order modes have to be considered.

2.7 Cascading of scattering matrices

If two discontinuities with scattering matrices S_L and S_R are cascaded, the overall resulting scattering matrix S_T is given by Ref. [6],

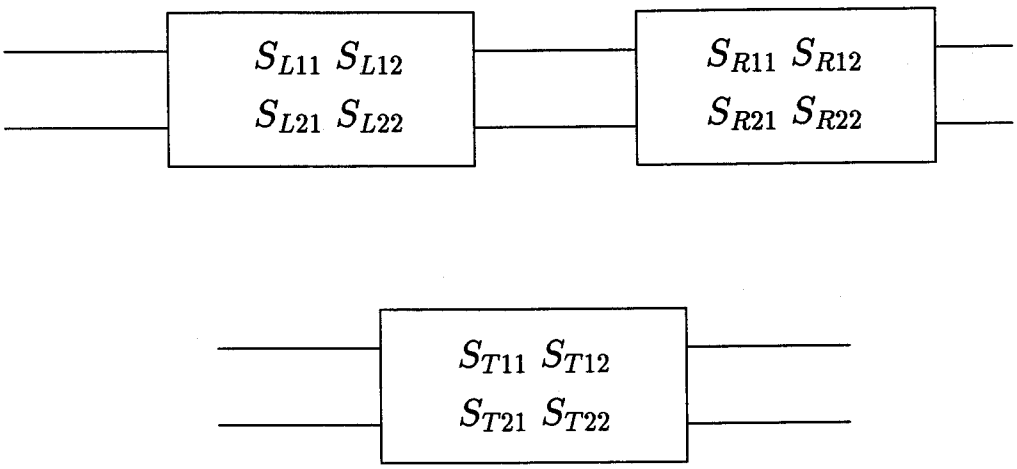

Figure 2.8: Cascading of S parameters

$$S_{T11} = S_{L11} + S_{L12}S_{R11}WS_{L21} \tag{2.14}$$

$$S_{T12} = S_{L12}(I + S_{R11}WS_{L22})S_{R12} \tag{2.15}$$

$$S_{T21} = S_{R21}WS_{L21} \tag{2.16}$$

$$S_{T22} = S_{R22} + S_{R21}WS_{L22}S_{R12} \tag{2.17}$$

where,

$$W = [I - S_{L22}S_{R11}]^{-1} \tag{2.18}$$

There is only one matrix inversion in the above equations. This is more efficient than the conventional equations used for cascading scattering matrices Ref. [15] where two matrix inversions are required.

Chapter 3

The Mode Matching Method

3.1 Introduction

The mode matching method [11] is one of the popular numerical techniques for the solution of waveguide discontinuities. The main advantage of the mode matching method is the inclusion of higher order modes and their interactions in the solution. In addition, the effect of evanescent (β is imaginary) TE and TM modes to the overall electromagnetic field is taken into consideration. The characterization of the waveguide discontinuity by the mode matching method is more accurate and the method can be programmed with much less effort when compared with other numerical techniques [11] like the Finite Element Method (FEM), the Finite Difference Time Domain (FDTD) or the Transmission Line Matrix (TLM) method.

The first step in the mode-matching procedure entails the expansion of unknown fields in the individual regions in terms of a complete set of normal modes whose amplitudes are adjusted so as to satisfy the boundary conditions at the discontinuity. This procedure eventually leads into an infinite set of linear simultaneous equations for the unknown modal coefficients. Since it is highly impossible to extract an exact solution of this infinite system of equations, an approximation is made by truncating the number of modes to a finite number.

Although the analysis is exact, difficulties can arise in the actual numerical calculations as a result of convergence problems. The use of a finite number of normal modes, may converge the solution to an incorrect value if an improper ratio is chosen between the number of modal terms retained in different regions. This phenomenon, popularly known as *relative convergence*, is discussed in Ref. [17, 18].

The Scattering matrix that characterizes the waveguide discontinuity is directly obtained by applying the mode matching method. Since the scattering matrix contains information on all the modes either above or below cutoff, a useful wideband equivalent network can be constructed for the analysis of interacting discontinuities in waveguides. Also, the method along with network theory can be applied very well for the complete design of passive structures like the waveguide filters, which is the objective of this thesis.

3.2 Characterization of Discontinuities

The problem of characterization of a general step discontinuity in a rectangular waveguide by the mode-matching method is considered in this section. Application of the mode-matching method can be better understood with an illustration and hence a specific case of a H-plane waveguide step discontinuity is considered in this section. Figure 3.1 shows a H-plane waveguide step discontinuity. A junction is formed between two waveguides 1 and 2 with widths a and c.

In order to do the mode-matching, the tangential components of electric and magnetic fields (E_y, H_x) are expanded at the junction in terms of the normal modes in each region. N number of modes are considered in waveguide 1 and M number of modes in waveguide 2.

For region 1,

$$E_y^1 = \sum_{i=1}^{N} \left\{ A_i^+ + A_i^- \right\} \phi_{1i} \tag{3.1}$$

$$H_x^1 = \sum_{i=1}^{N} Y_{1i} \left\{ A_i^+ - A_i^- \right\} \phi_{1i} \tag{3.2}$$

For region 2,

$$E_y^2 = \sum_{j=1}^{M} \left\{ B_j^+ + B_j^- \right\} \phi_{2j} \tag{3.3}$$

$$H_x^2 = \sum_{j=1}^{M} Y_{2j} \left\{ B_j^+ - B_j^- \right\} \phi_{2j} \tag{3.4}$$

where ϕ_{1i} and ϕ_{2j} are the normal modes in waveguides 1 and 2 with propagation constants γ_{1i} and γ_{2j} respectively. The normal modes are directly related with the type of discontinuity. For H-plane type of step discontinuity the normal modes are functions of x only. The propagation constants are given by,

$$\gamma_{1i} = \sqrt{\left(\frac{i\pi}{a}\right)^2 - k_o^2}, \qquad \gamma_{2j} = \sqrt{\left(\frac{j\pi}{c}\right)^2 - k_o^2} \tag{3.5}$$

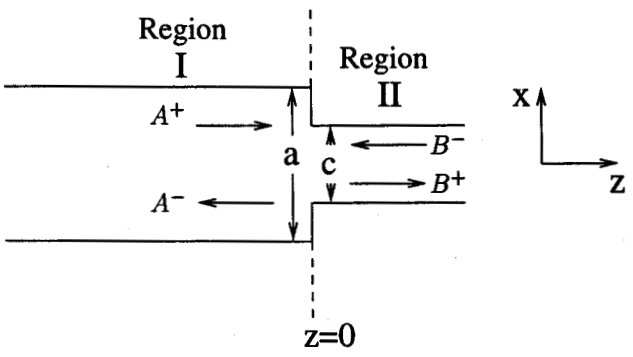

Figure 3.1: Waveguide step discontinuity

The wave admittances are given by,

$$Y_{1i} = \frac{\left(\frac{i\pi}{a}\right)^2 - k_o^2}{j\omega\mu_o\gamma_{1i}} \qquad Y_{2j} = \frac{\left(\frac{j\pi}{c}\right)^2 - k_o^2}{j\omega\mu_o\gamma_{2j}} \tag{3.6}$$

where k_o and μ_o have their usual meanings as defined in chapter 2.

The normal modes satisfy the orthogonality relation,

$$\int \phi_{mi}\,\phi_{mj}\,dx \;=\; \delta_{ij} = \begin{cases} 1 & i = j \\ 0 & i \neq j \end{cases} \qquad \text{m} = 1, 2 \tag{3.7}$$

where δ_{ij} is the Kronecker delta function. A_i^+ and B_j^- are the given incident field coefficients from regions 1 and 2, while A_i^- and B_j^+ are the unknown excited field coefficients in regions 1 and 2, In matrix form,

$$A^+ = \begin{bmatrix} A_1^+ \\ A_2^+ \\ \vdots \\ A_N^+ \end{bmatrix} \qquad B^+ = \begin{bmatrix} B_1^+ \\ B_2^+ \\ \vdots \\ B_M^+ \end{bmatrix} \tag{3.8}$$

$$A^- = \begin{bmatrix} A_1^- \\ A_2^- \\ \vdots \\ A_N^- \end{bmatrix} \qquad B^- = \begin{bmatrix} B_1^- \\ B_2^- \\ \vdots \\ B_M^- \end{bmatrix} \tag{3.9}$$

$$Y_1 = \begin{bmatrix} Y_{11} & 0 & \cdots & 0 \\ 0 & Y_{12} & \cdots & 0 \\ \vdots & \vdots & \ddots & \vdots \\ 0 & 0 & \cdots & Y_{1N} \end{bmatrix} \qquad Y_2 = \begin{bmatrix} Y_{21} & 0 & \cdots & 0 \\ 0 & Y_{22} & \cdots & 0 \\ \vdots & \vdots & \ddots & \vdots \\ 0 & 0 & \cdots & Y_{2M} \end{bmatrix} \tag{3.10}$$

By boundary conditions, the tangential electric field and the normal component of the magnetic field are continuous. Applying the boundary conditions at the junction gives,

$$\sum_{i=1}^{N} \left\{ A_i^+ + A_i^- \right\} \phi_{1i} = \sum_{j=1}^{M} \left\{ B_j^+ + B_j^- \right\} \phi_{2j} \tag{3.11}$$

$$\sum_{i=1}^{N} Y_{1i} \left\{ A_i^+ - A_i^- \right\} \phi_{1i} = \sum_{j=1}^{M} Y_{2j} \left\{ B_j^+ - B_j^- \right\} \phi_{2j} \tag{3.12}$$

By using the orthogonality property of the modal functions ϕ_{1i} and ϕ_{2j}, with the integration carried out over the smaller cross-section of the waveguide. We get,

$$A^+ + A^- = H(B^+ + B^-) \tag{3.13}$$

$$Y_1(A^+ - A^-) = HY_2(B^+ - B^-) \tag{3.14}$$

where,

$$H = \int_{-\frac{c}{2}}^{\frac{c}{2}} \phi_1 \, \phi_2 \, dx \tag{3.15}$$

Equations (3.13,3.14) are a set of linear simultaneous equations in matrix form for the unknown A. H is known as the coupling matrix and is of the order (N,M). Y_1 and Y_2 are the admittance matrices as defined by equation (3.10).

From the S-parameters definition,

$$A^- = S_{11} A^+ + S_{12} B^- \tag{3.16}$$

$$B^+ = S_{21} A^+ + S_{22} B^- \tag{3.17}$$

Rearranging equations (3.13) and (3.14) in the above form, the four scattering ma-

trices are given by [17],

$$S_{22} = \left[Y_2 + H^t Y_1 H\right]^{-1} \left[Y_2 - H^t Y_1 H\right] \tag{3.18}$$

$$S_{21} = 2\left[Y_2 + H^t Y_1 H\right]^{-1} H^t Y_1 = \left[U - S_{22}\right] H^t \tag{3.19}$$

$$S_{12} = 2\left[H Y_2^{-1} H^t Y_1 + U\right]^{-1} H = H\left[U + S_{22}\right] \tag{3.20}$$

$$S_{11} = \left[H Y_2^{-1} H^t Y_1 + U\right]^{-1} \left[H Y_2^{-1} H^t Y_1 - U\right] = -H S_{22} H^t \tag{3.21}$$

where U is the unity matrix, S_{22}, S_{21}, S_{12}, S_{11} are matrices of dimension (M, M), (M, N), (N, M) and (N, N), respectively. H^t is the transpose of the coupling matrix H.

Equations (3.18) to (3.21) can be used to find the scattering parameters of any type of waveguide step discontinuity. However, the coupling matrix H and the admittance matrices are not the same for different types of step discontinuities. The coupling matrix for H, E, and EH-plane step discontinuity are given in the following sections.

3.3 H-plane Step Discontinuity

The modal functions for symmetric H-plane waveguide step discontinuity (refer to Figure 3.1) are given by [1],

$$\phi_1 = \sqrt{\frac{2}{a}} \cos\left(\frac{n\pi x}{a}\right), \qquad n = 1, 3, 5..N \tag{3.22}$$

$$\phi_2 = \sqrt{\frac{2}{c}} \cos\left(\frac{m\pi x}{c}\right), \qquad m = 1, 3, 5..M \tag{3.23}$$

Since the discontinuity is only in the X-direction, the modal functions are depen-

dent only on x. It is sufficient to consider only odd number of modes as the even modes are not excited by the incident TE_{10} wave, due to the symmetric nature of the discontinuity. Thus, only TE_{n0} waves are excited at the junction where n is an odd integer. The coupling matrix is obtained as,

$$H = \frac{2}{\sqrt{ac}} \int_{-c/2}^{c/2} cos\,(ux)\ cos\,(vx)\ dx \tag{3.24}$$

where,

$$u = \frac{n\pi x}{a} \quad \text{and} \quad v = \frac{m\pi x}{c} \tag{3.25}$$

There are two cases, when $u = v$ and $u \neq v$.

$$H = \sqrt{\frac{c}{a}} if \qquad u = v \tag{3.26}$$

$$= \frac{4\,v\,(-1)^m}{\sqrt{ac}\,(v^2 - u^2)} cos\left(\frac{uc}{2}\right) if \qquad u \neq v \tag{3.27}$$

The coupling matrix is independent of frequency and this fact is utilized in increasing the speed of the analysis program where the S parameters for a number of frequency points are calculated. However, the admittance matrix is dependent on frequency and has to be calculated for each frequency point in the analysis program.

A separate subroutine is written for calculating the S matrix of the H-plane step discontinuity. Two other subroutines, one for calculating the coupling matrix H and the other for calculating the admittance matrices are developed. The input to the step analysis discontinuity subroutine are the two waveguide widths, frequency and the number of modes. The subroutine calculates and returns the $[S]$ matrix containing the four S parameters.

The susceptance normalized with respect to waveguide impedances is calculated

from,

$$B = \frac{1 - |S_{11}(0,0)|}{1 + |S_{11}(0,0)|} \tag{3.28}$$

The calculated susceptance for different number of modes in the two sides of the junction are shown in Table 3.3. $a/\lambda = 0.71$ and $c/a = 1/3$ are used for the calculation. The asymptotic value obtained from [11] is -7.7, which compares very well with the calculated value from the step subroutine. The equivalent circuit of a H-plane step discontinuity is shown in Figure 3.2.

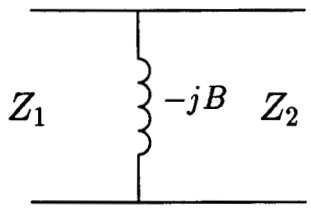

Figure 3.2: Equivalent circuit of a H-plane Step Discontinuity

Table 3.1: Normalized susceptance of a H-plane step discontinuity

N	M	B
10	4	7.675
20	7	7.731
30	10	7.745
40	14	7.737
50	17	7.739
10	10	7.597
20	20	7.688
30	30	7.710
40	40	7.719

The number of modes M in the smaller dimension is chosen by [18],

$$M = \frac{c}{a}N \tag{3.29}$$

The choice of modes is very crucial to avoid the relative convergence problem. At least 30 modes in the larger dimension is used for the analysis of waveguide filters in this thesis. If the smaller dimension is too small, so that the number of modes becomes very small in comparison with the number of modes in the larger dimension, then the number of modes in the smaller dimension is fixed with at least 5 and the number of modes in the larger dimension is calculated using the above equation (3.29). A large number of modes has to be chosen to obtain the asymptotic value, if equal modes are selected on both sides of the discontinuity. It can be seen from Table 3.3 that a convergence is obtained by selecting 30 modes on both sides of the discontinuity. Since the matrix size becomes very large (900) the computation speed is slow and large memory space is required to store the matrix. Hence, by choosing the number of modes according to equation (3.29) the relative convergence problem can be eliminated.

3.4 E-plane Step Discontinuity

The modal functions for symmetric E-plane waveguide step discontinuity (refer to Figure 2.1) are given by [1],

$$\phi_1 = \sqrt{\frac{2\epsilon_{no}}{b}}\, cos\left(\frac{2n\pi y}{b}\right), \qquad n = 0, 1, 2..N \tag{3.30}$$

$$\phi_2 = \sqrt{\frac{2\epsilon_{mo}}{d}}\, cos\left(\frac{2m\pi y}{d}\right), \qquad m = 0, 1, 2..M \tag{3.31}$$

Since the discontinuity is only in the Y-direction, the modal functions are dependent only on y. Only TE_{1n} modes, where n is an even integer, are excited at the junction due to the symmetric nature of the discontinuity. The coupling matrix is given as,

$$H = 2\sqrt{\frac{\epsilon_{no}\,\epsilon_{mo}}{b\,d}} \int_{-d/2}^{d/2} cos\,(uy)\; cos\,(vy)\; dy \tag{3.32}$$

where,

$$u = \frac{2n\pi y}{b} \quad ; \quad v = \frac{2m\pi y}{d} \tag{3.33}$$

and,

$$\epsilon_{io} = \begin{cases} \frac{1}{2} & i = 0 \\ 1 & i \neq 0 \end{cases} \tag{3.34}$$

After integrating for the different cases the result obtained is,

$$H = \sqrt{\frac{d}{b}} \qquad m = 0 \text{ and } n = 0 \tag{3.35}$$

$$= 0 \qquad n = 0 \text{ and } m \neq 0 \tag{3.36}$$

$$= \frac{2\sqrt{2}}{\sqrt{bd}} \frac{sin\left(\frac{ud}{2}\right)}{u} \qquad n \neq 0 \text{ and } m = 0 \tag{3.37}$$

$$H = 2\sqrt{\frac{d}{b}} \qquad m \neq 0,\ n \neq 0 \text{ and } u = v \tag{3.38}$$

$$= \frac{4\,u\,(-1)^m}{\sqrt{ac}\,(u^2 - v^2)} sin\left(\frac{ud}{2}\right) \qquad m \neq 0,\ n \neq 0 \text{ and } u \neq v \tag{3.39}$$

A separate subroutine is written for calculating the S matrix of the E-plane step discontinuity. The results obtained from mode matching method is compared with the results in [7] by calculating the susceptance normalized with respect to the wave impedances on both sides of the junction. The equivalent circuit of a E-plane step discontinuity is shown in Figure 3.3.

The proper choice of modes is very important in an efficient computation as it can be observed from Table 3.2. If equal number of modes are chosen on both sides

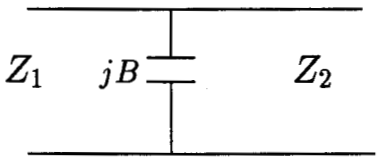

Figure 3.3: Equivalent circuit of an E-plane Step Discontinuity

Table 3.2: Normalized susceptance of an E-plane step discontinuity

N	M	B
10	6	0.129
20	12	0.129
30	18	0.129
40	23	0.129
50	29	0.129
100	57	0.129
10	10	0.128
20	20	0.129
40	40	0.129

Marcuvitz [7]
0.129

a = 22.86 mm, b = 10.16 mm, d = 5.78 mm, frequency = 9.2 GHz

of the junction, large number of modes (20) has to be selected while (10,6) modes are sufficient for obtaining the correct result. It can be readily observed that there is about six times reduction in the matrix size of the coupling matrix. Hence, relative convergence problem plays an important role in the memory requirements and computational speed. A separate program for computing the susceptance using Ref. [7] is developed to validate the results obtained from the mode matching method.

3.5 EH-plane Step Discontinuity

Numerical characterization of a double step discontinuity or EH-plane discontinuity (refer Figure 2.2) is usually carried out by a generalized analysis utilizing a linear superposition of TE_{mn} and TM_{mn} modes [12]. This approach, however, has a draw-

back of slow computation time and occupies large storage space as the matrix size is usually very large. A modified TE^x_{mn} mode approach [13] consumes less memory and CPU time and provides improved convergence behaviour without sacrificing the accuracy. The TE^x_{mn} approach is based on the fact that the E_x component is fairly small and is assumed to be zero. This drastically reduces the computation time compared to the TE_{mn} and TM_{mn} approach as many higher order terms are required to approximate a small or even zero E_x component.

The modal functions for a symmetric EH-plane waveguide step discontinuity are given by,

$$\phi_1 = \sqrt{\frac{2\epsilon_{no}}{ab}} \cos\left(\frac{(2m+1)\pi x}{a}\right) \cos\left(\frac{2n\pi y}{b}\right) \quad \begin{cases} m = 0,1,2..N \\ n = 0,1,2..M \end{cases} \tag{3.40}$$

$$\phi_2 = \sqrt{\frac{2\epsilon_{qo}}{cd}} \cos\left(\frac{(2p+1)\pi x}{c}\right) \cos\left(\frac{2q\pi y}{d}\right) \quad \begin{cases} p = 0,1,2..P \\ q = 0,1,2..Q \end{cases} \tag{3.41}$$

The coupling matrix is obtained from,

$$H = \int_{-d/2}^{d/2}\int_{-c/2}^{c/2} \phi_1 \, \phi_2 \, dx \, dy \tag{3.42}$$

where (N,P), (M,Q) are the number of modes considered in the larger and smaller waveguide, respectively. The number of modes are chosen according to equation (3.29) in order to facilitate efficient convergence of the solution.

For simplification purpose, we can write,

$$k_1 = \frac{(2m+1)\pi}{a} \quad ; \quad k_3 = \frac{(2p+1)\pi}{c} \tag{3.43}$$

$$k_2 = \frac{2n\pi}{b} \quad ; \quad k_4 = \frac{2q\pi}{d} \tag{3.44}$$

Evaluating the coupling matrix integral for different cases results in,

case 1: $k_2 = 0$ and $k_4 \neq 0$

$$H = 0 \tag{3.45}$$

case 2: $k_2 \neq 0$ and $k_4 = 0$

if $k_1 = k_3$

$$H = \sqrt{\frac{8}{abcd}}\, sin\left(\frac{k_2\, d}{2}\right) \frac{c}{k_2} \tag{3.46}$$

if $k_1 \neq k_3$

$$H = \sqrt{\frac{8}{abcd}} \frac{4\, k_3\, (-1)^p}{k_2\ (k_1^2 - k_3^2)} cos\left(\frac{k_1 c}{2}\right) sin\left(\frac{k_2\, d}{2}\right) \tag{3.47}$$

case 3: $k_2 = 0$ and $k_4 = 0$

if $k_1 = k_3$

$$H = \sqrt{\frac{cd}{ab}} \tag{3.48}$$

if $k_1 \neq k_3$

$$H = \sqrt{\frac{4}{abcd}} \frac{2\, k_3\, (-1)^p}{(k_1^2 - k_3^2)} cos\left(\frac{k_1 c}{2}\right) d \tag{3.49}$$

case 4: $k_2 \neq 0$ and $k_4 \neq 0$

if $k_1 = k_3$ and $k_2 = k_4$,

$$H = \sqrt{\frac{cd}{ab}} \tag{3.50}$$

if $k_1 \neq k_3$ and $k_2 = k_4$,

$$H = \sqrt{\frac{1}{abcd}} \frac{4\, k_3\, (-1)^p}{(k_1^2 - k_3^2)} \cos\left(\frac{k_1 c}{2}\right) d \tag{3.51}$$

if $k_1 = k_3$ and $k_2 \neq k_4$,

$$H = \sqrt{\frac{1}{abcd}} \frac{4\, k_2\, (-1)^q}{(k_2^2 - k_4^2)} \sin\left(\frac{k_2 d}{2}\right) c \tag{3.52}$$

if $k_1 \neq k_3$ and $k_2 \neq k_4$,

$$H = \sqrt{\frac{16}{abcd}} \frac{4\, k_2\, (-1)^q\, k_3\, (-1)^p}{(k_1^2 - k_3^2)\,(k_2^2 - k_4^2)} \cos\left(\frac{k_1 c}{2}\right) d \sin\left(\frac{k_2 d}{2}\right) c \tag{3.53}$$

An appropriate arrangement of a single index is used for normal modes with double indices. The modes are arranged in ascending order with respect to their cutoff frequencies facilitating the use of single index for the double indices. The admittance matrices are calculated from,

$$\gamma_{1ij} = \sqrt{k_1^2 + k_2^2 - k_o^2} \tag{3.54}$$

$$\gamma_{2ij} = \sqrt{k_3^2 + k_4^2 - k_o^2} \tag{3.55}$$

$$Y_{1ij} = \frac{k_1^2 - k_o^2}{j\omega\mu_o\gamma_{1ij}} \qquad Y_{2ij} = \frac{k_3^2 - k_o^2}{j\omega\mu_o\gamma_{2ij}} \tag{3.56}$$

A subroutine is written for calculating the S matrix of the EH-plane step discontinuity. The results obtained from the subroutine developed using the mode matching method are compared with those in Ref. [14]. The normalized susceptance from Ref. [14] for case 1 and case 2 are 2.978 and 19.189 respectively. The agreement

between the two results is good as seen from Table 3.3.

Table 3.3: Normalized susceptance of an EH-plane step discontinuity

a = 22.86 mm, b = 10.16 mm , f = 11 GHz

P	Q	Case 1	Case 2
5	5	2.950	19.275
10	5	2.952	19.341

Case 1: c = 11.43 mm, d = 5.08 mm;
Case 2: c = 6.86 mm, d = 3.16 mm;

3.6 E-plane Iris

Iris type discontinuities are characterized by cascading the individual S matrices of a step, a section of transmission line and a second step in that order as shown in Figure 3.4. The overall S matrix is given by,

$$K = \left(I - DS_{22}^{A} DS_{11}^{B}\right)^{-1} \tag{3.57}$$

$$S_{11}^{T} = S_{11}^{A} + S_{12}^{A} DS_{11}^{B} KDS_{21}^{A} \tag{3.58}$$

$$S_{21}^{T} = S_{21}^{B} KDS_{21}^{A} \tag{3.59}$$

$$S_{12}^{T} = S_{12}^{A} D\left(I + S_{11}^{B} KDS_{22}^{A} D\right) S_{12}^{B} \tag{3.60}$$

$$S_{22}^{T} = S_{22}^{B} + S_{21}^{B} KDS_{22}^{A} DS_{12}^{B} \tag{3.61}$$

where I is the unity matrix and D is the diagonal matrix as given in chapter 2.

Figure 3.5 shows the equivalent circuit of an E-plane iris discontinuity. The equivalent circuit is valid only for the fundamental dominant mode. However, the contributions due to the higher order modes are taken into account when the mode matching

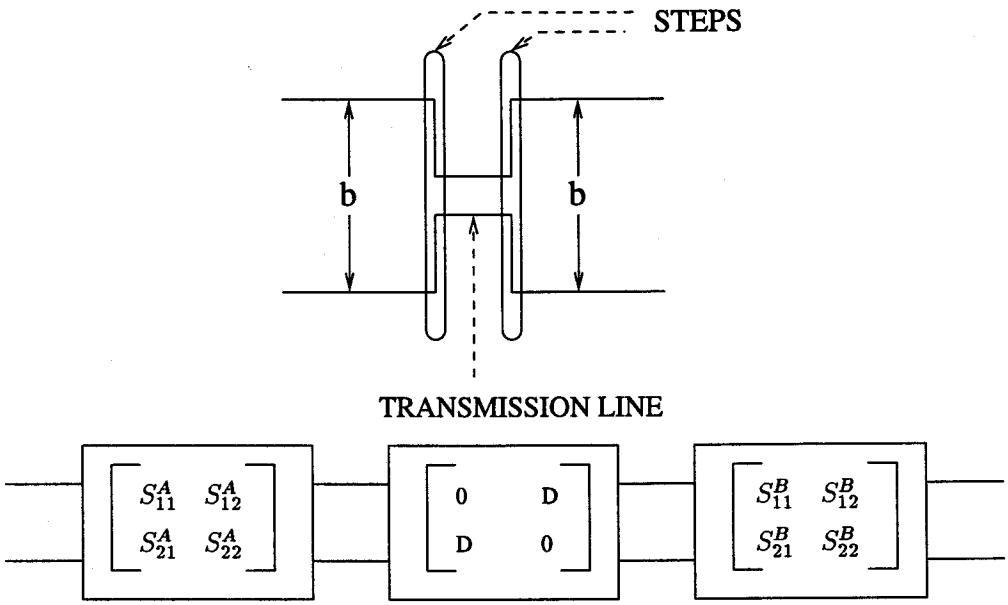

Figure 3.4: Characterization of an E-plane Iris Discontinuity

method is used to obtain the equivalent circuit. The results obtained from the mode

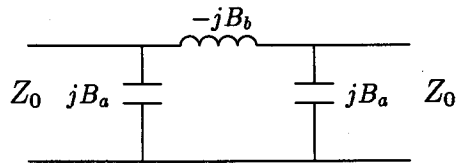

Figure 3.5: Equivalent circuit of an E-plane Iris Discontinuity

matching method are compared with Marcuvitz [7]. The normalized susceptance obtained by both the mode matching and [7] are tabulated for different iris openings in Table 3.6. The agreement between the two methods is very good.

Table 3.4: E-plane Iris Discontinuity

a = 22.86 mm, b = 10.16 mm, f = 20 GHz
thickness of iris = 3 mm and N = 40

Mode Matching			Marcuvitz [7]		
M	B_b	B_a	B_b	B_a	d/b
5	10.657	9.626	10.780	9.584	0.1
8	5.390	5.325	5.390	5.288	0.2
12	3.593	3.611	3.593	3.600	0.3
16	2.694	2.638	2.695	2.625	0.4
20	2.155	2.013	2.156	1.970	0.5
23	1.794	1.517	1.797	1.505	0.6
28	1.537	1.181	1.540	1.171	0.7
31	1.345	0.942	1.348	0.935	0.8
35	1.197	0.777	1.198	0.775	0.9

3.7 Summary

In this chapter, the characterization of different types of waveguide discontinuities by using the mode matching method is discussed in detail. The relative convergence problem encountered in the mode matching method is considered and the method for overcoming this problem is discussed as given by [18]. Application of the mode matching method to characterize E-plane, H-plane and EH-plane type of waveguide step discontinuities are given in detail. Other types of discontinuity problems can be solved similarly following the method described. The results from the traditional method [7] are used to validate the results obtained from the mode matching method. The agreement between the results is very good. Marcuvtiz's method fails when more than one mode propagates through the waveguide and has many limitations as of the size of the step considered while the mode matching method includes the evanescent modes very accurately in the solution of the discontinuity and has no limitations on the size of the step. It can be concluded that the mode matching method is an effective numerical method for solving waveguide discontinuity problems and it is fast, accurate and robust when compared with the traditional method [7].

Chapter 4

Synthesis and Analysis

In the previous chapter the characterization of waveguide discontinuities using the mode matching method is explained. In this chapter the CAD method for the design of tapered corrugated waveguide bandpass and low-pass filters is presented in detail. The CAD method for designing waveguide filters involves a synthesis method and an analysis method. The synthesis method determines the physical dimensions of the filter and the analysis method accurately simulates the frequency response of the filter for verifying the design of the filter.

The synthesis method is based on distributed transmission line theory and the conventional low frequency network theory. It determines the geometrical dimension of each coupling iris and the distance between two consecutive irises in the waveguide filter structure. The synthesis method uses the analysis method for obtaining the data required for the determination of opening of each coupling iris. The design procedure greatly relies on the accurate characterization of the waveguide discontinuities inherent to the type of filter. The mode matching method described in the previous chapter is most efficient for the characterization of waveguide discontinuities having a relatively simple geometry. The mode matching method is used in the design procedures developed in this chapter.

4.1 Bandpass Filter Design

4.1.1 Performance Parameters

The design procedure commences with a review of the performance parameters of the waveguide bandpass filter to be designed. The performance is expressed by a set of parameters characterizing the frequency response of the filter. Figure 4.1 shows the insertion and return loss characteristics as a function of frequency of a bandpass filter.

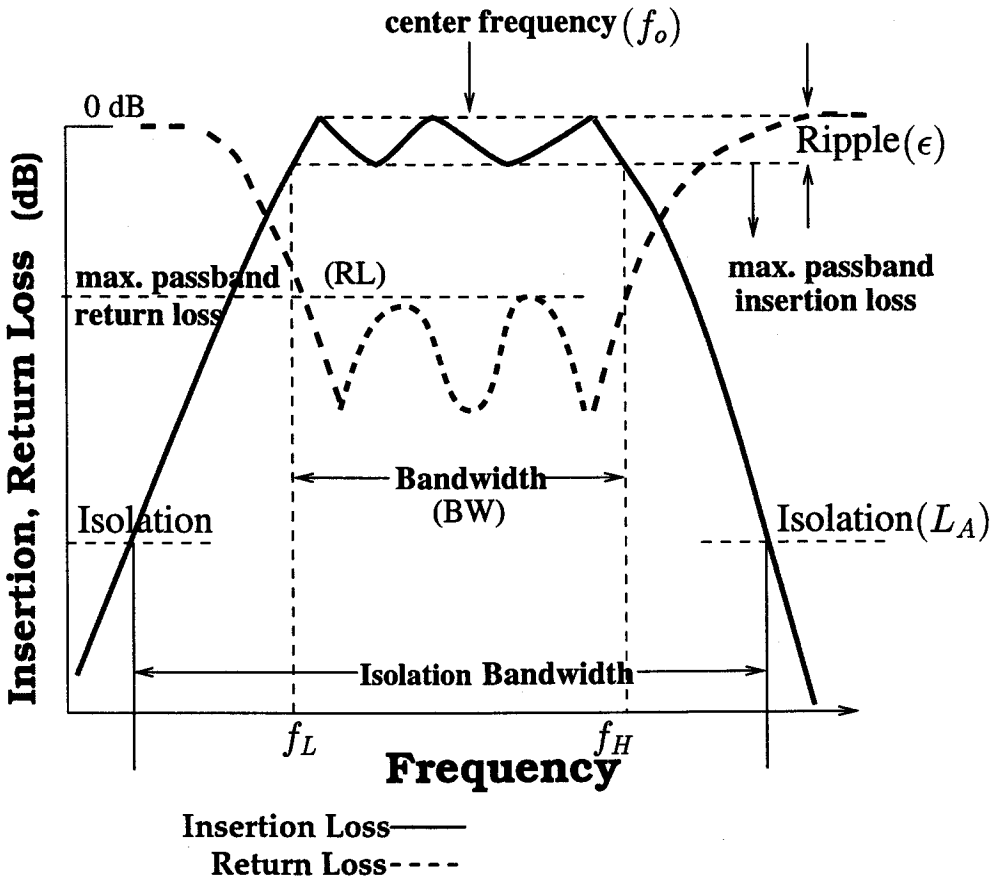

Figure 4.1: Passband characteristics of a bandpass filter

Some of the common terms that are used to describe the filter frequency response are as follows:

- Bandwidth, BW
- Lower cutoff frequency, f_L
- Upper cutoff frequency, f_H
- Passband return loss, RL
- Passband ripple, ϵ
- Isolation bandwidth factor, γ
- Isolation, L_A

Further,

Center frequency is the mean of the lower and upper cutoff frequencies.

Bandwidth is usually expressed in absolute frequency or in relative percentage of the center frequency of bandpass filters.

Isolation is expressed in decibels (dB) and it is the minimum stopband insertion loss.

$$L_A = 20\, log\, \frac{1}{|S_{12A}|} \tag{4.1}$$

where S_{12A} is the maximum value of the magnitude of S_{12}, the transmission coefficient in the stopband. For example, 50 dB isolation means the undesired frequencies should be attenuated by at least 50 dB with respect to passband signal amplitude.

Isolation bandwidth factor (γ) is the ratio of isolation bandwidth to bandwidth.

In addition, the dimensions of the waveguide (width and height), the tapering profile and iris thickness form a part of the design specifications. The peak power handling capacity [4] of the filter is used in some cases as an additional specification. The number of modes to be considered is specified as input to the computer code developed for the filter design.

4.1.2 Synthesis Method

The synthesis method is based on a formulation proposed by Rhodes for a distributed step-impedance bandpass prototype [19]. Chebyshev type of response is considered in the design method. The generalized lumped element prototype for the bandpass filter is shown in Figure 4.2 (a) and the equivalent distributed prototype containing impedance inverters is shown in Figure 4.2 (b). The distributed prototype consists

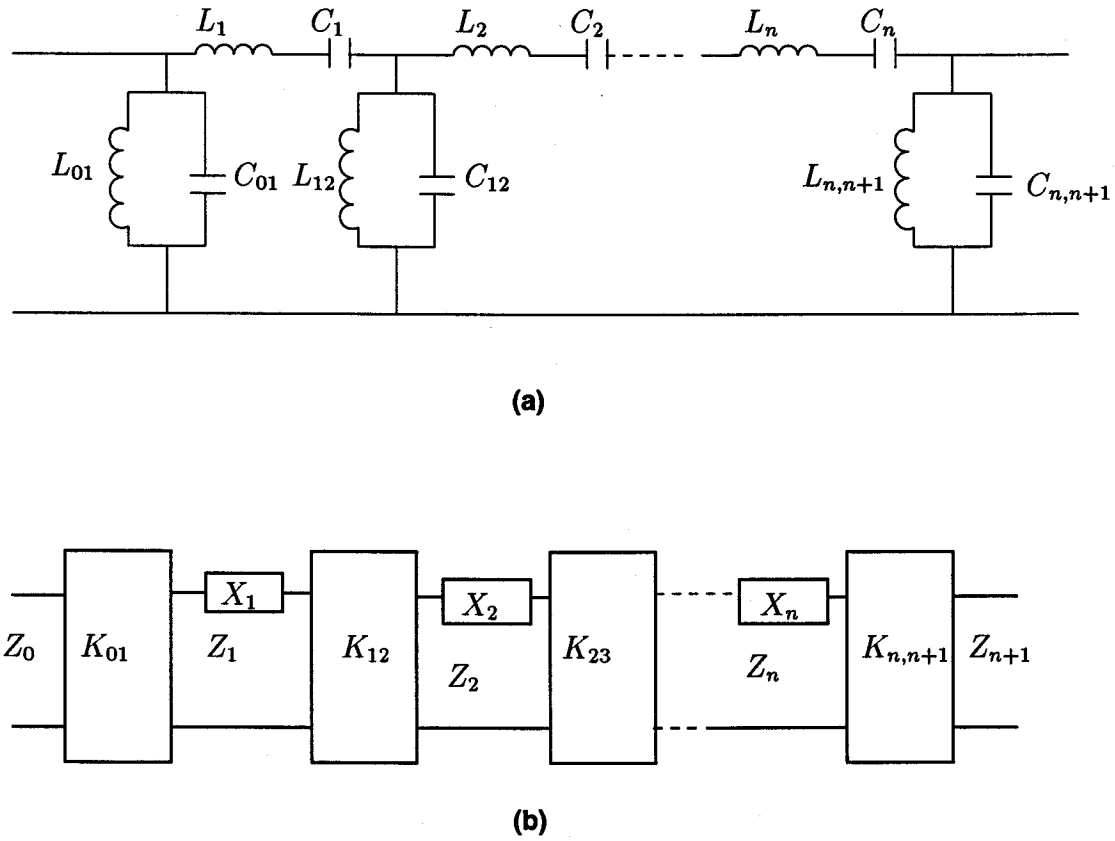

Figure 4.2: Equivalent models of the corrugated waveguide filter including impedance inverters: (a) bandpass filter prototype (b) bandpass filter containing impedance inverters

of a cascade of impedance inverters connected by transmission line sections. Parallel-resonant circuits of the bandpass filter in Figure 4.2 (a) are replaced by impedance inverters K_{ij} as shown in Figure 4.2 (b). An impedance inverter of impedance K can

be defined as a two port network which, looking into its input port, inverts and scales to impedance K any impedance Z connected to its output port. Since in waveguides an arrangement consisting of series and parallel resonators is difficult to realize, the use of impedance inverters in the synthesis method is a quite practical approach.

Two types of structures are possible for realizing the bandpass filters using waveguides. In the first type, E-plane irises are utilized in realizing the K-inverters as shown in Figure 4.3. In the second type, H-plane irises are utilized in realizing the K-inverters as shown in Figure 4.4.

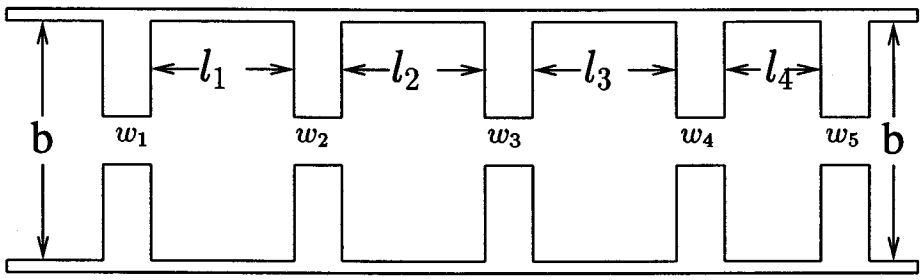

Figure 4.3: Waveguide bandpass filter with E-plane iris discontinuities

In both types, the series resonators as shown in Figure 4.2(b) are realized by waveguide sections of length $\lambda_{go}/2$, where λ_{go} is the guide wavelength of the line at the center frequency of the filter. The waveguide section acts like a transmission line and when the length is made equal to $\lambda_{go}/2$ and $Z_R = \infty$ (open circuit), the input impedance of the line given by [1],

$$Z_{in} = Z_o \left(\frac{Z_R cos\,\beta l + j Z_o sin\,\beta l}{Z_o cos\,\beta l + j Z_R sin\,\beta l} \right) \tag{4.2}$$

goes to infinity. Z_R, Z_o and β are the terminating impedance, the characteristic impedance and the propagation constant of the transmission line. This corresponds to conditions in the parallel-resonant circuit (the low-frequency analogue), which has an infinite impedance if resistance is neglected.

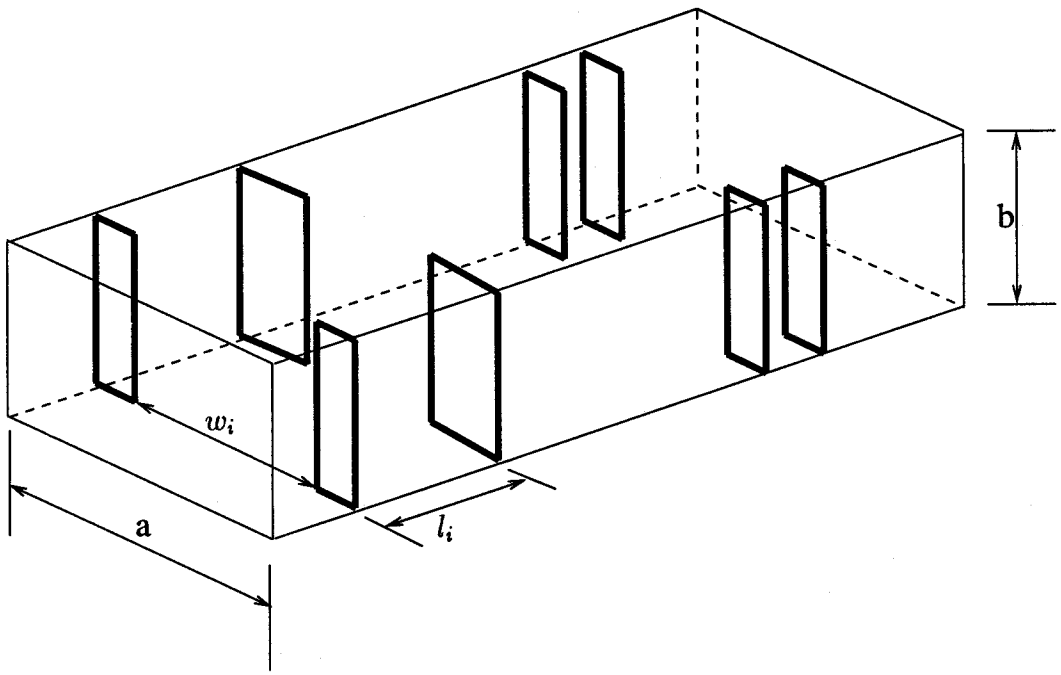

Figure 4.4: Waveguide bandpass filter with H-plane iris discontinuities

In the waveguide structure shown in Figure 4.4 the iris opening is increased and decreased in the X-direction to realize the K-inverter values, which has led to the name **H-plane corrugated waveguide filter** by which it is commonly known. Similarly, in Figure 4.3 the iris opening w_i is raised or lowered in the Y-direction to realize the K-inverter values, which has led to the name of **E-plane corrugated waveguide filter.** Since the waveguide sections between any two irises are equal in width, and equal in height for the H-plane and E-plane structures, respectively, the structures are said to be *uniformly* corrugated. It is possible to have waveguide sections of unequal width or unequal height between any two iris discontinuities and such a structure is known as *nonuniform* corrugated waveguide filters. Usually, a particular profile (square, cosine, linear etc.) is followed to have waveguide sections of unequal height or width. This profile is called the tapering profile, and *tapered* corrugated waveguide filters are used instead of *nonuniform* corrugated waveguide filters.

The procedure for designing H-plane or E-plane tapered corrugated waveguide band-pass filters is as follows [19]:

1. The midband guide wavelength λ_{go} is determined by solving,

$$\lambda_{gL} sin(\frac{\pi \lambda_{go}}{\lambda_{gL}}) + \lambda_{gH} sin(\frac{\pi \lambda_{go}}{\lambda_{gH}}) = 0 \tag{4.3}$$

where λ_{gL} and λ_{gH} are the guide wavelengths in the resonator section at the lower f_L and upper f_H cutoff frequencies. For a narrow-band case,

$$\lambda_{go} \approx \frac{\lambda_{gL} + \lambda_{gH}}{2} \tag{4.4}$$

A suitable numerical method such as the Newton Raphson [20] is applied for solving the above equation (4.3).

2. Scaling parameter α is obtained from,

$$\alpha = \frac{\lambda_{go}}{\lambda_{gL} sin(\frac{\pi \lambda_{go}}{\lambda_{gL}})} \tag{4.5}$$

3. The number of resonators N is determined by [21],

$$N \geq \frac{(L_A + RL + 6)}{20 log(\gamma + \sqrt{\gamma^2 - 1})} \tag{4.6}$$

4. The impedances of the distributed element Z and impedance inverter values K are determined by,

$$Z_n = \frac{2\alpha}{y} sin\left[\frac{(2n-1)\pi}{2N}\right]$$

$$-\frac{1}{4y\alpha}\left\{\frac{y^2+sin^2(\frac{n\pi}{N})}{sin\frac{(2n+1)\pi}{2N}}\right\}$$

$$-\frac{1}{4y\alpha}\left\{\frac{y^2+sin^2\left[\frac{(n-1)\pi}{N}\right]}{sin\frac{(2n-3)\pi}{2N}}\right\}, \quad n=1,...,N \tag{4.7}$$

and,

$$k'_{n,n+1}=\frac{\sqrt{y^2+sin^2(\frac{n\pi}{N})}}{y}, \qquad n=0,...,N \tag{4.8}$$

where,

$$y=sinh\left[\frac{1}{N}sinh^{-1}\frac{1}{\epsilon}\right] \tag{4.9}$$

5. In uniform corrugated waveguide filters, the characteristic impedances of the resonator sections are identical and hence by scaling the impedance Z_n to unity, and the K-inverters are normalized by,

$$K_{n,n+1}=\frac{k'_{n,n+1}}{\sqrt{Z_nZ_{n+1}}}, \quad n=0,...,N \tag{4.10}$$

$$Z_o=Z_{n+1}=1 \tag{4.11}$$

6. In tapered corrugated waveguide filters, the characteristic impedances of the resonator sections are not identical, and hence normalization of the K-inverter values with the characteristic impedances is done so that the quantity $K/\sqrt{Z_n,Z_{n+1}}$ is made invariant when matching a practical network to a prototype.

$$K'_{n,n+1}=\frac{K_{n,n+1}}{\sqrt{Z'_nZ'_{n+1}}}, \quad n=0,...,N \tag{4.12}$$

$$Z'_o=Z'_{n+1}=1 \tag{4.13}$$

where, Z'_n is the characteristic impedance of the resonator section n.

7. The filter structure can be represented by using the asymmetrical impedance inverter as shown in Figure 4.5. The width of iris is determined so that the required impedance inverter value is realized via Ref. [8],

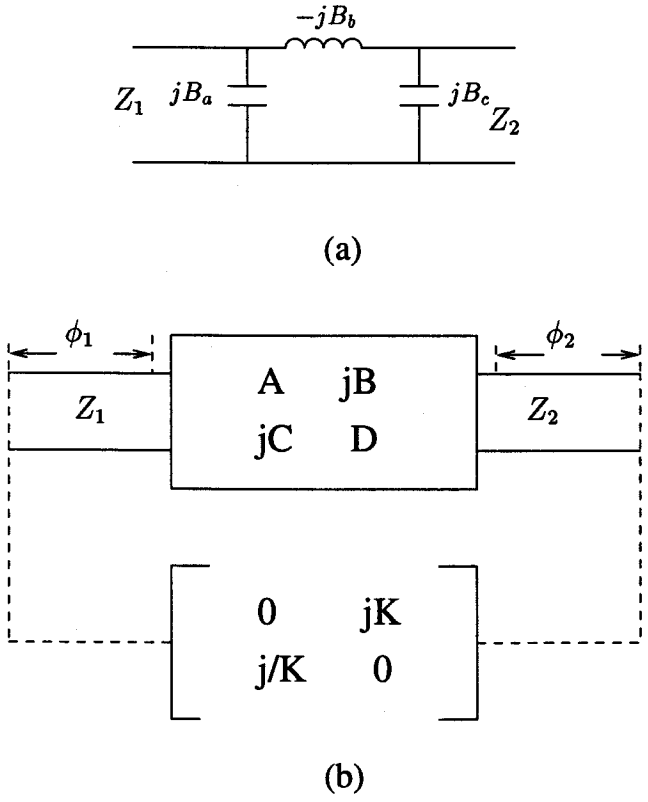

Figure 4.5: (a) Equivalent circuit of an asymmetrical iris (b) Equivalent impedance inverter representation

$$K = \sqrt{Z_1 Z_2}(\sqrt{L} - \sqrt{L-1}) \tag{4.14}$$

$$L = 1 + \frac{1}{4}\left\{(a-d)^2 + (b-c)^2\right\} \tag{4.15}$$

$$a = A\sqrt{\frac{Z_2}{Z_1}} \qquad b = \frac{B}{\sqrt{Z_1 Z_2}} \tag{4.16}$$

$$c = C\sqrt{Z_2 Z_1} \qquad d = D\sqrt{\frac{Z_1}{Z_2}} \tag{4.17}$$

where a, b, c, and d are normalized elements of the $ABCD$ matrix, and Z_1 and Z_2 are normalized guide impedances of the tapered waveguide resonator sections. The reference planes are obtained from the equations,

$$tan2\phi_1 = \frac{2(bd - ac)}{(a^2 - d^2) + (b^2 - c^2)} \tag{4.18}$$

$$tan2\phi_2 = \frac{2(ab - cd)}{(d^2 - a^2) + (b^2 - c^2)} \tag{4.19}$$

where the angles ϕ_1 and ϕ_2 are expressed in radians.

The K-values can also be obtained directly from the scattering matrix S without converting the S matrix into the $ABCD$ matrix. The voltage standing wave ratio (VSWR) seen at one port of the inverter when the other port is terminated in its characteristic impedance is given by,

$$\text{VSWR} = \frac{1 + |S_{11}|}{1 - |S_{11}|} \text{ and} \tag{4.20}$$

$$K = \frac{1}{\sqrt{\text{VSWR}}} \tag{4.21}$$

where $|S_{11}|$ is the absolute value of the reflection coefficient seen at one port when the other is terminated in its characteristic impedance. The reference plane locations are given by the following equations:

$$\phi_1 = -\angle S_{11}/2 + \pi/2$$

$$\phi_2 = -\angle S_{22}/2 + \pi/2 \tag{4.22}$$

A root-seeking program is implemented to find the value of the iris width. Newton-Raphson method using the derivative [20] is implemented for faster convergence to the solution. Since the method uses gradient information, it is very efficient in converging towards the solution. The gradient is calculated using the perturbation method as the function is unknown in analytical form.

The iris subroutine which is a part of the analysis program is used to find out the S matrix of the iris type discontinuity. The obtained S matrix is converted into ABCD matrix and the K-inverter values are found out using the above formulae. The obtained K-inverter values are then compared to the K-inverter values calculated from the distributed stepped impedance method. The root-seeking program alters the iris widths, starting from an initial guess, until the error between the two K-inverter values is sufficiently small. An error tolerance of 1.0e-4 is used in this program.

8. Finally, the physical length of the resonator formed by the ith and $(i+1)$th iris is found by,

$$l_i = \frac{\lambda_{go}}{2\pi}\left[\pi + \frac{(\phi_i + \phi_{i+1})}{2}\right] \tag{4.23}$$

where λ_{go} is the guide wavelength. The guide wavelength remains a constant for the E-plane structures as the guide wavelength for the dominant TE_{10} mode does not depend on the height of the guide. However, in H-plane tapered corrugated waveguide filter structures the change in width of the cavities between any two iris type of discontinuities changes the guide wavelength. Hence, the appropriate guide wavelength for each of the cavity should be substituted in place of $\lambda_{go}/2$ when calculating the length of the cavity or resonator. In practice, ϕ_1 and ϕ_2 may be realized as negative values and by absorbing such a negative value into the positive adjacent length, the final network can be shortened.

4.2 Low-pass Filter Design

Waveguide low-pass filters are used in numerous antenna feed systems, most often for rejection of spurious harmonics from transmitters. A very simple type of harmonic rejection filter is a cascade of thick capacitive irises closely spaced in a uniform waveguide [9] as shown in Figure 4.6. Since it is impossible to realize capacitive reactance using H-plane discontinuities, only E-plane low-pass filters are possible. Since the waveguide has a cutoff frequency, the filters cannot operate to DC as most of the low-pass filters do. Waveguide low-pass filters can be made to have very low passband loss because of its waveguide construction, and it can be expected to have a higher power rating than equivalent TEM-mode filters.

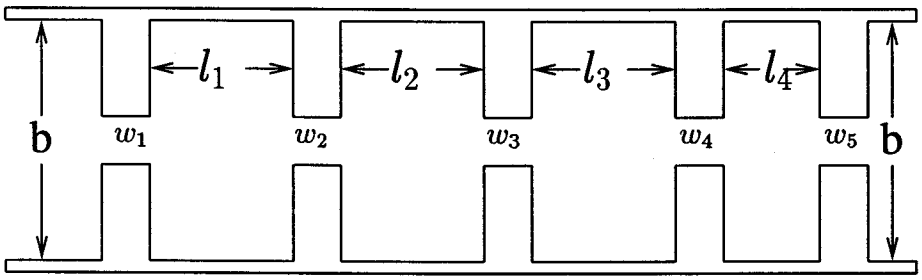

Figure 4.6: E-plane uniform corrugated waveguide low-pass filter
Resonator lengths: l_1, l_2, l_3, l_4 Iris openings: w_1, w_2, w_3, w_4, w_5

The irises are spaced by lengths of waveguide less than $\lambda_g/4$ at the cutoff frequency of the filter. Typically, it is $\lambda_g/8$. The uniform corrugated waveguide filters suffers from following disadvantages:

- the stopband cannot readily be made to be free of spurious responses
- there will be numerous spurious responses in the stopband region for higher order modes, which are easily excited at frequencies above the normal TE_{10} operating range of the waveguide.

Due to the presence of the corrugations in the guide, modes having variations in the direction of the waveguide height will be cut off up to very high frequencies. Therefore, TE_{n0} modes will be the only ones that need to be considered. Also the TE_{20}, TE_{40}, and other even order modes will not be excited because of the symmetric nature of the iris discontinuity in the filter structure. The first higher order mode that will be able to cause trouble is the TE_{30} mode which has a cutoff frequency three times that of the TE_{10} mode.

In order to improve the stopband of the filter, tapered corrugated waveguide filter structure shown in Figure 4.7 is used. The synthesis technique for designing the tapered corrugated waveguide low-pass filter commences by specifying the performance parameters of the waveguide low-pass filter to be designed. Some of the steps involved in the design of waveguide low-pass filter is the same as that for the design of a bandpass filter given in the previous section.

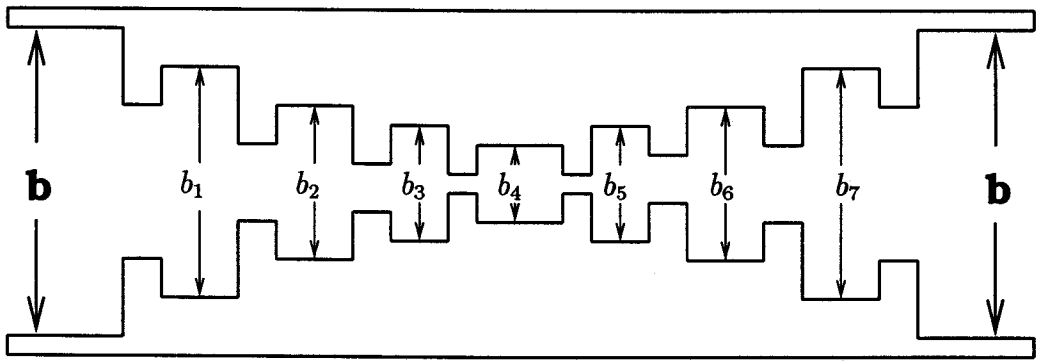

Figure 4.7: E-plane tapered corrugated waveguide low-pass filter (5 pole)
Waveguide heights: $b, b_1, b_2, b_3, .., b_7$

4.2.1 Performance Parameters

The common performance parameters that are used to describe the filter frequency response are shown in Figure 4.8 and defined below [21].

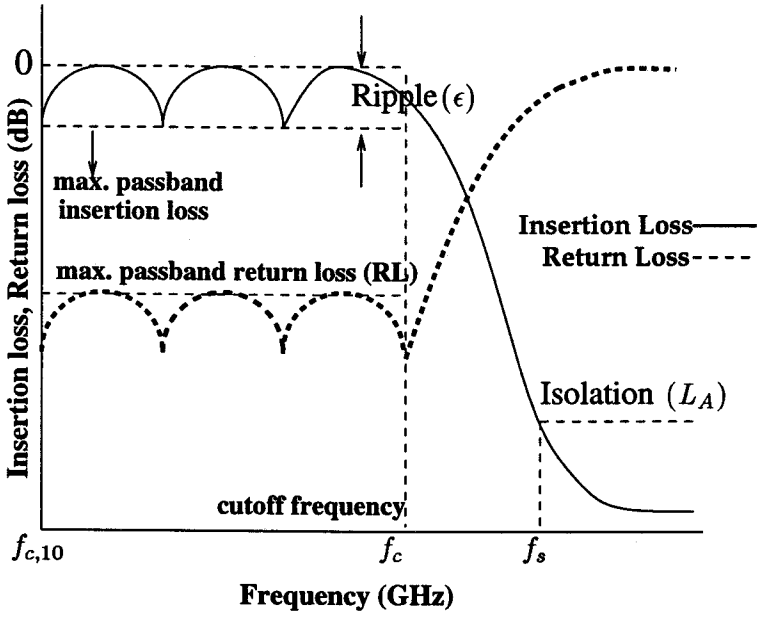

Figure 4.8: Passband characteristics of a low-pass filter

- Cutoff frequency, f_c
- Fractional bandwidth,

$$w_g = \frac{4\theta_o}{\pi} \tag{4.24}$$

  where θ_o is the electrical length corresponding to the cutoff frequency of the low-pass filter.

- Passband return loss, RL
- Passband ripple, ϵ

- Isolation bandwidth factor (γ), is the ratio of the cutoff frequencies of the stop-band to passband.

$$\gamma = \frac{f_s}{f_c} \tag{4.25}$$

- Isolation, L_A

In addition to the performance parameters, the dimensions of the waveguide (width and height), the tapering profile, iris thickness and the number of modes to be considered form a part of the design specifications.

4.2.2 Synthesis Method

The synthesis method for the design of tapered corrugated waveguide low-pass filter [22] closely follows the synthesis method for the design of bandpass filters discussed in the previous section. The generalized distributed low-pass prototype is shown in Figure 4.9. It consists of a cascade of generalized impedance inverters connected by sections of transmission line each of electrical length θ_o. The generalized impedance inverter can be realized by any reciprocal, passive two port.

The use of generalized impedance inverters in the design of tapered corrugated waveguide filters is of special importance, since in this filter type the waveguide discontinuity (iris) acting as an impedance inverter is asymmetrical. Consequently, such an impedance inverter is connected to waveguide sections of different characteristic impedances. The tapered corrugated waveguide filters, significantly reduces the filter length due to the elimination of input/output transformers, which are required if symmetrical impedance inverters are used in the design method.

The steps which are variant from that of bandpass filter design are as follows:

The scaling parameter α is determined by,

$$\alpha = sin\left(\frac{\pi w_g}{4}\right) \tag{4.26}$$

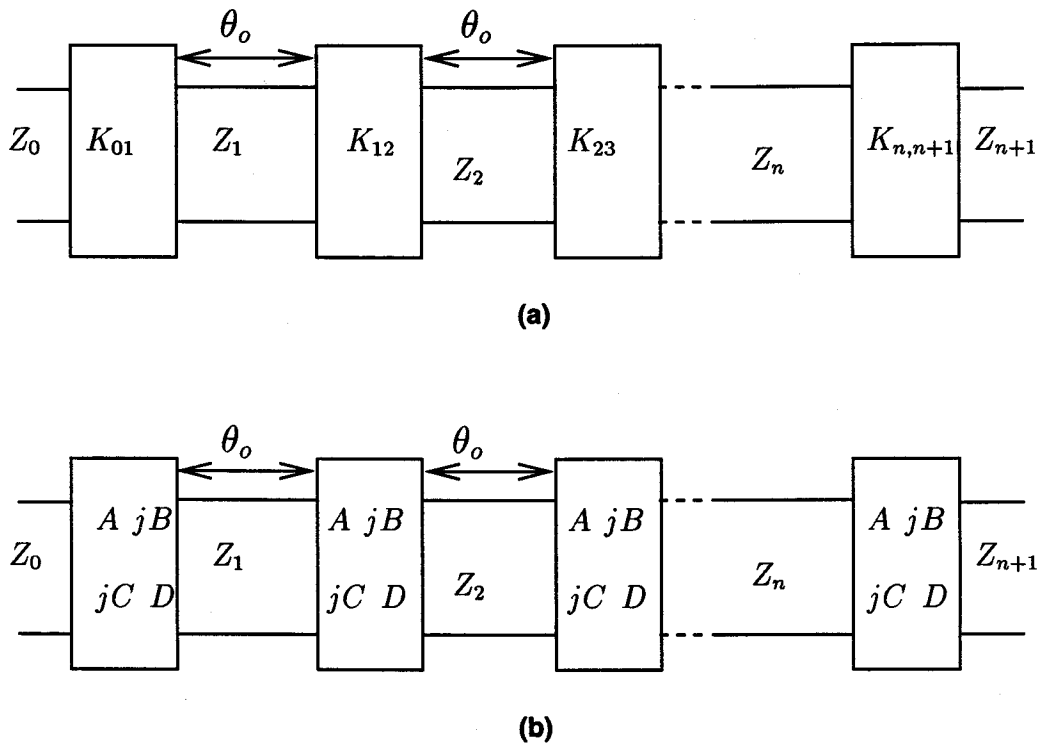

Figure 4.9: Equivalent models of the corrugated waveguide filter including generalized impedance inverters: (a) low-pass prototype (b) physical equivalent of the prototype

The impedance of the distributed element Z_n is calculated by,

$$Z_n = \frac{2}{y\,\alpha} sin\left[\frac{(2n-1)\pi}{2N}\right]$$

$$-\frac{\alpha}{4y}\left\{\frac{y^2 + sin^2(\frac{n\pi}{N})}{sin\frac{(2n+1)\pi}{2N}}\right\}$$

$$-\frac{\alpha}{4y}\left\{\frac{y^2 + sin^2\left[\frac{(n-1)\pi}{N}\right]}{sin\frac{(2n-3)\pi}{2N}}\right\}, \quad n = 1, ..., N \tag{4.27}$$

The length of the iris formed by the ith and $(i+1)$th iris is found by,

$$l_i = \frac{\lambda_{go}}{2\pi}\left[\frac{\pi}{8} - \frac{(\phi_i + \phi_{i+1})}{2}\right] \tag{4.28}$$

4.3 Advantages of CAD Synthesis Method

The major advantages of the synthesis method are as follows:

1. The filters can be constructed directly from the dimensions printed out by the output of the synthesis program.
2. No major experimental adjustments are required. However, minor tuning adjustments may be required to compensate for mechanical tolerances, especially in small waveguide sizes and extremely narrow band filters.
3. More compact and efficient filters can be designed.
4. Better control over stopband requirements as stopband performance is also predicted.
5. It is possible to get high attenuation near the cutoff frequency.
6. Tradeoffs may be made with passband insertion loss, bandwidth, isolation and power handling capability.

4.4 Analysis

The analysis method can be used to obtain S-parameters of various discontinuities in waveguides. This data is very useful in characterization of impedance inverters in

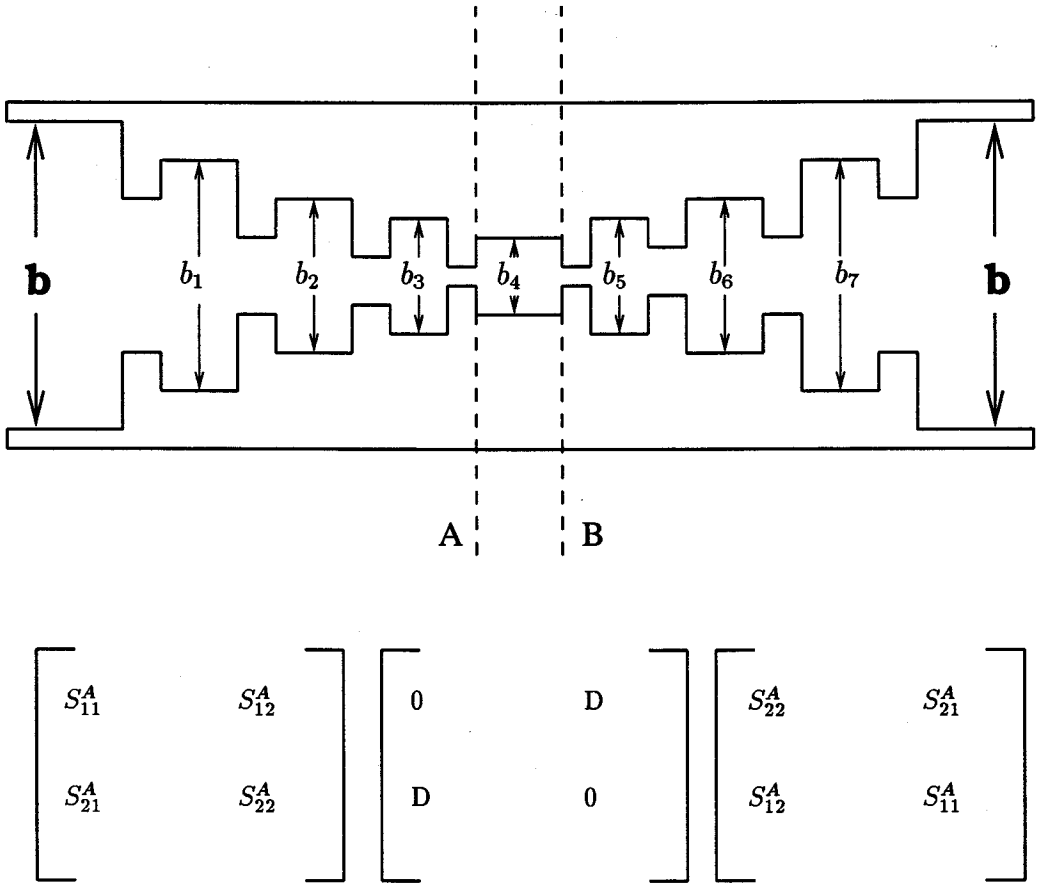

Figure 4.10: Analysis of symmetric waveguide filters

the synthesis method. In addition, the analysis method can be used in the verification of the design of the complete filter. After finding the dimensions of the filter using the synthesis method, the frequency response of the filter is simulated by the analysis program. At each frequency point the S matrix of the irises and the resonators are cascaded to obtain the overall S matrix of the filter and hence the frequency response characteristics of the filter.

Since only symmetric structures are used in this thesis, calculating the overall matrix is relatively a simple process in comparison with the asymmetric structures. Figure 4.10 shows the analysis procedure for analysing a symmetric tapered corrugated waveguide filter structure with odd number of resonators. The overall matrix

up to half the number of resonators (vertical line A in the figure) is sufficient as the overall matrix for the other half of the structure (vertical line B in the figure) is the same with S_{22}, S_{11} and S_{12}, S_{21} interchanged, respectively. This reduces the computational time for the simulation of frequency response characteristics by about half when compared with the asymmetric structures. For an even number of resonators, instead of a resonator section between A and B an iris will be present but a similar method utilizing the symmetric property can be applied for calculating the overall matrix.

4.5 Optimization

Since in the computer aided synthesis method developed, the higher order mode interaction between adjacent K-inverters are neglected, in some cases a final tuning of the filter is required. This final tuning of the filter, if required, is done by optimizing the dimensions of the waveguide filter in order to obtain the desired frequency response. An error function $F(\overline{x})$ to be minimised is defined as,

$$F(\overline{x}) = \sum_{N_s} \left(\frac{L_s}{|S_{21}|} \right)^2 + \sum_{N_p} \left(\frac{|S_{21}|}{L_p} \right)^2 \tag{4.29}$$

where N_s and N_p are the number of frequency sampling points in the stopband and passband, respectively. L_s and L_p are the minimum stopband and maximum passband attenuation levels, respectively, and $|S_{21}|$ is the calculated value of the filter attenuation. For a given iris thickness, the parameters $\overline{x}$ to be optimized are the resonator lengths l_i and iris widths w_i. The optimization computer program used in this thesis is developed by the Electrical Engineering Department and Institute for Systems Research, University of Maryland, College Park, USA. The program is written in C high level language and driving functions are written to call this program

whenever optimization of the filter is required.

4.6 Summary

In this chapter the computer aided design methods for designing bandpass and low-pass filters are developed. The mode matching method is used for characterizing the waveguide discontinuities and two types of structures namely, uniformly corrugated and tapered corrugated waveguide filter design methods are given. The various advantages of the synthesis method developed are listed and a brief introduction to the optimization of the design is described. Complete computer aided design of filters has three steps namely, synthesis, analysis and optimization.

Chapter 5

Results and Discussion

This chapter presents the results of several types of corrugated waveguide low-pass and bandpass filters, obtained from the developed computer code based on the design methods developed in the previous chapter. It is highly impractical to verify the design process experimentally by making and testing a large number of filters. Therefore, the analysis method developed is used for simulating the complete characteristic response of a filter designed from the synthesis method. Hence the verification of the developed analysis method is very important.

This chapter commences with an introduction to the various filter structures that are designed later in the chapter. This is followed by the verification of the analysis method by comparing the simulated results with experimental results for both E-plane and H-plane waveguide filter structures. The rest of the chapter furnishes the results arising from the design and analysis of bandpass and low-pass filters along with a discussion of the results. The filter structures presented in this thesis are designed with X-band (8-12 GHz) and Ku-band (12-18 GHz) waveguides.

5.1 Filter Structures

There are various waveguide structures that are used to realize both bandpass and low-pass filters. It can be broadly classified as E-plane and H-plane structures as discussed in chapter 4. E-plane and H-plane corrugated waveguide filter structures for realizing bandpass filters are shown in Figures 4.3 and 4.4, respectively. H-plane low-pass filters are not possible since it it impossible to realize capacitive reactance using H-plane discontinuities. E-plane uniform corrugated and tapered corrugated waveguide filter structure for realizing low-pass filters are shown in Figures 4.6 and 4.7, respectively.

Instead of uniform height or width of the waveguide in the resonator sections between the two irises, tapering of the width or height of the waveguide can be done as mentioned in chapter 4. A number of tapering profiles are used in the tapered corrugated structures and are defined as below.

- square

$$tm = tc + \alpha(i-k)(i-k) \tag{5.1}$$

$$\alpha = \frac{(t-tc)}{k^2} \tag{5.2}$$

- cosine

$$tm = t - (t-tc)sin\left(\frac{i\pi}{(n+1)}\right) \tag{5.3}$$

- exponential

$$tm = te^{2\alpha i} \tag{5.4}$$

$$\alpha = -log\left(\frac{t}{tc}\right)/(n+1) \tag{5.5}$$

- linear

$$tm = t - \alpha i \tag{5.6}$$

$$\alpha = \frac{t - tc}{n} \tag{5.7}$$

$$\text{where,} \quad t_i = t_{n-i+1} = tm \tag{5.8}$$

$$k = \frac{n+1}{2} \qquad i = 1..k \tag{5.9}$$

Here tc is the width or height of the central waveguide section, t is the width or height of the input or output waveguide section and n is the number of resonators. In practice, the tapering profile and the minimum height or width of the central waveguide section is specified for a tapered corrugated waveguide filter. For instance, E-plane cosine (5mm) tapering implies cosine tapering profile with height of the central waveguide section equal to 5mm. The tapering profile is symmetric as given by equation (5.8).

All the filter structures designed in this thesis are symmetric i.e.,

$$w_i = w_{n+1-i} \qquad for \quad i = 1..k \tag{5.10}$$

$$l_i = l_{n-i} \qquad for \quad i = 1..k \tag{5.11}$$

$$\text{where,} \quad k = \begin{cases} (n+1)/2 & for \quad even \quad n \\ (n/2) & for \quad odd \quad n \end{cases} \tag{5.12}$$

5.2 Verification of the Analysis Method

In this section two waveguide filter structures, one with E-plane discontinuities and the other with H-plane discontinuities, are analysed to obtain the complete frequency response characteristics. The results obtained from the analysis method developed in

this thesis is compared with experimental and existing published results for verifying the computer code based on the design methods developed in this thesis.

5.2.1 H-plane Structure Analysis

Figure 5.1 shows a H-plane uniform corrugated waveguide filter structure that is used for the verification of the analysis method. The structure is analysed to obtain the complete frequency response using the developed analysis method. The dimensions of the filter structure are taken from [23]. Table 5.1 shows the iris widths, resonator lengths and other dimensions like thickness of the iris and waveguide dimensions. All the lengths are expressed in milli-metre (mm).

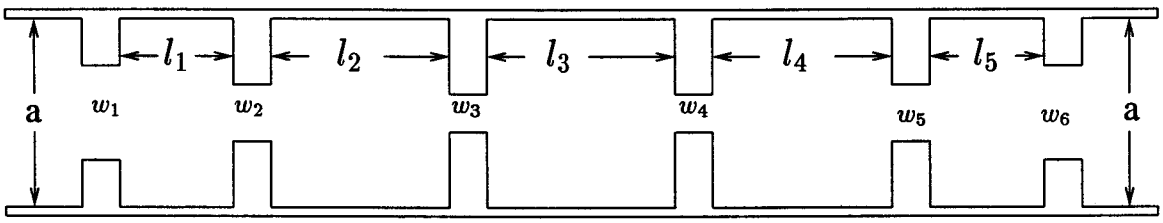

Figure 5.1: Filter structure with H-plane discontinuities

Figure 5.2 shows the comparison between simulated and experimental [23] frequency response characteristics. It can be seen that a very good agreement between the two results is achieved. The results provided in [23] is the measured response of the five resonator waveguide filter structure shown in Figure 5.1. It is found that the cutoff frequencies, the passband ripple level and the stopband attenuation are in excellent agreement. Table 5.2 highlights the comparison between the computed and measured performance.

Table 5.1: Dimensions of the filter (mm)

Waveguide dimensions: a = 19.05 b = 9.52		
No.	Iris width (w)	Resonator Length (l)
1	11.05	11.835
2	7.952	13.763
3	7.2	14.079
4	7.2	13.763
5	7.952	11.835
6	11.05	-
Thickness of all the irises : 2		

Table 5.2: Comparison between computed and measured performance

Parameter	Analysis Method	Experimental Results [23]
Lower cutoff frequency (GHz)	11.7	11.7
Upper cutoff frequency (GHz)	12.6	12.6
Maximum return loss (dB)	-26	-26
Insertion loss (dB) at 13.5 GHz	-40	-40

5.2.2 E-plane Structure Analysis

The analysis method developed for analysing an E-plane waveguide filter structure is verified in this section. A 9 pole E-plane uniform corrugated waveguide filter structure is considered and the dimensions of the filter structure are shown in Table 5.3. The filter dimensions and the experimental results are obtained from **Microwaves Development Company**, North Andover, MA, USA. The performance characteristics of the filter is simulated and compared with the experimental results. A comparison between the simulated passband return loss and the experimental results is shown in Figure 5.3.

The maximum return loss in the passband is accurately predicted. The reason for the discrepancies between the two results may be due to the misalignment of the filter

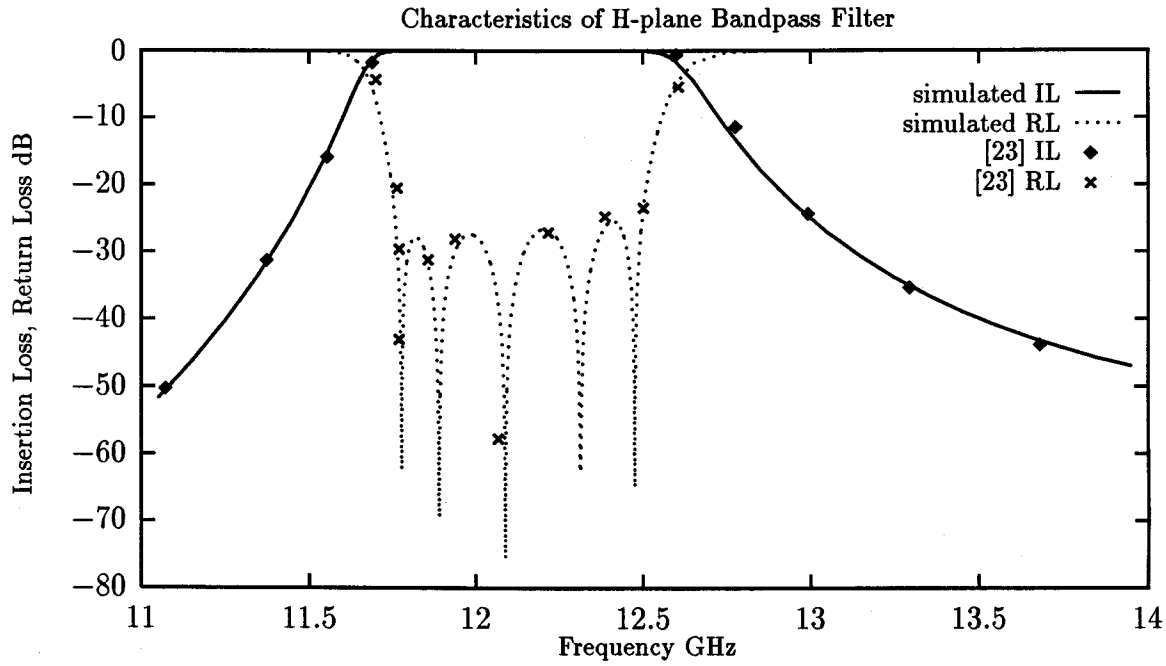

Figure 5.2: Comparison between simulated and measured performance of a H-plane bandpass filter

at the input and output flanges. In addition, mechanical limitations due to machine tolerance in the manufacturing process may be another reason for the discrepancies between the two results.

Figure 5.4 shows the simulated wide band characteristics of the filter and a comparison with the measured experimental results. It can be seen that the cutoff frequency of the filter is accurately predicted and the agreement of the passband insertion loss is good. However, the measured performance in the stopband is full of harmonics. This clearly proves the misalignment of the filter at the input and output flanges. There is almost a difference of 60 dB between the two results at 36 GHz frequency. However, the slope above the cutoff and the cutoff are the main concerns and it can be seen that they are predicted accurately.

Table 5.3: Dimensions of the filter (mm)

Waveguide dimensions: a = 9.144 b = 3.708		
No.	Iris width (w)	Resonator Length (l)
1	2.12	3.498
2	1.027	2.817
3	0.617	2.474
4	0.503	2.362
5	0.472	2.337
Thickness of all the irises: 0.508		

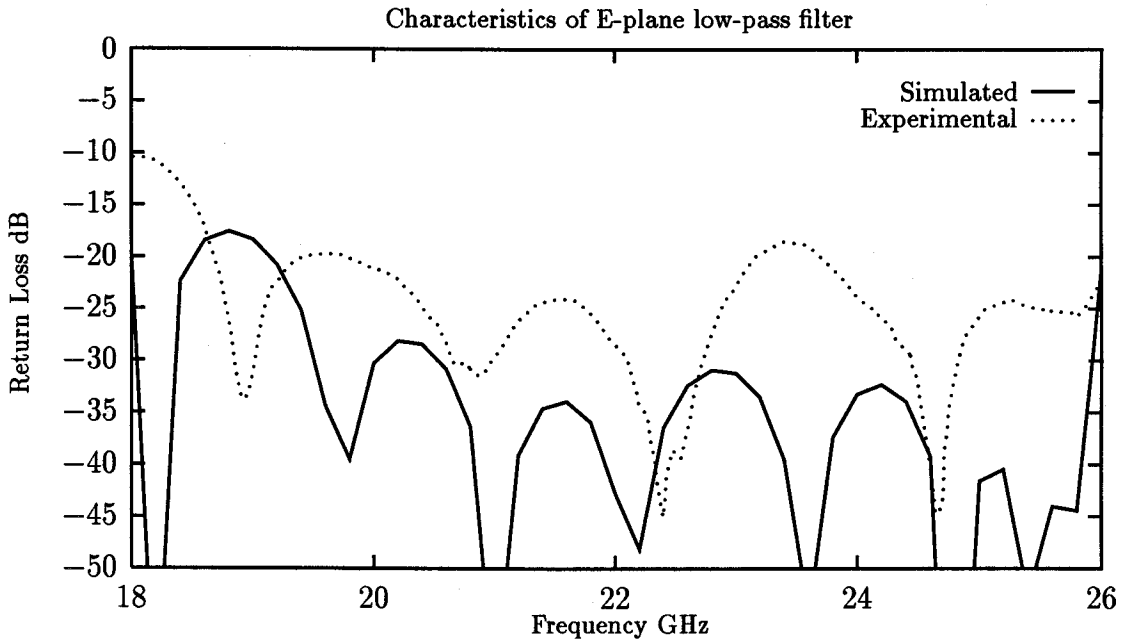

Figure 5.3: Comparison of simulated and experimental passband return loss

Figure 5.5 shows the comparison of simulated stopband characteristics of another E-plane uniform corrugated waveguide low-pass filter structure with the experimental results. The filter dimensions and the experimental results are obtained from **Microwaves Development Company**, North Andover, MA, USA. The dimensions of

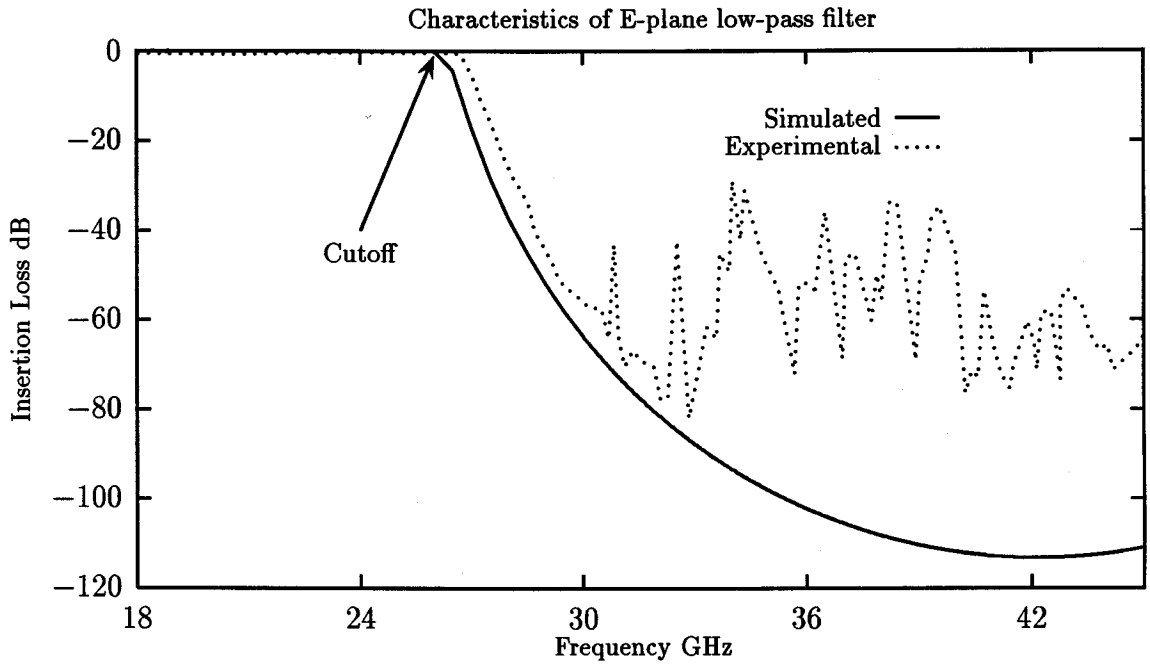

Figure 5.4: Comparison of simulated and experimental insertion loss

the filter is shown in Table 5.4. The filter is designed for 9 GHz cutoff frequency, the passband ripple level is 0.002 dB and the iris thickness is 2.54 mm. The number of resonators is 9.

As with the previous example, the cutoff frequency is exactly predicted. However, the stopband insertion loss at frequencies higher than the cutoff frequency there is a considerable difference between the two results. This discrepancy in results is due to the misalignment of the filter at the input and output flanges.

The effect of misalignment is predominant at higher frequencies. In the case of filter with 26 GHz cutoff frequency, due to the misalignment, the insertion loss in the stopband is reduced to as low as -30 dB. But in the case of filter with 9 GHz cutoff the insertion loss in the stopband is reduced to as low as -40 dB.

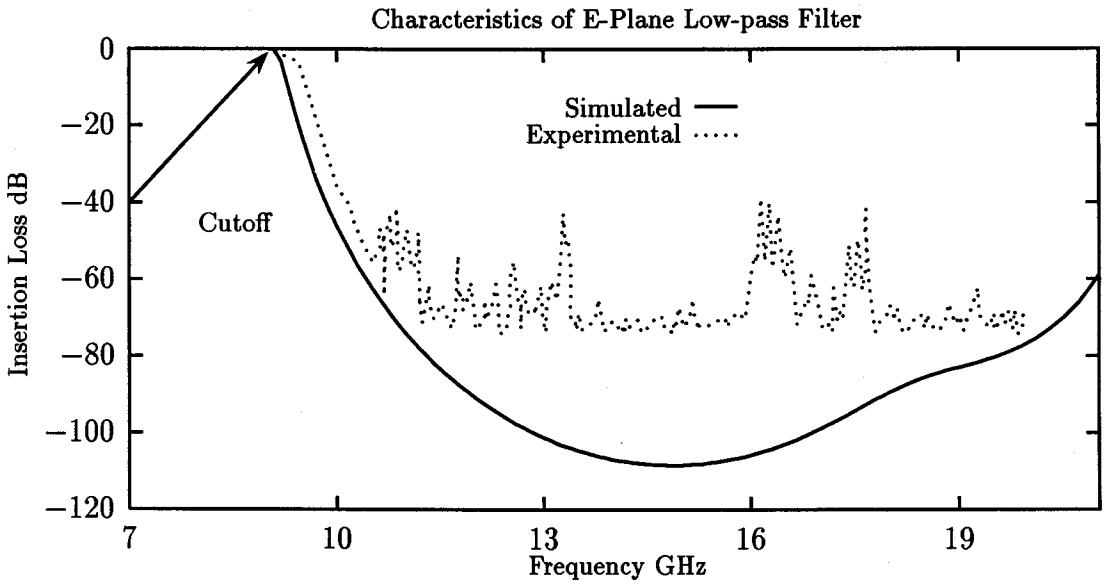

Figure 5.5: Comparison of simulated and experimental insertion loss

Table 5.4: Dimensions of the filter (mm)

Waveguide dimensions: a = 28.4988 b = 7.112		
No.	Iris width (w)	Resonator Length (l)
1	4.365	9.157
2	2.149	7.321
3	1.333	6.309
4	1.100	5.966
5	1.037	5.888
Thickness of all the irises: 2.54		

Thus the analysis computer program developed based on the analysis method for analysing E-plane and H-plane types of waveguide filter structures is verified in this section. The following sections present a few examples of waveguide filters designed using the computer aided design method developed in this thesis.

5.3 Design Examples

5.3.1 H-plane Bandpass Filter

In this section waveguide bandpass filter structures with H-plane discontinuities are designed. The specifications are as follows:

- Waveguide dimensions = 22.86 x 10.16 Iris thickness = 2
- Bandwidth = 10.0 to 10.2 GHz
- Isolation Bandwidth Factor = 2.5
- Isolation = 30 dB
- Passband Return Loss = 16 dB
- Passband ripple = 0.1 dB

H-plane uniform corrugated waveguide bandpass filter

One of the simplest realizations of bandpass filters using waveguide are uniform corrugated waveguide bandpass filters (see Figure 4.4). The dimensions of the filter are calculated from the synthesis method described in chapter 4 and is given in Table 5.5. The analyzed response of the filter is shown in Figure 5.3.1.

An excellent agreement with the desired frequency response is achieved. The parameter which is most difficult to achieve is the return loss in the passband. But the desired passband return loss is also achieved with very good accuracy. The stopband performance characteristics of the filter is shown in Figure 5.7.

Table 5.5: Dimensions of the H-plane uniform corrugated waveguide bandpass filter (mm)

Uniform height = 10.16	
Iris width (w)	Resonator length (l)
10.055	16.933
6.206	18.365
5.790	-

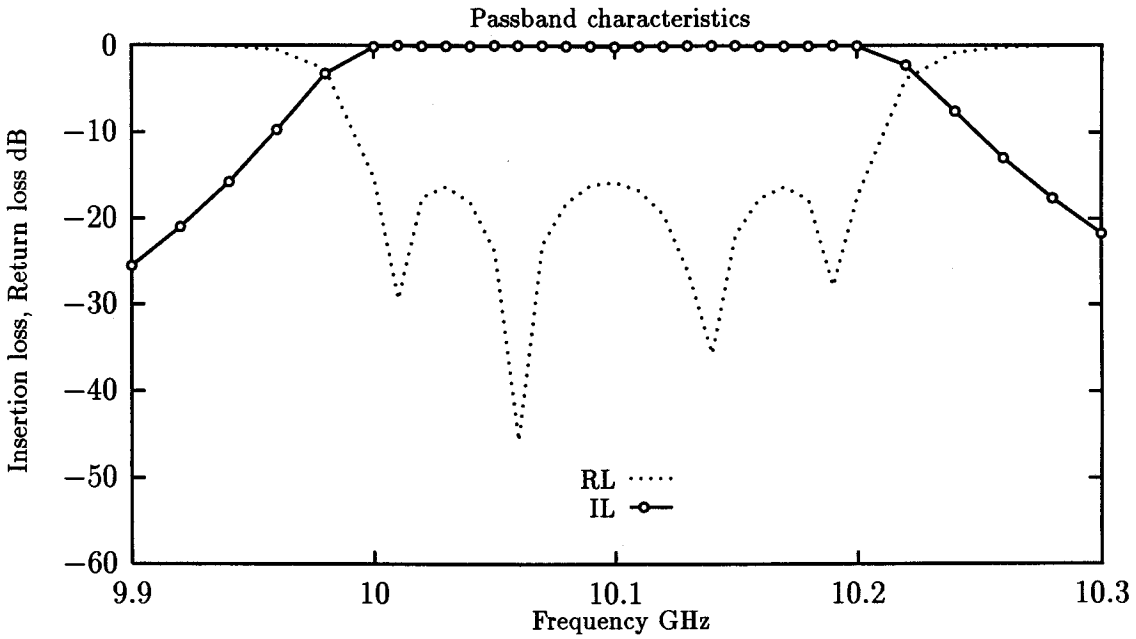

Figure 5.6: Performance characteristics of the uniform bandpass filter

The presence of spurious harmonics in the stopband is highly undesirable. Due to harmonics, it can be observed that the signal is passed without any attenuation at around 16.5 GHz. In recent years, much effort has been devoted to the study of design of bandpass filters with improved stopband performance. Several solutions

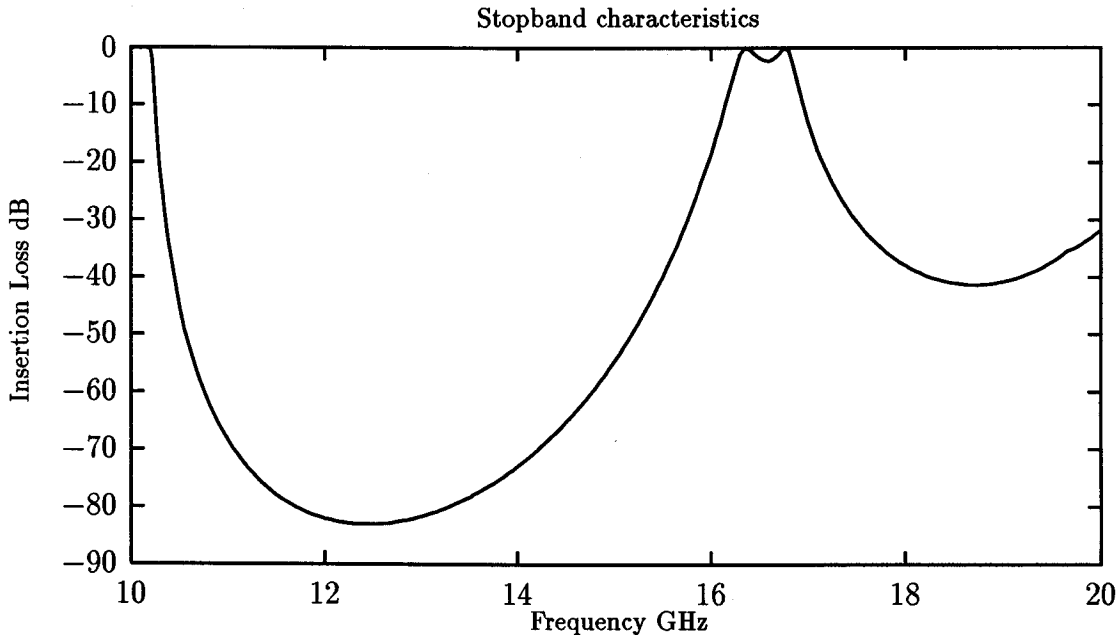

Figure 5.7: Stopband characteristics of the uniform bandpass filter

have been proposed.

- The cutoff frequency of the fundamental mode within the filter resonators may be suitably reduced by increasing the waveguide width.
- Using resonators of different cutoff frequency. This is achieved by employing sections of rectangular waveguide in which all the waveguide sections are resonant at the same fundamental frequency. However, due to different guide wavelengths in the different sections, all the sections are not simultaneously resonant at any higher frequency, resulting in an improved stopband attenuation.

Design for improvement in the stopband is investigated and the following few sections present the design for alleviating the problem of very low attenuation in the stopband.

H-plane bandpass filters with improved stopband performance

With the same specifications used for designing the uniform corrugated waveguide H-plane bandpass filter in the previous section, the structure shown in Figure 5.8 is designed. The filter dimensions obtained from the synthesis method are given in Table 5.6. The structure is a symmetric waveguide filter.

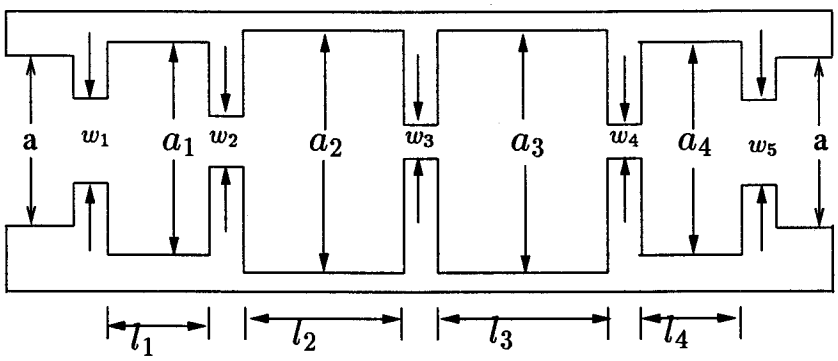

Figure 5.8: Tapered corrugated waveguide bandpass filter

Table 5.6: Dimensions of the tapered corrugated waveguide bandpass filter (mm)

Cosine Tapering		
Iris width (w)	Resonator length (l)	waveguide width (a)
10.227	15.463	27.06
6.410	16.179	29.65
6.033	-	-

Figure 5.9 shows the comparison of stopband characteristics between the uniform and cosine tapering filters designed. The harmonic which appears at 16.5 GHz in the uniform case is shifted to 17.5 GHz when tapered corrugated waveguide filter structure with increased width as shown in Figure 5.8 is used. The resonator length is also smaller in comparison with the resonator length obtained for a uniform waveguide

structure. This decreases the overall length. However, one drawback of this type of filters is the bandwidth of the filter increases when the width of the waveguide, used for realizing the resonators, is increased.

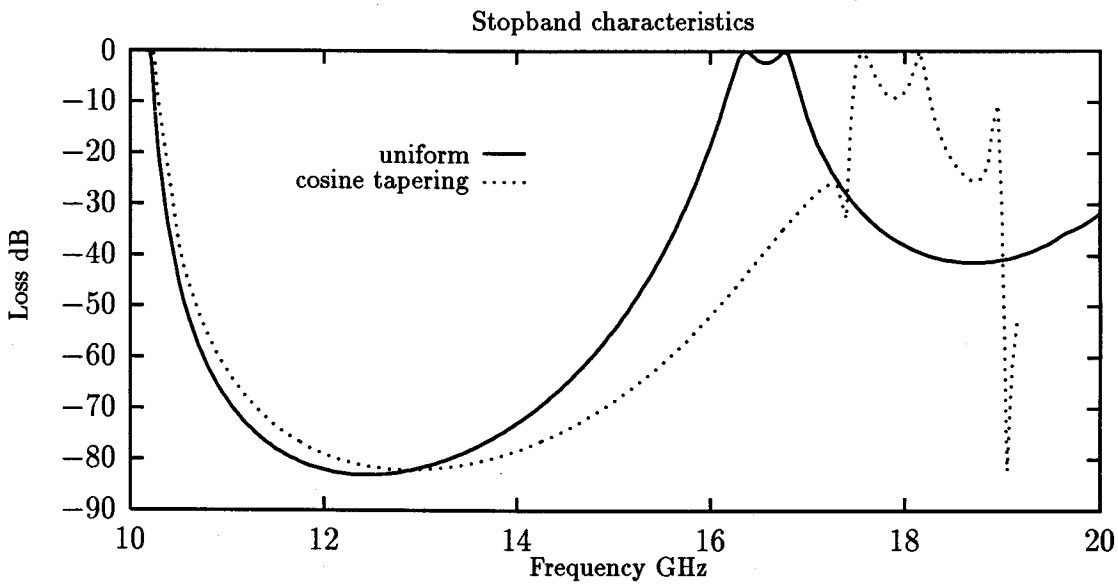

Figure 5.9: Comparison of stopband characteristics

An optimum tapering profile can be obtained by repeated synthesis and analysis with slightly modified required performance to remove all the discrepancies between the simulated and actual required performance. Optimization method can also be used to obtain a satisfactory performance. However, satisfactory results are obtained with direct synthesis method making the optimization method redundant. This reduces the computational time for the complete design process considerably.

Another structure is formed by making the waveguide widths of the resonator sections all equal to 25 mm while the input and output waveguides of the filter structure are 22.86 mm wide. The filter dimensions obtained from the synthesis method are given in Table 5.7.

Table 5.7: Dimensions of the filter for 25mm *through* tapering (mm)

25mm *through* Tapering	
Iris width (w)	Resonator length (l)
10.145	16.034
6.278	17.366
5.856	-

Figure 5.10 shows the comparison of stopband characteristics between the uniform and 25 mm *through* tapering filters designed.

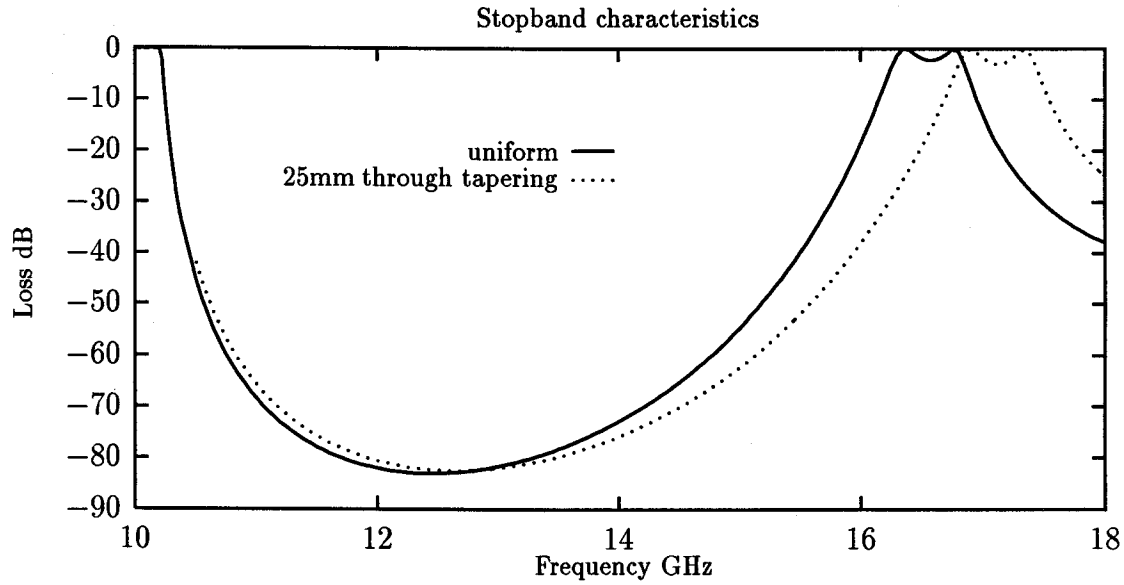

Figure 5.10: Comparison of stopband characteristics

The harmonic which appears at 16.5 GHz in the uniform case is shifted to 17.0 GHz. The passband characteristics of 25mm through tapering is shown in Figure 5.11. There is a slight increase in bandwidth. Since the overall performance characteristics

of the filter is satisfactory no optimization is required.

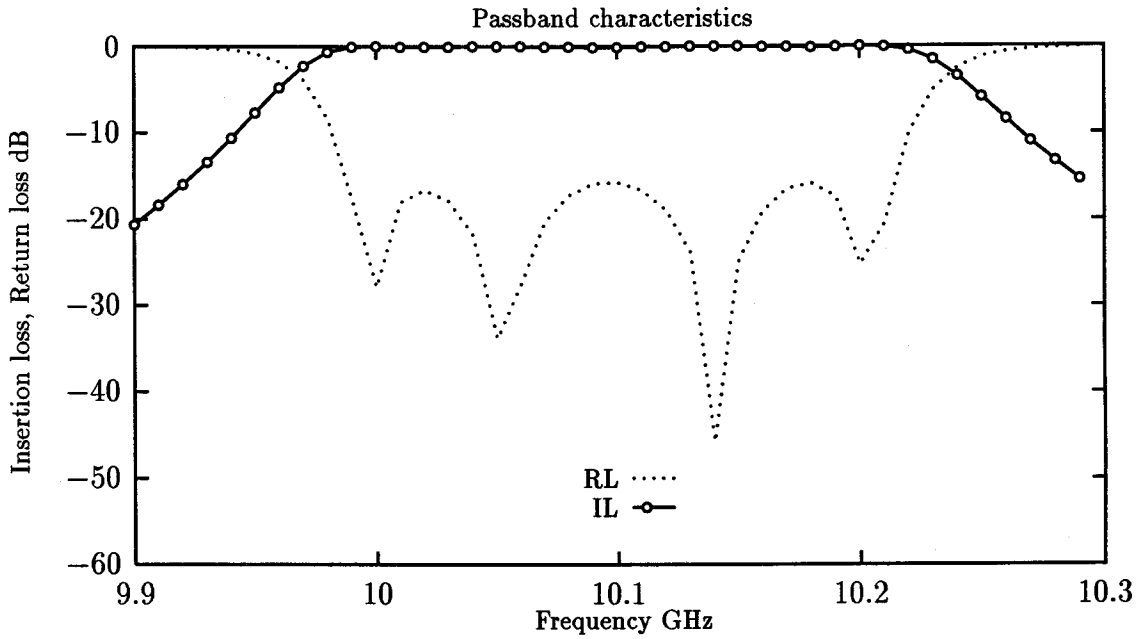

Figure 5.11: Passband characteristics of 25mm through tapering

Instead of increasing the waveguide width in all the resonators following a particular tapering profile, a structure with resonators having widths which are larger and smaller as compared with the input and output waveguide width is studied in this section. Same design parameters are used and the dimensions of the filter are given in Table 5.8.

Another structure with 25 and 20 mixed tapering is designed and the dimensions are given in Table 5.9.

Figure 5.12 shows the comparison of stopband characteristics between the uniform and the filters designed with 25 and 19 tapering and 25 and 20 mixed tapering. 25 and 19 tapering structure stopband response is very poor while the 25 and 20 tapering structure stopband response is extended compared with the uniform tapering. There

Table 5.8: Dimensions of the filter for 25mm and 19mm mixed tapering (mm)

25mm and 19mm mixed Tapering		
Iris width (w)	Resonator length (l)	waveguide width (a)
10.145	16.041	25
6.222	22.383	19
5.768	-	-

Table 5.9: Dimensions of the filter for 25mm and 20mm mixed tapering (mm)

25mm and 20mm mixed Tapering		
Iris width (w)	Resonator length (l)	waveguide width (a)
9.950	19.219	20
6.208	17.376	25
5.856	-	-

are number of possible tapering profiles which would give satisfactory performance in both passband and stopband frequency response characteristics. Hence, several designing and redesigning may be required to obtain a filter with a satisfactory performance. The passband characteristics of 25 and 20 mixed tapering structure is shown in Figure 5.13.

5.3.2 E-plane Bandpass Filter

E-plane bandpass filters are known mainly as variants of the more commonly used H-plane bandpass filters designed in the previous section. The resonator lengths of H-plane filters are some what shorter than 180^o electrical length, while those of E-plane filters are longer. E-plane filters possess an advantage in that bandwidth remains fairly constant when the filter is tuned over a wide frequency range and the

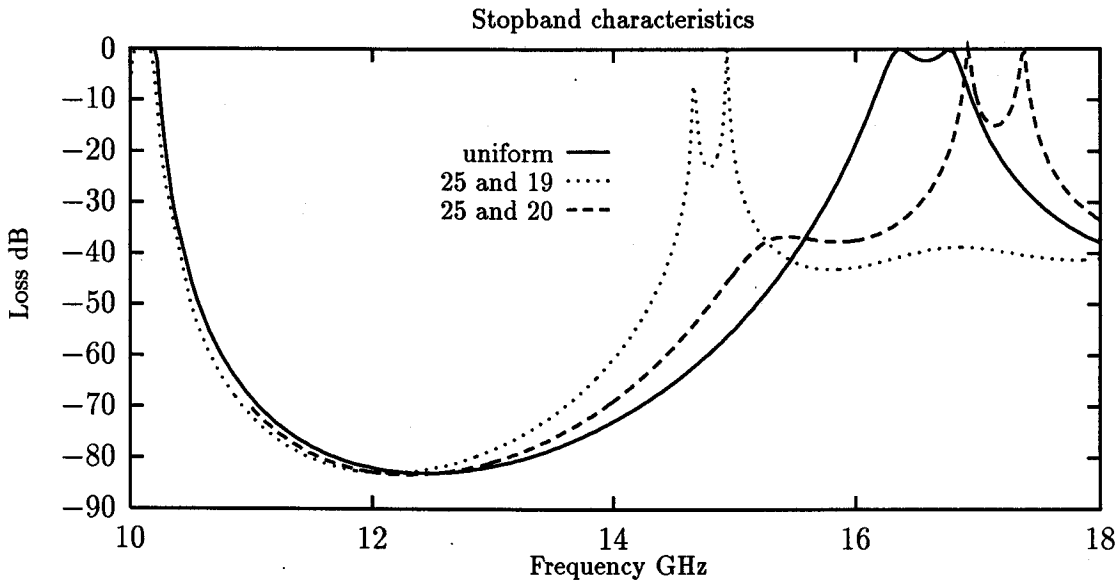

Figure 5.12: Comparison of stopband characteristics

rate of cutoff is more rapid above the upper cutoff frequency band edge compared with the lower frequency band edge, the reverse situation holding for H-plane filters. The disadvantages of E-plane filters are that it is difficult to produce large capacitive susceptances in waveguides, so that narrow-band filters are not feasible, and the harmonic rejection capability is a little better than that of the H-plane version since the resonators are long, and so possess harmonic passbands at comparatively low frequencies above the main pass-band. The problem of harmonic passbands can be alleviated by tapered corrugated waveguide E-plane filter structures. Tapering in the E-plane raises the cutoff frequencies of the higher order TE_{1n} modes and hence a slight improvement in the stopband can be achieved.

E-plane bandpass filters with the following specifications are designed in this section.

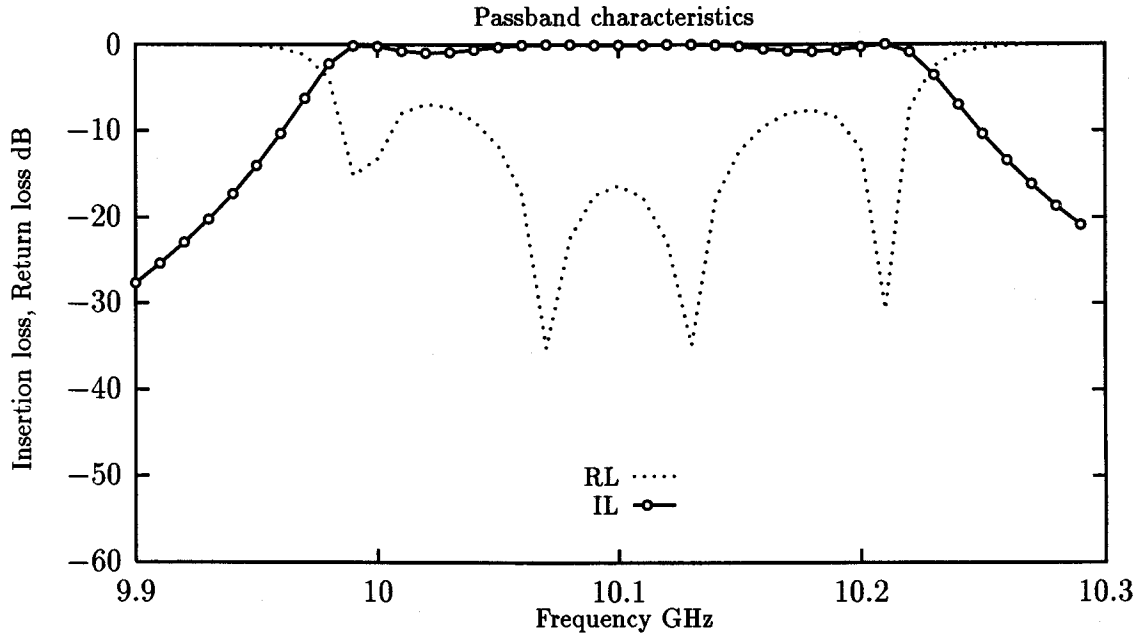

Figure 5.13: Passband characteristics of 25 and 20 mixed tapering filter

- Waveguide dimensions = 22.86 x 10.16 Iris thickness = 3
- Bandwidth = 9.0 to 9.5 GHz
- Isolation Bandwidth Factor = 2
- Isolation = 35 dB
- Passband Return Loss = 16 dB
- Passband ripple = 0.1 dB

E-plane uniform corrugated waveguide bandpass filter

E-plane uniform corrugated waveguide bandpass filter (see Figure 4.3) is designed for the above specifications and the dimensions of the filter obtained from the synthesis method are shown in Table 5.10. The number of resonators in the filter is equal to 5

and the filter is a symmetric filter ie. ($w_1 = w_6$, $w_2 = w_5$, $w_3 = w_4$, $l_1 = l_5$ and $l_2 = l_4$). Figure 5.14 shows the passband frequency response characteristics of the designed

Table 5.10: Dimensions of the E-plane uniform corrugated waveguide bandpass filter (mm)

Uniform width = 22.86	
Iris width (w)	Resonator length (l)
2.652	26.355
0.746	24.659
0.545	24.447

uniform corrugated waveguide filter. The lower cutoff frequency is exactly predicted while the upper cutoff frequency is slightly less than the desired 9.5 GHz. Hence, the bandwidth predicted is slightly lower than the required bandwidth. Figure 5.15 shows the stopband frequency response characteristics of the uniform corrugated waveguide filter. The rate of cutoff is more rapid above the upper cutoff frequency band edge but it has harmonics present in the stopband at low frequencies above the main passband. For instance at frequency 11 GHz, the insertion loss is reduced to -100 dB which is highly desirable. However, there are harmonic spikes at 14 GHz and 19 GHz which are highly undesirable. At 14 GHz, the signal is passed without any attenuation. At frequencies which are around 1.5 times the center frequency of the bandpass filter, the performance is greatly disrupted. This disruption arises because higher order modes have different guide wavelengths than that for the TE_{10} mode. As a result the pass and stop bands for energy in the higher order modes occur at quite different frequencies than for the TE_{10} mode.

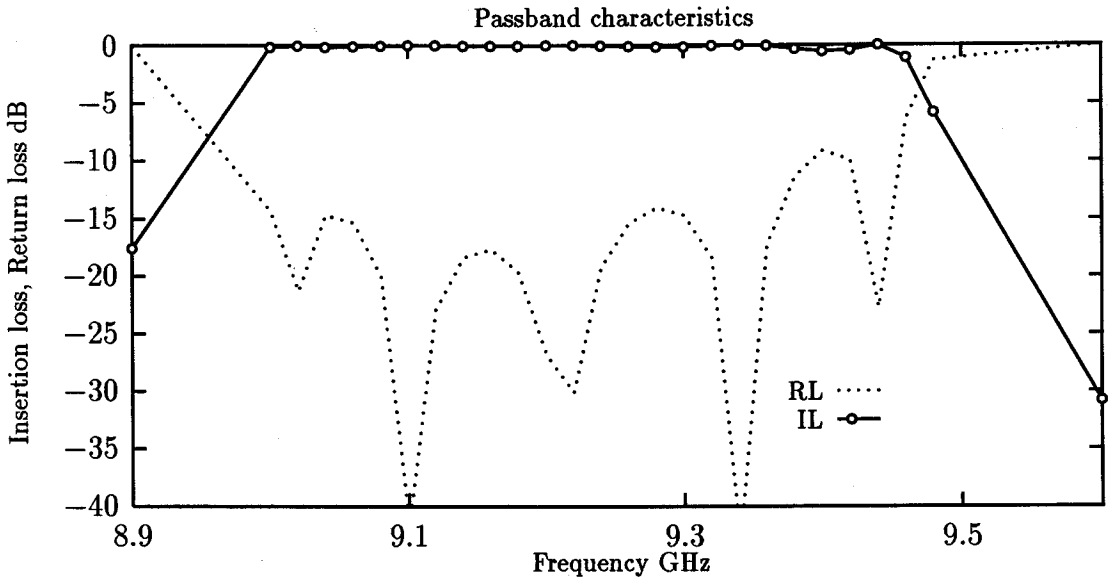

Figure 5.14: Passband characteristics of the E-plane uniform corrugated waveguide bandpass filter

Tapered corrugated waveguide bandpass filter

The uniform corrugated waveguide bandpass filter structure given in the previous section has additional pass bands at frequencies which are multiples of their first passband frequencies. To alleviate the problem of harmonics present in the stopband of the E-plane uniform corrugated waveguide bandpass filters, E-plane tapered corrugated waveguide bandpass filter structures are designed. Reducing the height of the narrow dimension of the waveguide in the filter structure would move up the cutoff frequencies of the TE_{1n} produced, which would result in an improvement of the stopband. However, substantial improvement in the stopband attenuation requires the tapering in the H-plane or adding transmission line stubs which would eliminate the harmonic spikes. These structures are highly complex to be analysed.

In this section, the design of E-plane tapered corrugated waveguide filters and

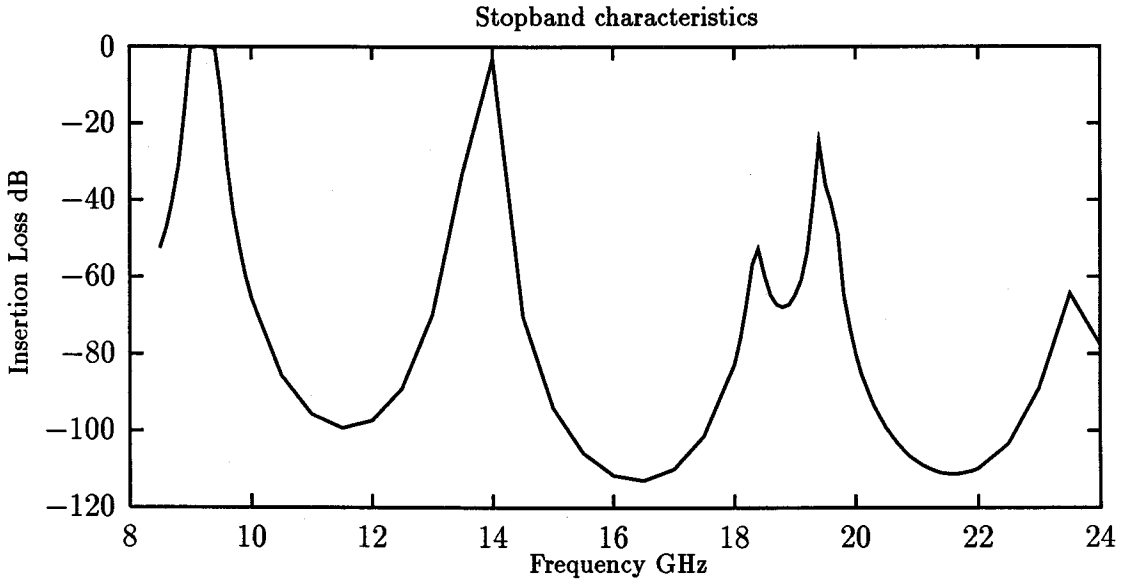

Figure 5.15: Stopband characteristics of an E-plane uniform corrugated waveguide bandpass fitler

the effect of tapering on the frequency response of the filter is studied. Tapered corrugated waveguide bandpass filters with the same specifications used for designing the uniform corrugated waveguide filter in the previous section is designed. Two filters with cosine tapering profile are designed and the dimensions of the filter are given in Tables 5.11 and 5.12.

Figure 5.16 shows the comparison of stopband characteristics between the uniform and cosine tapered (minimum height = 5mm) and (minimum height = 6mm) corrugated waveguide bandpass filters. It can be seen, that at 14 GHz there is an improvement in the insertion loss for both the cases of tapered filters when compared with the uniform corrugated filter. For the case of (minimum height = 6mm) central section height, about -20 dB attenuation is achieved while for the case of (minimum height = 5mm) central section height, about -30dB attenuation is achieved. Hence, decreasing the central section height results in better stop band attenuation. How-

Table 5.11: Dimensions of the E-plane cosine tapered (minimum height = 5mm) corrugated waveguide bandpass filter (mm)

Cosine Tapering		
Iris width (w)	Resonator length (l)	waveguide height (b)
2.961	26.646	7.58
0.625	25.512	5.691
0.323	25.257	5.0

Table 5.12: Dimensions of the E-plane cosine tapered (minimum height = 6mm) corrugated waveguide bandpass filter (mm)

Cosine Tapering		
Iris width (w)	Resonator length (l)	waveguide height (b)
2.810	26.570	8.08
0.645	25.276	6.557
0.363	25.006	6.0

ever, the harmonic spike which appears at around 19 GHz is not improved by the tapering.

Figure 5.17 shows the passband characteristics of E-plane cosine tapered (5mm) corrugated waveguide filter. The passband response is very poor and there is a substantial shrinkage in bandwidth compared with the desired bandwidth. Hence, there is a tradeoff between the passband and stopband. To get a satisfactory frequency response, several design and redesigns might be required. An Optimization method may also be applied for obtaining a satisfactory performance. However, sometimes it would not be possible to obtain a filter with good passband and stopband characteristics by using a tapered structure alone. The next section deals with a filter designed by optimization to improve the passband of the tapered corrugated waveguide filter

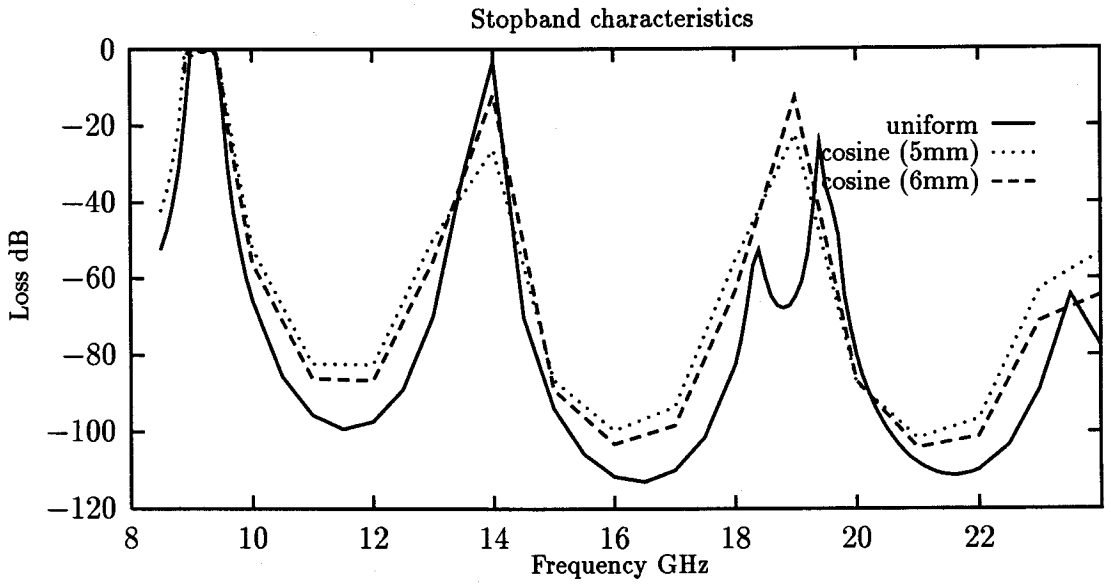

Figure 5.16: Comparison of stopband characteristics between uniform and tapered corrugated waveguide filters

designed in this section.

E-plane Optimized Filter

The dimensions of the filter are adjusted in order to satisfy the design specification using the optimization procedure and are shown in Table 5.13. It is interesting to note that the resonator lengths are increased and decreased in contrary to the common method of tapering in which the resonator lengths are either only increased or decreased based on a tapering profile.

Figure 5.18 shows the passband characteristics of the optimized bandpass filter. The desired bandwidth is achieved and the return loss is also achieved according to the design specification.

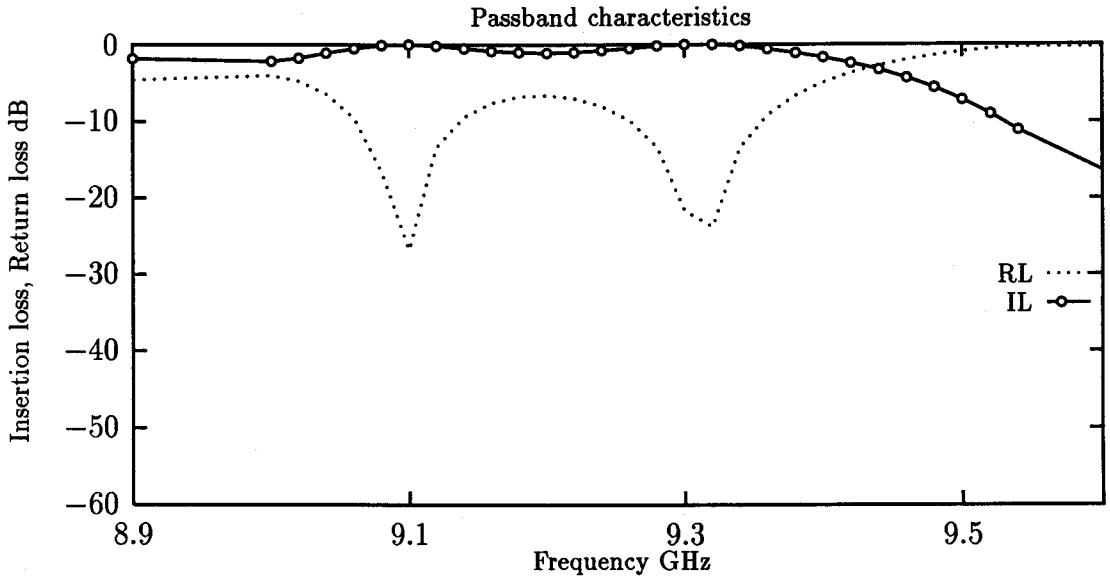

Figure 5.17: Passband characteristics of E-plane cosine (5mm) tapered corrugated waveguide bandpass filter

Table 5.13: Dimensions of the E-plane optimized tapered corrugated waveguide bandpass filter (mm)

Optimized values		
Iris width (w)	Resonator length (l)	waveguide height (b)
3.095	26.947	9.722
0.832	26.820	5.357
1.124	22.950	7.140

The stopband characteristics is shown in Figure 5.19. However, the stopband characteristics are not satisfactory. This clearly indicates that there is a tradeoff between the passband and stopband characteristics. But, there are number of designs possible by varying the tapering profile and by designing, optimizing and redesigning so that a satisfactory filter may be designed. The design process, however, is slow

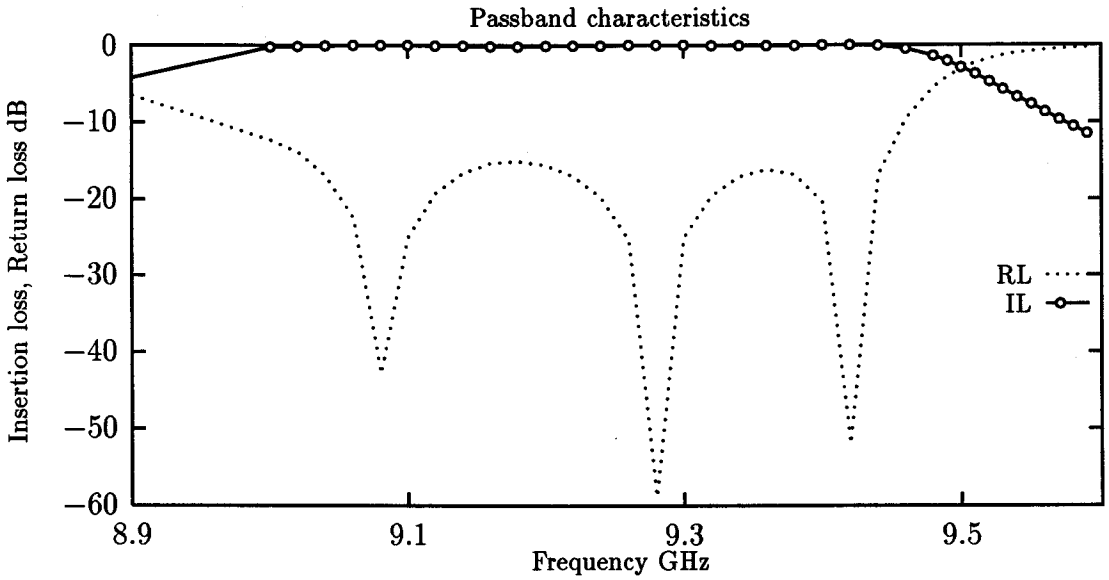

Figure 5.18: Passband characteristics of E-plane optimized tapered corrugated waveguide bandpass filter

but considerably faster and less laborious compared with experimentally tuning the filters with tuning screws.

5.3.3 E-plane Low-pass Filter

Low-pass filters, as mentioned in the previous chapter, are used for rejection of spurious harmonics from transmitters. In this section, an E-plane low-pass filter design is presented. Design of an uniform corrugated waveguide low-pass filter is presented first, followed by the design of a tapered corrugated waveguide low-pass filter. Three tapering profiles are used in the tapered corrugated waveguide case, namely, cosine, square and exponential profile. The specifications of the filter designed are as follows:

- Waveguide dimensions = 15.799 x 7.899 Iris thickness = 0.508
- Cutoff frequency = 20 GHz

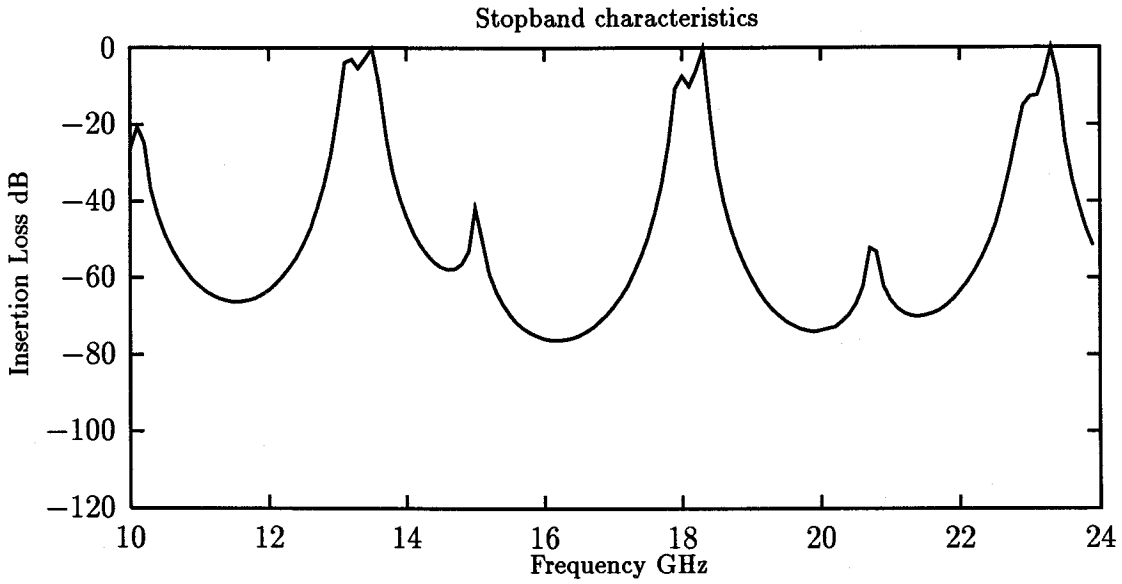

Figure 5.19: Stopband characteristics of an E-plane optimized tapered corrugated waveguide bandpass filter

- Fractional bandwidth = 0.7
- Isolation Bandwidth Factor = 2.5
- Isolation = 50 dB
- Passband Return Loss = 26 dB
- Passband ripple = 0.01 dB

E-plane uniform corrugated waveguide low-pass filter

A very simple type of harmonic rejection filter is a cascade of thick capacitive irises closely spaced in a uniform waveguide, as shown in Figure 4.6. The dimensions of the filter designed with the above specifications is shown in Table 5.14. The filter is uniform in the broad dimension, however, longitudinal slots as in the case of a waffle-

iron filter [4] can be incorporated. These filters are highly complicated to design both theoretically and mechanically. However, these filter structures can be avoided in many applications by using tapered corrugated waveguide filters. The waveguide narrow dimension is tapered in the tapered corrugated waveguide filters to move up the cutoff frequency of the TE_{1n} modes to obtain a better stopband compared with the uniform corrugated filters.

Table 5.14: Dimensions of the E-plane uniform corrugated waveguide low-pass filter (mm)

Uniform width = 15.799, height = 7.899	
Iris width (w)	Resonator length (l)
5.1183	4.057
3.352	3.352
2.412	2.952
2.063	2.84

Figure 5.20 shows the passband characteristics of E-plane uniform corrugated waveguide low-pass filter. The cutoff frequency of 20 GHz is predicted exactly and the return loss of 26 dB is also achieved. The passband response of the filter closely compares with the required specifications. Figure 5.21 shows the stopband characteristics of E-plane uniform corrugated waveguide low-pass filter.

From the stopband characteristics, it can be observed that the insertion loss is very high at frequencies above cutoff frequency. For instance, the insertion loss is -116 dB at 30 GHz. This gives an excellent isolation at frequencies above the cutoff frequency. However, there is a harmonic spike at a frequency of 39 GHz at which the insertion loss is very low. Hence, the range of this filter is restricted to 38 GHz which is a severe limitation considering the fact that especially these filters find applications in rejection of spurious harmonics from transmitters.

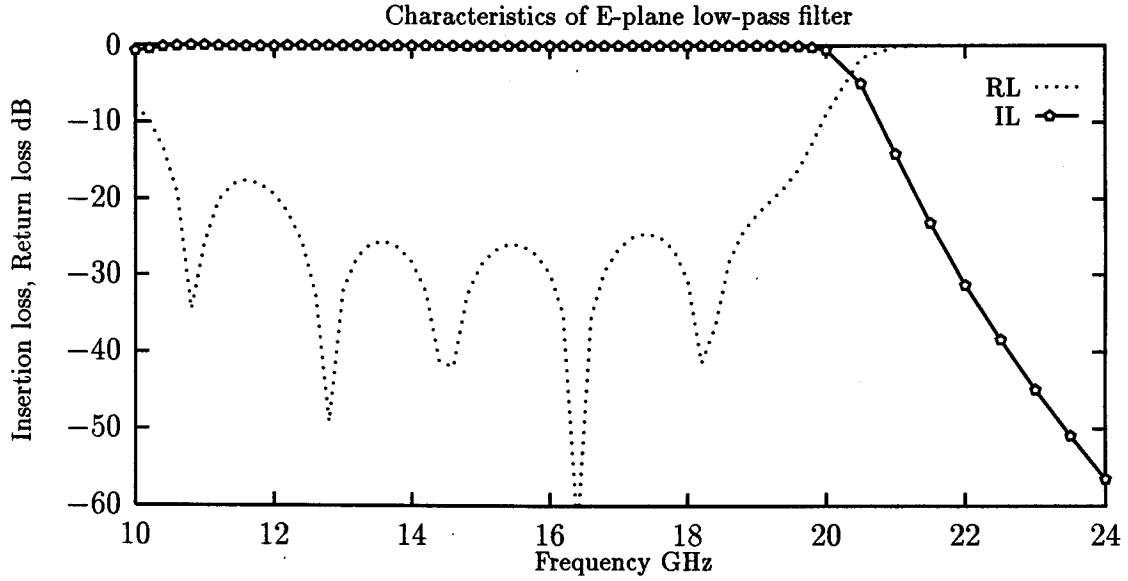

Figure 5.20: Passband characteristics of E-plane uniform corrugated waveguide low-pass filter

E-plane tapered corrugated waveguide low-pass filter

As mentioned in the previous section, the operation of the uniform corrugated waveguide filter designed is restricted to up to 38 GHz due to the harmonic spike at 39 GHz. In order to improve the stopband characteristics tapered corrugated waveguide filter structures are used. The narrow dimension of the waveguide is reduced to 5mm and filters following three different profiles, namely, cosine, square and exponential are designed in this section. The dimensions of tapered corrugated waveguide filters are shown in Tables 5.15, 5.16 and 5.17. Figures 5.22, 5.23 and 5.24 shows the passband characteristics of tapered corrugated waveguide low-pass filter with cosine, square and exponential tapering profile respectively. It is seen that the cutoff frequency obtained is in the higher side in all the three cases. The return loss achieved is in good agreement with the required return loss from the specifications.

Table 5.15: Dimensions of the E-plane cosine tapered (minimum height = 5mm) corrugated waveguide low-pass filter (mm)

Cosine tapering		
Iris width (w)	Resonator length (l)	waveguide height (b)
4.740	4.413	6.790
2.381	3.441	5.849
1.295	3.021	5.221
0.935	2.865	5.0

Table 5.16: Dimensions of the E-plane square tapered (minimum height = 5mm) corrugated waveguide low-pass filter (mm)

Square tapering		
Iris width (w)	Resonator length (l)	waveguide height (b)
4.695	4.493	6.631
2.297	3.448	5.725
1.262	3.016	5.181
0.929	2.865	5.0

Table 5.17: Dimensions of the E-plane exponential tapered (minimum height = 5mm) corrugated waveguide low-pass filter (mm)

Exponential tapering		
Iris width (w)	Resonator length (l)	waveguide height (b)
4.818	4.323	7.046
2.581	3.403	6.285
1.465	2.982	5.606
0.997	2.865	5.0

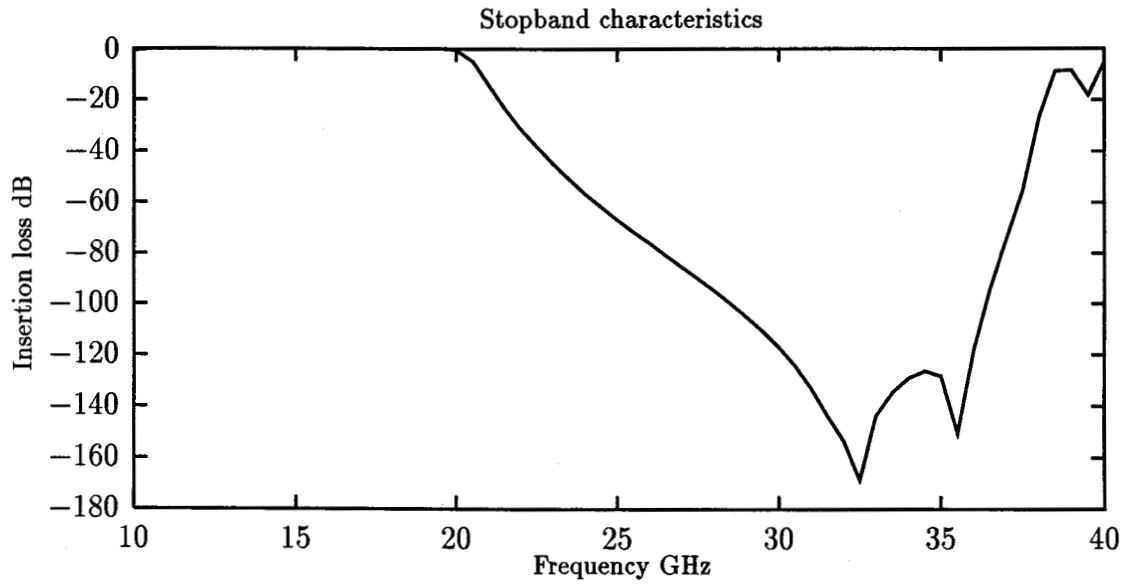

Figure 5.21: Stopband characteristics of an E-plane uniform corrugated waveguide low-pass filter

Figure 5.25 shows the comparison of stopband characteristics of all the three tapered corrugated waveguide filters with the uniform corrugated waveguide filter designed in the previous section. In all the three cases, the harmonic which appears at 39 GHz in the uniform corrugated waveguide filter case is eliminated and the attenuation at 39 GHz for all the three cases is close to -60 dB. It can be observed that all the three cases follow closely with each other. However, the maximum attenuation is restricted to approximately -70 dB compared with the uniform case where -160 dB attenuation is achieved. But, the -70 dB attenuation satisfies the required -50 dB isolation at the stopband frequencies. Hence, the tapered corrugated waveguide low-pass filters have very good stopband characteristics and can be used for operation up to 45 GHz without any spurious harmonic passband.

In order to see the effect of tapering on the frequency response of the filter, two other structures with a minimum height of 4mm and 3mm are designed and the

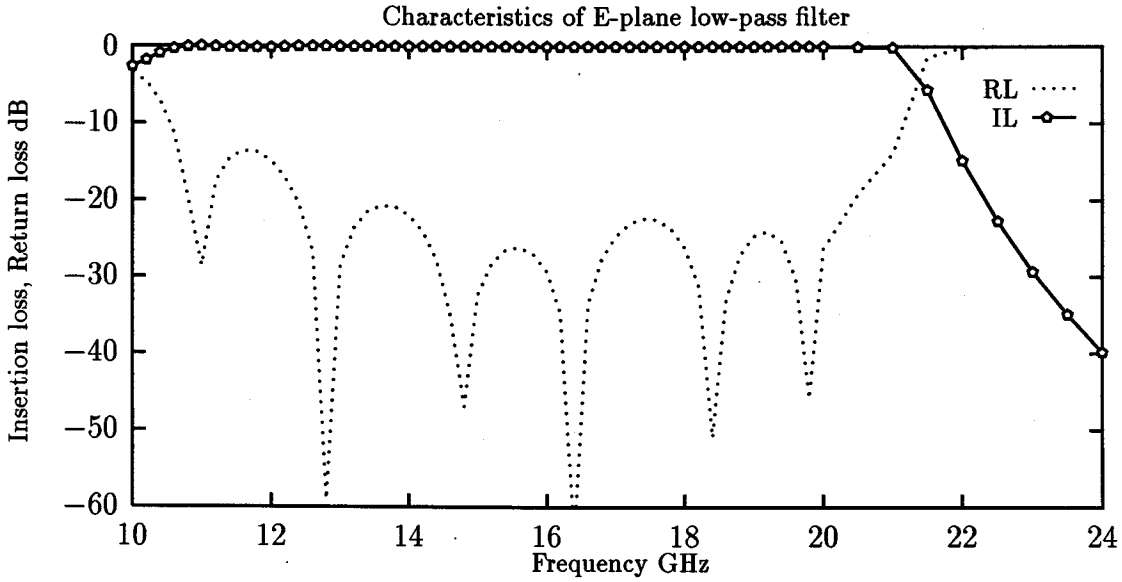

Figure 5.22: Passband characteristics of E-plane tapered corrugated waveguide low-pass filter: cosine tapering (5mm) profile

dimensions obtained from the synthesis computer program are shown in Tables 5.18 and 5.19. Figure 5.26 shows the comparison of stopband characteristics for different minimum height 5mm, 4mm and 3mm for cosine tapering profile. It can be seen that reducing the minimum height increases the insertion loss slightly at the frequencies where the harmonics occur for the uniform corrugated waveguide filters. At 39 GHz, the insertion loss of -58 dB, -58 dB and -53 dB is obtained for minimum height 5mm, 4mm and 3mm, respectively.

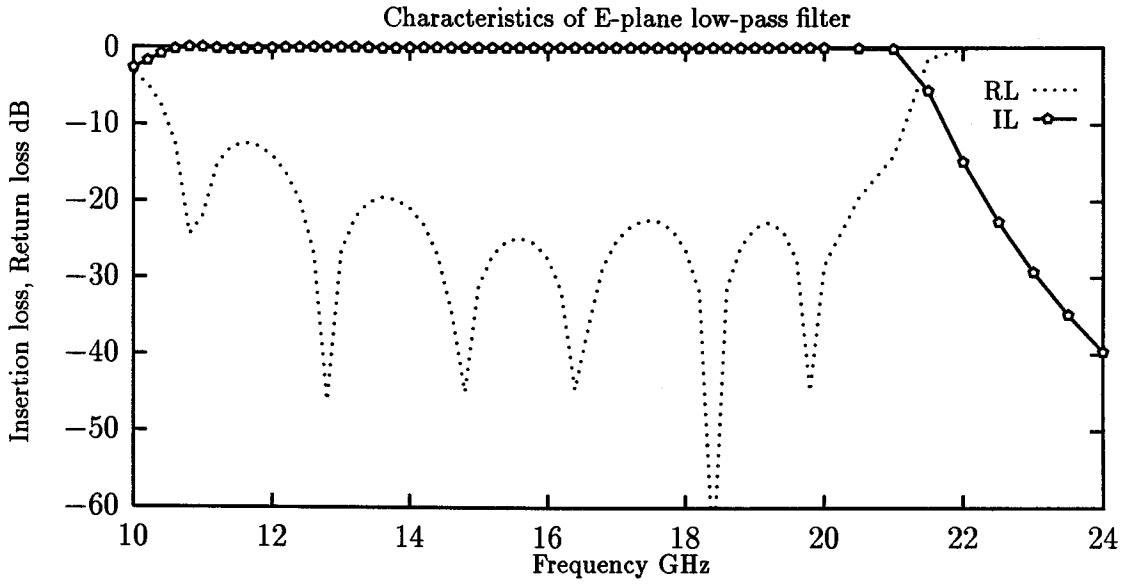

Figure 5.23: Passband characteristics of E-plane tapered corrugated waveguide low-pass filter: square tapering profile

Table 5.18: Dimensions of the E-plane cosine tapered (minimum height = 4mm) corrugated waveguide low-pass filter (mm)

Cosine tapering = 4mm		
Iris width (w)	Resonator length (l)	waveguide height (b)
4.639	4.539	6.407
2.075	3.486	5.142
0.983	3.06	4.297
0.653	2.876	4.0

Figures 5.27 and 5.28 shows the passband characteristics of the low-pass filter structures with cosine tapering of minimum height 4mm and 3mm, respectively.

The passband response for both the type of filters are satisfactory. The cutoff

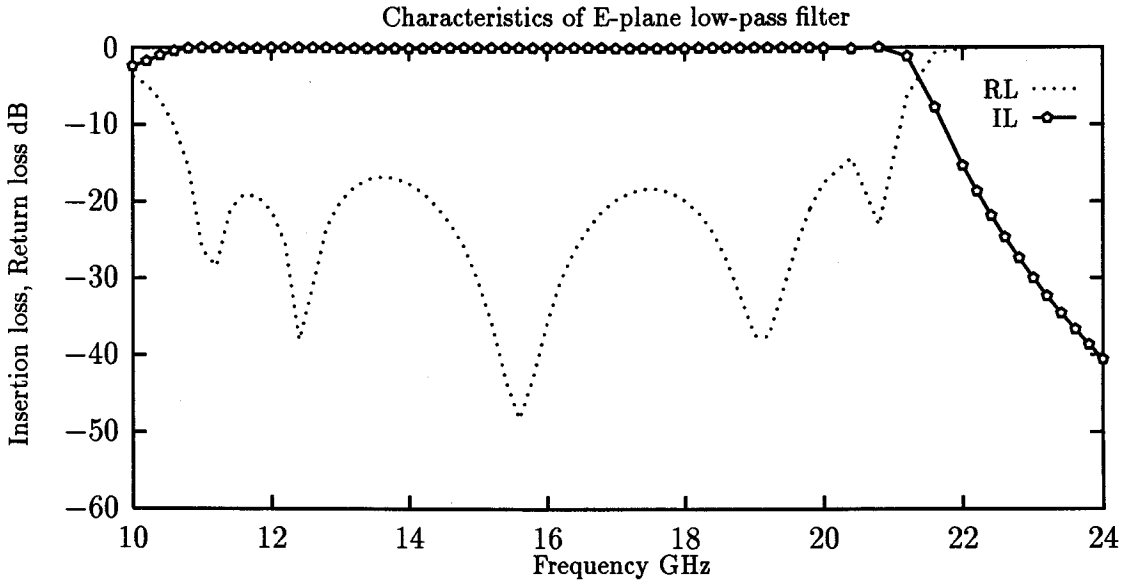

Figure 5.24: Passband characteristics of E-plane tapered corrugated waveguide low-pass filter: exponential tapering profile

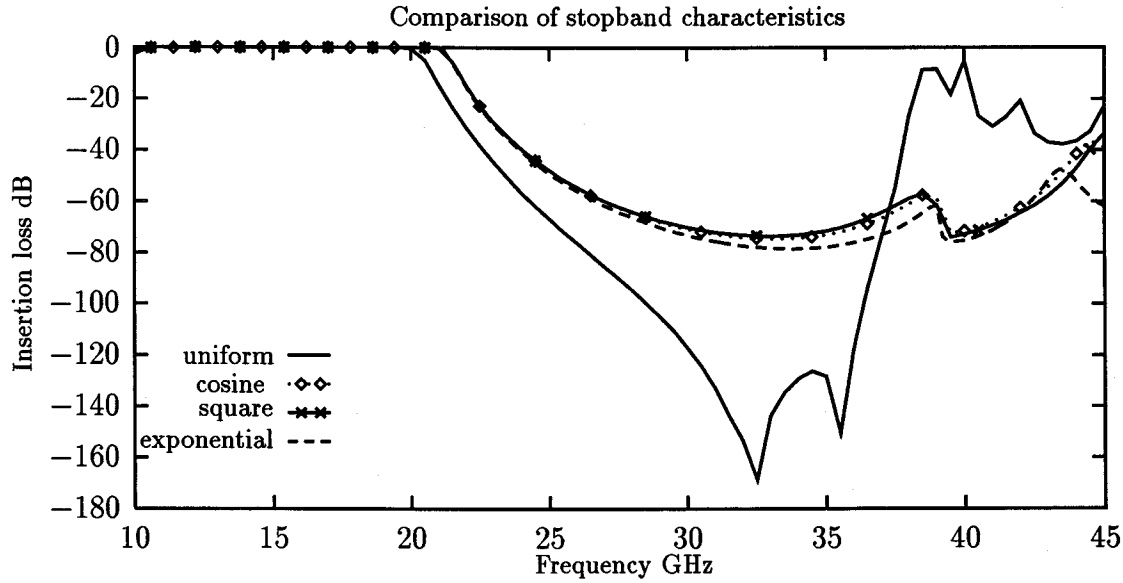

Figure 5.25: Comparison of stopband characteristics

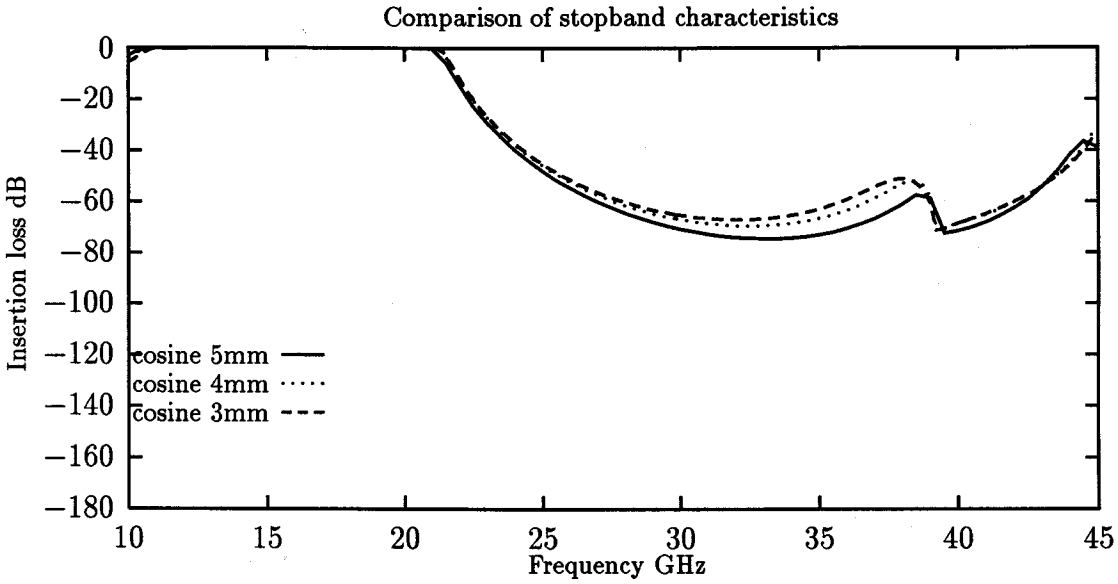

Figure 5.26: Comparison of stopband characteristics

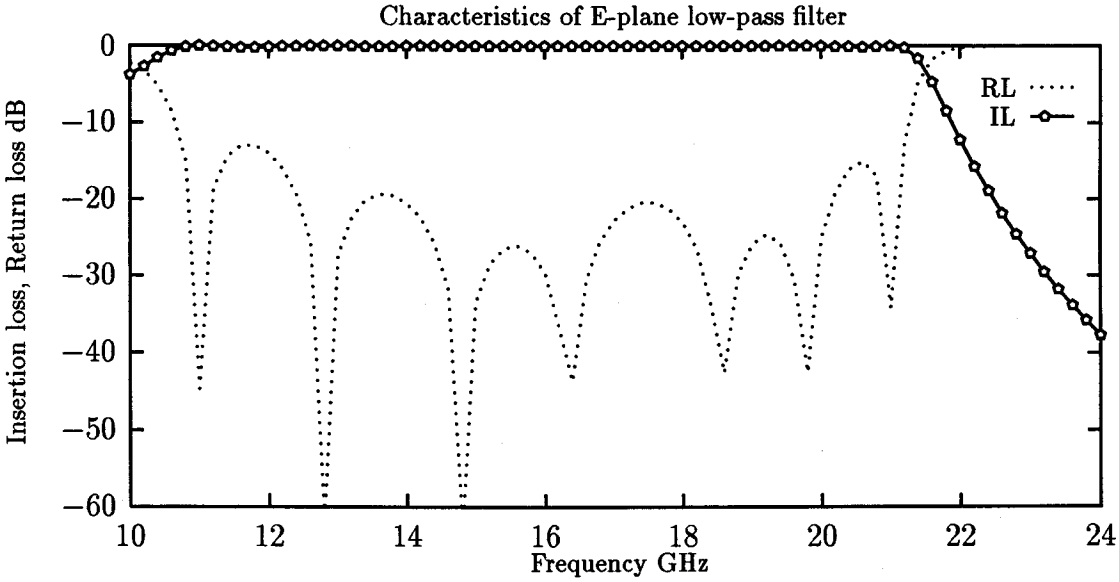

Figure 5.27: Passband characteristics of E-plane tapered corrugated waveguide low-pass filter: cosine tapering (4mm) profile

Table 5.19: Dimensions of the E-plane cosine tapered (minimum height = 3mm) corrugated waveguide low-pass filter (mm)

Cosine tapering = 3mm		
Iris width (w)	Resonator length (l)	waveguide height (b)
4.567	4.667	6.024
1.784	3.532	4.435
0.714	3.115	3.373
0.415	2.892	0.761

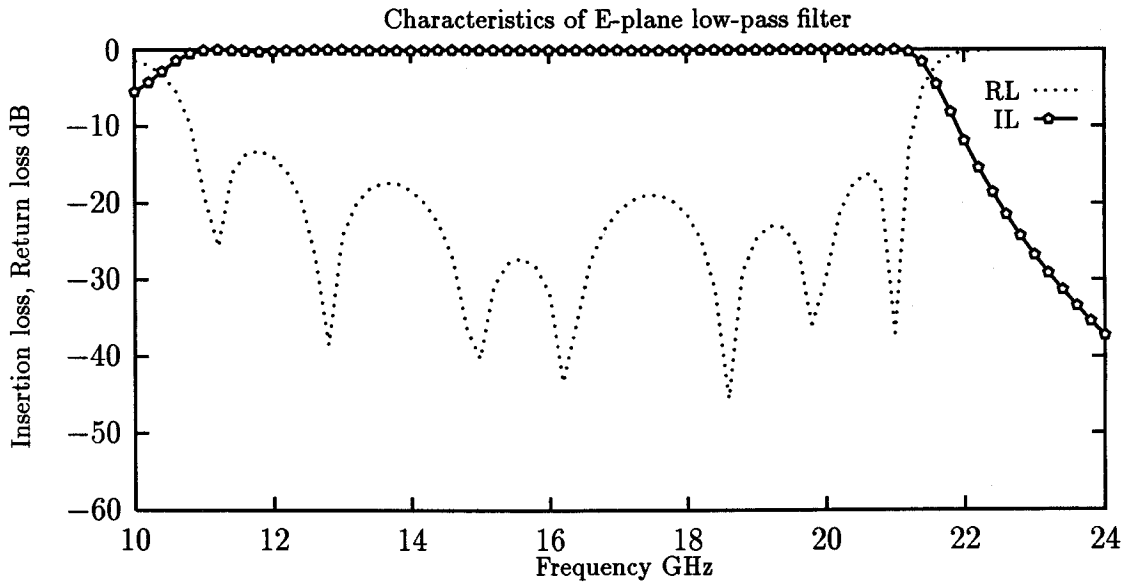

Figure 5.28: Passband characteristics of E-plane tapered corrugated waveguide low-pass filter: cosine tapering (3mm) profile

frequency is higher than the required 20 GHz for both the cases. However, this does not adversely affect the filter performance because the two main concerns in the design of a low-pass filter are the passband performance below 20 GHz and the stopband performance, especially the harmonic passband at 39 GHz.

5.4 Summary

In this chapter, the results obtained from the computer aided design methods developed in this thesis are presented. The verification of the computer program based on the analysis method developed is presented. Results obtained are in good agreement with experimental and published results. The synthesis method verification is done by synthesising several band-pass and low-pass filters. Simple structures, like E-plane uniform corrugated waveguide low-pass, bandpass filters and H-plane uniform corrugated waveguide bandpass filters are designed and the frequency response characteristics of these filters are simulated. In order to improve the stopband performance characteristics of the uniform corrugated waveguide filters, tapered corrugated waveguide filters are designed and the effect of tapering is studied. Tapering improved the stopband performance of the H-plane bandpass filters but it is very difficult to get a satisfactory performance in both the stopband and passband for the case of E-plane bandpass filters, even after applying optimization procedure. Tapering improved the stopband performance of the low-pass filters and a satisfactory performance of the filter is achieved. Thus, the computer aided design methods and computer programs developed are verified. The design process in the mass production of filters can be greatly simplified with the use of the computer aided design method. Compact, efficient and tuning screw free filters can be designed without undergoing the difficulties of using complex empirical formulae and following a trial and error based method in the design procedure.

Chapter 6

Conclusions

The objectives of this thesis as stated previously in chapter 1 are:

1. To develop efficient computer aided design and analysis methods for the design of a large variety of existing waveguide filters without requiring post-production tuning

2. To use the developed methods to design new efficient and compact waveguide filter structures

In accordance with the above objectives, the conclusions of the thesis are as follows:

A complete computer aided design method is developed for the design of waveguide filters. Several designs of existing structures like the H-plane uniform corrugated waveguide bandpass filters, E-plane uniform corrugated waveguide bandpass and low-pass filters are designed. The stopband performance characteristics of these structures contains passband harmonics which are undesirable.

R. Levy [9] proposed E-plane tapered corrugated waveguide low-pass filters for better stopband performance compared with the existing uniform corrugated structures. But the design procedure used empirical formulae for the solution of the S-matrix of the discontinuities present in the waveguide filter structure. In this thesis, the

computer aided design method based on the mode matching method and distributed transmission line theory is used for the design of tapered corrugated waveguide structures. The computer aided design method not only eliminates the complex empirical formulae used by Levy method but also provides better performing compact filters. The filters designed following Levy method require post-production tuning. But the filter designed with the computer aided design method developed in this thesis does not require post-production tuning for most of the filter structures to obtain the required performance.

E-plane tapered corrugated waveguide low-pass filters are designed successfully with satisfactory performance in both the passband and stopband. The filter structures designed would perform satisfactorily without tuning screws for most of the cases except for filter with very small waveguide dimensions.

Bandpass filters with both E-plane and H-plane tapered corrugated waveguide structures are designed to improve the stopband performance characteristics. With E-plane bandpass filters satisfactory passband and stopband performance is not achieved and the optimization procedure could not be of much help in this regard. On the other hand, very good results are obtained for H-plane bandpass filters. Hence, it can be concluded that the E-plane bandpass filters are very good for a single mode operation with excellent stopband isolation for frequencies less than twice the center frequency of the filter. The stopband isolation at higher frequencies than the upper cutoff frequency of the H-plane bandpass filter is not as good as that of E-plane bandpass filters. However, the stopband harmonics are eliminated in H-plane bandpass filters by tapering and allowing the H-plane filters to be used with systems having more than single mode of operation. Some of the structures, namely the mixed tapering and the tapering profile with increasing widths in the H-plane bandpass filters are **entirely new structures** and these structures provide very good performance in both the passband and stopband without any optimization.

The distributed transmission line theory [21] with K-inverter design for synthesising filter structures proved to be very efficient and accurate. The usual procedure of following the optimization to design filters with desired performance is not required. This reduced the computational time for the entire design procedure considerably. The mode matching method used in the design procedure proved to be a powerful, efficient and highly accurate numerical method for solving waveguide discontinuity problems which are inherently present in several microwave passive structures using waveguides.

6.1 Limitations

Some of the limitations of the computer aided design method developed in this thesis are as follows:

- Only symmetrical filters are designed.
- The filters designed are considered to be lossless.
- Practical difficulties like the misalignment of the filter with the input and output flanges and the machine tolerance are not included in the computer aided design method.

6.2 Future work

- By slight modifications of the developed methods asymmetric filters can be designed.
- The thickness of iris is kept constant in the filter structures considered in this thesis. The effect of varying the iris thickness can be studied.

- Designing of filter structures with both E and H-plane waveguide discontinuities can be studied.
- Several other waveguide discontinuity problems like T-junction, bends can be solved by the mode matching method and new structures utilizing these discontinuities can be designed and studied.
- More complex structures like multiplexers can be designed by following similar procedures described in this thesis.
- A better optimization method for final fine tuning of the filters can be developed.
- Waveguide filters with different dielectric filling can be studied.

Bibliography

[1] R.E.Collin, *Foundations for microwave engineering.* McGraw-Hill Book Company, 1966.

[2] I. Bahl and P. Bhartia, *Microwave Solid State Circuit Design.* John Wiley and Sons, 1988.

[3] M. E. V. Valkenburg, *Network Analysis.* Prentice-Hall, Inc. Englewood Cliffs, N.J., 1964.

[4] G. L. Matthaei, L. Young, and E. M. T. Jones, *Microwave Filters, Impedance Matching Networks, and Coupling structures.* McGraw-Hill, New York, 1964.

[5] R. Levy and S. B. Cohn, "A History of Microwave Filter Research, Design, and Development," *IEEE Trans. on Microwave Theory and Techniques*, Vol. MTT-32, pp. 1055–1065, Sep. 1984.

[6] J. Uher, J. Bornemann, and U. Rosenberg, *Waveguide Components for Antenna Feed Systems: Theory and CAD.* Artech House, 1993.

[7] N. Marcuvitz, *Waveguide Handbook.* Artech House, 1991.

[8] R. Levy, "A Generalized Design Technique for Practical Distributed Reciprocal Ladder Networks," *IEEE Trans. on Microwave Theory and Techniques*, Vol. MTT-21, pp. 519–524, Aug. 1973.

[9] R. Levy, "Tapered Corrugated Waveguide Low-Pass Filters," *IEEE Trans. on Microwave Theory and Techniques*, Vol. MTT-21, pp. 525–532, Aug. 1973.

[10] A. Wexler, "Computation of Electromagnetic Fields," *IEEE Trans. on Microwave Theory and Techniques*, Vol. MTT-17, pp. 416–439, Aug. 1969.

[11] T. Itoh, ed., *Numerical Techniques for Microwave and Millimeter-Wave Passive Structures.* John Wiley and Sons, 1989.

[12] R. Safavi-Naini and R. H. Macphie, "Scattering at Rectangular-to-Rectangular Waveguide Junctions," *IEEE Trans. on Microwave Theory and Techniques*, Vol. MTT-30, pp. 2060–2063, Nov. 1982.

[13] J. Bornemann and R. Vahldieck, "Characterization of a Class of Waveguide Discontinuities Using a Modified TE^{x}_{mn} Mode Approach," *IEEE Trans. on Microwave Theory and Techniques*, Vol. MTT-38, pp. 1816–1821, Dec. 1990.

[14] Z. Shen and R. H. Macphie, "An Improved Modal Expansion Method for Two Cascaded Junctions and Its Application to Waveguide Filters," *IEEE Trans. on Microwave Theory and Techniques*, Vol. MTT-43, pp. 2719–2723, Dec. 1995.

[15] K.C.Gupta, *Computer-Aided Microwave Circuit Design.* Department of Electrical and Computer Engineering, University of Colorado, Boulder, Fall 1995.

[16] J. A. Dobrowolski, *Introduction to Computer Methods for Microwave Circuit Analysis and Design.* McGraw-Hill, New York, 1991.

[17] Y.C.Shih and K.G.Gray, "Convergence of numerical solutions of step-type waveguide discontinuity problems by modal analysis," *IEEE MTT-S Int. Microwave Symp. Dig.*, pp. 233–235, 1983.

[18] S. W. Lee, W. R. Jones, and J. J. Campbell, "Convergence of Numerical Solutions of Iris-Type Discontinuity problems," *IEEE Trans. on Microwave Theory and Techniques*, Vol. MTT-19, pp. 528–536, June 1971.

[19] L. Q. Bui, D. Ball, and T. Itoh, "Broad-Band Millimeter-Wave E-Plane Bandpass Filters," *IEEE Trans. on Microwave Theory and Techniques*, Vol. MTT-32, pp. 1655–1658, Dec. 1984.

[20] W. H. Press, S. A. Teukolsky, W. T. Vetterling, and B. P. Flannery, *Numerical Recipes in C.* Cambridge University Press, 1992.

[21] J.D.Rhodes, *Theory of Electrical Filters.* John Wiley and Sons, 1976.

[22] K. J. Button, ed., *Topics in Millimeter Wave Technology.* Vol. 1, Academic Press, Inc., 1988.

[23] M. Guglielmi, G. Gheri, M. Calamia, and G. Pelosi, "Rigorous Multimode Network Numerical Representation of Inductive Step," *IEEE Trans. on Microwave Theory and Techniques*, Vol. MTT-42, pp. 317–325, Feb. 1994.

[24] C. Lawrence, J. L. Zhou, and A. L. Tits, *A C Code for Solving (Large Scale) Considered Nonlinear (Minimax) Optimization Problems, Generating Iterates Satisfying All Inequality Constraints.* Electrical Engineering Department and Institute for Systems Research, University of Maryland, College Park, MD 20742, 1996.

Appendix A

Computer program for synthesis of E-plane low-pass filter

```
/*****************************************************************
This is the source code for the synthesis of E-plane low-pass filters
It is divided into three files.
The file input1.cc is used for inputting the various performance
parameters required for the synthesis. It also calculates the
K-values for the low-pass filter using Rhode's formulae.
The file jenstep.cc
finds the S matrix of the E-plane step and iris discontinuity using
the mode matching method. The file Eplow_kval.cc is a root seeking
routine which matches the
K(Impedance Inverter) values from mode matching method and Rhode's
method.
*****************************************************************/
#include <iostream.h>
#include <iomanip.h>
#include <math.h>
#include <assert.h>
#include "header.h"
#include "input1.cc"
#include "jenstep.cc"
#include "Eplow_kval.cc"

main()
{
  float a_width, b_h[20],d_h,i_th, freq;
  float fc,bw,ibw,idb,rl,fac,amc,amo,amd,f1,f2,df;
  int N,nf,law;
```

```
  filter_in(fc,bw,ibw,idb,rl,fac,nf);
  rect_in(a_width,b_h,i_th,N,law);
   d_h = 0.1 * b_h[1];
  freq = fc;
  amc = 2*a_width;
  amo = VEL/freq;
  amd = amo/sqrt(1-pow((amo/amc),2));
  cout <<"Computing the iris widths and resonator
            lengths..Please wait"<<endl;
  iris_synth(a_width,b_h,i_th,freq,nf,N,amd);

  return 0;

}
/*****************************************************************
 input1.cc
*****************************************************************/
#include <iostream.h>
#include <Complex.h>

int n;
void filter_in(float &fc ,float &bw,float &ibw,float &idb,
float &rl,float &fac,int &nf)
{
float t,alpha,epsilon,temp1,temp2,y,Y[20],f1,f2,f3,J,R;
int r;
cout << " Enter the Cutoff frequencyin Ghz="<<endl;
 cin >> fc;
cout <<endl <<" Enter the Fractional Bandwidth=";
  cin >>bw;
cout << endl<<" Enter Isolation  Bandwidth Factor =";
  cin >>ibw;
cout << endl<<" Enter Isolation in dB  =";
  cin >>idb;
cout << endl<<" Enter Passband return loss  in dB  =";
  cin >>rl;
cout << endl<<"Enter Passband ripple level in dB = ";
  cin >>R;
t = (idb + rl + 6)/(20*log10(sqrt(ibw*ibw-1) + ibw));
nf = (int)ceil(t);
 n = nf;
cout << endl<<" Required filter order = "<<nf <<endl;
```

```
/* Rhode's Formulae */
alpha = sin(M_PI*bw/4);
t     = pow(10,0.1*R);
epsilon = sqrt(t - 1);
temp1 = 1/epsilon;
temp2 = asinh(temp1)/nf;
y = sinh(temp2);
Y[0] = 1;
Y[nf+1] = 1;

for(r=1;r<nf+1;r++)
{
f1 = 2*sin((2*r-1)*M_PI/(2*nf))/(y*alpha);
f2 = (y*y +pow(sin(r*M_PI/nf),2))/sin((2*r+1)*M_PI/(2*nf));
f3 = (y*y +pow(sin((r-1)*M_PI/nf),2))/sin((2*r-3)*M_PI/(2*nf));
Y[r] = f1 - (alpha/(4*y))*(f2+f3);
}

for(r=0;r<nf+1;r++)
{
J = sqrt(y*y+pow(sin(r*M_PI/nf),2))/y;
K[r] = J/sqrt(Y[r]*Y[r+1]);
cout <<"K["<<r<<"]= "<<K[r]<<"\n";
}}
/* Inputting the  waveguide dimensions */
void rect_in(float &a_width,float b_h[],float &i_th,
 int &N ,int &law)
{
 float bc,b,alpha,bm;
 int i,k;
cout << endl<<"Enter the width of the waveguide a= ";
 cin >> a_width;
k = (n+1)/2;
 cout << endl<<"Enter the  height of the  waveguide b= ";
 cin >> b ;
 cout << endl<<"Enter the  height of the central section bc= ";
 cin >> bc ;
  b_h[0] = b_h[n+1] = b;
 cout << "Enter the Height Distribution law" << endl;
 cout << "1 for Square Law" << endl;
 cout << "2 for Cosine Law" << endl;
```

```
cout << "3 for Exponential Law" << endl;
cout << "4 for Linear Law" << endl;
cout << "5 for Uniform Law" << endl;
cin >> law;
switch(law){
case 1:
    // square law
       alpha = (b-bc)/(k*k);
       for(i=1;i<=k;i++){
         bm = alpha*(i-k)*(i-k)+bc;
          b_h[i] = b_h[n-i+1] = bm;
         }
        break;
case 2:
    // cosine law
     for(i=1;i<=k;i++){
        bm = b - (b-bc)*sin(i*M_PI/(n+1));
        b_h[i] = b_h[n-i+1] = bm;
       }
        break;
 case 3:
     // exponential law
      alpha = -log(b/bc)/(n+1);
      for(i=1;i<=k;i++){
         bm = b * exp(2.0*alpha*i);
         b_h[i] = b_h[n-i+1] = bm;
        }
        break;
 case 4:
      // Linear law
       alpha = (b-bc)/n;
       for(i=1;i<=k;i++){
        bm = b -alpha*i;
        b_h[i] = b_h[n-i+1] = bm;
      }
       break;
  case 5:
      // Uniform law
        bm = b ;
      for(i=1;i<=k;i++)
       b_h[i] = b_h[n-i+1] = bm;
       break;
```

```
        default:
         cout << "Enter a number 1-5 please,BYE" << endl;
        exit(0);
    }
if (n % 2 == 0) k = n/2+1;
 k = n/2;
 for(i=1;i<=n/2+1;i++)
  {
   z[i] = b_h[i]/b_h[i-1]; //Normalizing the impedance
   z[n-i+1] = z[i];
  }
  z[0] = z[n+1] = 1;
for(i=0;i<=n;i++)
  {
  K[i] /= sqrt(z[i]*z[i+1]);
   }
for(i=0;i<=n+1;i++){
cout << "b["<<i<<"]="<<b_h[i]<<endl;
cout << "z["<<i<<"]="<<z[i]<<endl;
}
for(i=0;i<=n;i++)
cout << "K["<<i<<"]="<<K[i]<<endl;
cout << endl<<"Enter the  Iris thickness of the waveguide i_th= ";
cin >>i_th;
 cout <<endl<<"Enter the value of  N the no of modes";
 cout << "N= "<<endl;
 cin >> N ;
}

void anal_in(float &f1,float &f2,float &df)
{
cout << endl<<" Enter the Lower Frequency bound in Ghz";
cin >> f1;
cout << endl<<" Enter the Upper Frequency bound in Ghz";
cin >> f2;
cout << endl<<" Enter the frequency step  in Ghz";
cin >> df;
}
```

```
/*****************************************************************
****************jenstep.cc *****************
Mode Matching Method to characterize the E-plane iris discontinuity
*****************************************************************/

void iris(float a_width,float b_h,float d_h,float b_h1, float i_th,
float freq, int &N,Complex &S11I,Complex &S12I,
Complex &S21I, Complex &S22I)
 {
        int M;
        Complex en;
        M = 10;
        N  = (int)(b_h/d_h)*M;
        if(N > 40){ M =5;
        N  = (int)(b_h/d_h)*M;
        }
        array L(M,M),*I,*Y2,*U1;
        array *S22R,*S21R,*S12R,*S11R,*S11F,*S12F,*S21F,*S22F;
        array *S11T,*S12T,*S21T,*S22T;
        Y2 = new array(M,M);
        U1 = new array(M,M);
        S22R = new array(M,M);
        S21R = new array(N,M);
        S12R = new array(M,N);
        S11R = new array(M,M);
        S11F = new array(N,N);
        S12F = new array(N,M);
        S21F = new array(M,N);
        S22F = new array(M,M);
        S11T = new array(N,N);
        S12T = new array(N,N);
        S21T = new array(N,N);
        S22T = new array(N,N);

        jenstep(a_width,b_h,d_h,freq,N,M,S11F,S12F,S21F,S22F);
        jenstep(a_width,b_h1,d_h,freq,N,M,S22R,S21R,S12R,S11R);

        *Y2 = jenY(a_width,d_h,freq,M);
        I = new array(M,M);
        for(int i=0;i<M;i++) (*I)(i,i) = Complex(1,0);
```

```
        en = Complex(0,1.0);
        for(int i=0;i<M;i++)
            {
            if(imag((*Y2)(i,i)) == 0 )
           L(i,i) = exp(-en*(*Y2)(i,i)*i_th);
            else
           L(i,i) = exp(imag((*Y2)(i,i))*i_th);
            }

        *U1 = ~(*I - L*(*S22F)*L*(*S11R));
        *S11T = *S11F + (*S12F)*L*(*S11R)*(*U1)*L*(*S21F);
        *S21T = *S21R*(*U1)*L*(*S21F);
        *S12T = *S12F*L*(*I + (*S11R)*(*U1)*L*(*S22F)*L)*(*S12R);
        *S22T = *S22R + *S21R*(*U1)*L*(*S22F)*L*(*S12R);

        S11I = (*S11T)(0,0);
        S12I = (*S21T)(0,0);
        S21I = (*S12T)(0,0);
        S22I = (*S22T)(0,0);

        delete I;
        delete Y2;
        delete S22R;
        delete S21R;
        delete S12R;
        delete S11R;
        delete S11F;
        delete S12F;
        delete S21F; delete S22F; delete U1;
 }

void abcd(Complex S11, Complex S12, Complex S21, Complex S22,
Complex &A, Complex &B,Complex  &C,Complex  &D,float zn1,
float zn2)

{
   Complex DS,Dr;
   DS = S11*S22-S12*S21;
   Dr = 2*S21*sqrt(zn1*zn2);

   A = (zn1 + zn1*S11-zn1*S22-zn1*DS)/Dr;
   B = (zn1*zn2 + zn1*zn2*S11 + zn1*zn2*S22 +zn1*zn2*DS)/Dr;
```

```
   C = (1 - S11 - S22 + DS)/Dr;
   D = (zn2 - zn2*S11 + zn2*S22 - zn2*DS)/Dr;
}

void jenstep(float c_w,float b_h,float d_h,float freq, int N, int M,
array *S11, array *S12,array *S21, array *S22)
 {
        array H(N,M),*I,*temp;
        int i,j;
        H = jenHmn(c_w,b_h,d_h,N,M,freq);

        temp = new array(N,N);
        I = new array(N,N);
        for(i=0;i<N;i++) (*I)(i,i) = Complex(1,0);
        *temp = ~(H*(!H)+(*I));
        *S11 = (*temp)*(H*(!H)-(*I));
        *S12 = (*temp)*H;
        for(i=0;i<N;i++)
                for(j=0;j<M;j++)
                        (*S12)(i,j) *= Complex(2,0);
        *S21 = (!H)*(*I-(*S11));
        delete I;
        I = new array(M,M);
        for(i=0;i<M;i++) (*I)(i,i) = Complex(1,0);
        *S22 = (*I) - (!H)*(*S12);
        delete temp;
        delete I;
}


array jenHmn(float a_width,float b,float d,int N, int M,float freq)
{
        array h(N,M),Y1(N,N),Y2(M,M); int i,j; float u,v;

        Y1 = jenY(a_width,b,freq,N);
        Y2 = jenY(a_width,d,freq,M);
        h(0,0) = Complex(sqrt(Y2(0,0)/Y1(0,0)*(d/b)));
        for(i=1;i<N;i++)
        {
           for(j=1;j<M;j++)
             {
```

```
            u = 2*M_PI*i/b;
            v = 2*M_PI*j/d;
        h(0,j) = 0;
        h(i,0) = Complex(2*sqrt(2)*sqrt(Y2(0,0)/Y1(i,i))
                  *sin(u*d/2)/(u*sqrt(b*d)));
        if (u == v ) h(i,j) = Complex(2*sqrt(d/b)*sqrt(Y2(j,j)/Y1(i,i)));
        else
        h(i,j) = Complex(sqrt(Y2(j,j)/Y1(i,i))*4*u*cos(M_PI*j)
                  *sin(u*d/2)/((sqrt(b *d)*(u*u - v*v))));
           }}
           return(h);
}

array jenY(float a, float b,float freq,int M)
{
        array y(M,M);
        double k0;
        double gamma;
        int i,j;

        k0 = 2*M_PI*freq/VEL;
        for(i=0;i<M;i++)
        {
                gamma = (pow(k0,2)-pow(M_PI/a,2) - pow(2*i*M_PI/b,2));
                if(gamma > 0)
                y(i,i) = Complex(sqrt(gamma),0);
                else
                y(i,i) = Complex(0,-sqrt(-gamma));
        }

        return(y);
}

/*****************************************************************
Root seeking routine. K-values from Mode matching method
and the Rhode's formulae are matched.
*****************************************************************/

#define UNUSED (-1.11e30)
#define MAXIT 60
#define acc 0.0001
```

```
void iris_synth(float a_width,float b_h[],float i_th,float freq,
                int nf,int N,float amd)
{
 double km,d_h,pha,phb;
 float b_h1,b_h2,d_hl,d_hu;
 float ph1[30],ph2[30],k_calc[30];
 int i;
 float f1, f2, df;
for(i=0;i<=nf/2;i++)
{
   b_h1 = b_h[i];
   d_hl = 0.02*b_h[i];
   b_h2 = b_h[i+1];
   d_hu = pow(0.85,i)*b_h[i];

   solve(a_width,b_h1,d_hl,d_hu,b_h2,i_th,freq,N,i,d_h,pha,phb,km);

   ph1[i]  = pha;
   ph2[i]  = phb;
   ph1[nf-i]=ph1[i];
   ph2[nf-i]=ph2[i];
   k_calc[i] = km;
   k_calc[nf-i] = k_calc[i];
   w[i] = d_h;
   w[nf-i] = d_h;
}

  for(i=0;i<=nf/2;i++)
   L[i] = amd*(ph2[i]+ph1[i+1]+ M_PI/8)/(2*M_PI);
  for(i=0;i<=nf/2;i++)
   L[nf-i-1] = L[i];
  for(i=0;i<=nf;i++)
   {
   cout <<"W["<<i+1<<"]= "<<w[i]<<"\t";
   cout <<"KI["<<i<<"]= "<<k_calc[i]<<"\t";
   cout <<"K["<<i<<"]= "<<K[i]<<"\n"<<endl;
   }
  for(i=0;i<nf;i++)
   cout <<"\n L["<<i+1<<"]= "<<L[i]<<"\n"<<endl;
}

void  K_values(const Complex S11I,const Complex S12I,const
```

```
Complex S21I, const Complex S22I,double &k1,double &ph1,
double &ph2, int i)
{
  k1  = sqrt((1-abs(S11I))/(1+abs(S11I)));
  k1  = k1/sqrt(z[i+1]*z[i]);
  ph1 = arg(S11I)/2 + M_PI/2 ;
  ph2 = arg(S22I)/2 + M_PI/2 ;
}

void solve(float a_width,float b_h1,float d_h1,float d_h2,float b_h2,
float i_th,float freq,int N,int i,double &d_h,double &ph1,
double &ph2,double &km)
{
   double err1, err2,dk, errm, k1, k2,temp;
   double dxold,rts,dx,d_hl,d_hu;
   int j;
   Complex S11I, S12I, S21I , S22I;

   iris(a_width,b_h1,d_h1,b_h2,i_th,freq,N,S11I,S12I,S21I,S22I);
   K_values(S11I,S12I,S21I,S22I,k1,ph1,ph2,i);
   iris(a_width,b_h1,d_h2,b_h2,i_th,freq,N,S11I,S12I,S21I,S22I);
   K_values(S11I,S12I,S21I,S22I,k2,ph1,ph2,i);

   err1 = (K[i] - k1)/K[i];
   err2 = (K[i] - k2)/K[i];
   cout << err1<<"\t" << err2 << endl;
   if (err1 < 0.0) {
        d_hl = d_h1;
        d_hu = d_h2;
   } else {
        d_hl = d_h2;
        d_hu = d_h1;
   }
    rts = 0.5*(d_hl+d_hu);
    dxold = fabs(d_hu-d_hl);
    dx   = dxold;
    funcd(a_width,b_h1,rts,b_h2,i_th,freq,N,i,km,ph1,ph2,dk);
          errm = (K[i] - km)/K[i];

     for(j=0;j<=MAXIT;j++){
        if ((((rts-d_hu)*dk-km)*((rts-d_hl)*dk-km) >= 0.0)//
              || (fabs(2.0*km) > fabs(dxold*dk))) {
```

```
          dxold = dx;
          dx = 0.5*(d_hu-d_hl);
          rts = d_hl+dx;
          //cout << "errm = " << errm << endl;
          if(fabs(errm) <= acc){d_h=rts; return;}
          } else {
           dxold = dx;
           dx = km/dk;
           temp = rts;
           rts -= dx;
          //cout << "errm = " << errm << endl;
           if(fabs(errm) <= acc){d_h=rts; return;}
          }
          //cout << "errm = " << errm << endl;
          if (fabs(errm) < acc){d_h=rts; return;}
          funcd(a_width,b_h1,rts,b_h2,i_th,freq,N,i,km,ph1,ph2,dk);
           errm = (K[i] - km)/K[i];
          if (errm < 0.0)
             d_hl = rts;
          else
             d_hu = rts;
        }
       cout << "Max number of iterations exceeded"<< endl;
     }

//Function to find the differentiation using the pertubration method
void funcd(float a_width,float b_h1,double rts,float b_h2,float i_th,
float freq,int N,int i,double &km,double &ph1, double &ph2,double &dk)
{
  Complex S11,S12,S22,S21;
  double rts_inc,k_inc;

   iris(a_width,b_h1,rts,b_h2,i_th,freq,N,S11,S12,S21,S22);
   K_values(S11,S12,S21,S22,km,ph1,ph2,i);
   rts_inc = rts + 0.1*rts;
   iris(a_width,b_h1,rts_inc,b_h2,i_th,freq,N,S11,S12,S21,S22);
   K_values(S11,S12,S21,S22,k_inc,ph1,ph2,i);
   dk = (k_inc -km)/0.1;

}
```

Appendix B

Computer program for analysing E-plane low-pass filter structures

```
/*****************************************************************
This is the source code for analysis of E-plane filter structures.
File nf.cc inputs the filter dimensions and the frequency points for
analysis. File iris.cc finds the S-matrix of the iris discontinuity
using the mode matching method. analyse.cc analyses the structure for
each frequency point and prints out the Insertion and Return loss.
*****************************************************************/

#include <Complex.h>
#include <fstream.h>
#include <iostream.h>
#include <iomanip.h>
#include <stdlib.h>
#include "header.h"
#include "nf.cc"
#include "iris.cc"
#include "analyse.cc"


char infile[f_size];

main(void)
{
float a_width,b_h[20],d_h,i_th,freq,f1,f2,df;
float bw,ibw,idb,rl,fac,amc,amo,amd,bc;
int i,j,nf,N,M,law;
char check;
ofstream dFile;
```

```
cout << "Please type y to enter data or any
         other char for file input " << endl;
cin >> check;
if (check == 'y') {
   dFile.open("default.dat",ios::out);
   filter_in(nf);
   dFile <<  nf<<endl;
   rect_in(a_width,b_h,bc,law,i_th,N);
   dFile << a_width << endl << b_h[0] <<endl << bc << endl
         << law << endl  << i_th << endl << N << endl;
   anal_in(f1,f2,df);
   dFile << f1 << endl << f2 <<endl<< df<<endl;
   if(nf%2 == 0) M = nf/2;
   else M = (nf-1)/2;
   for(i=0;i <=nf; i++){
       cout <<"W["<<i<<"]= \t";
       cin >> w[i];
        dFile << w[i] << endl;
     }
   for(i=0;i <nf; i++){
       cout <<"L["<<i<<"]= \t";
       cin >> L[i];
        dFile << L[i] << endl;
    }

   dFile.close();

   cout << "Data is saved in the Default
           file 'default.dat'" << endl;

 }
else {
   cout << "Enter the file to read" << endl;
cin >> infile;
// cin.getline(infile,f_size);
   ifstream  iFile(infile,ios::in);
       if(!iFile){
         cerr << "Could not open the file " << endl;
         cout.write(infile,f_size);
         exit(-1);
        }
```

```
     filter(nf,iFile);
    rect(a_width,b_h,i_th,N,iFile);
    anal(f1,f2,df,iFile);
        if(nf%2 == 0) M = nf/2;
          else M = (nf-1)/2;
        for(i=0;i <=M; i++){
            iFile >> w[i];
            w[nf-i] = w[i];
           }
        for(i=0;i <=M; i++){
            iFile >> L[i];
            L[nf-i-1] = L[i];
          }
  iFile.close();

}
   analysis(a_width,b_h,i_th,N,f1,f2,df,nf);
  cout << "Do you want to do the analysis again? "<<endl;
  cin >> check;
   if (check == 'y'){ anal_in(f1,f2,df);
     analysis(a_width,b_h,i_th,N,f1,f2,df,nf);
   }
  cout << "Do you want to do the analysis again? "<<endl;
  cin >> check;
   if (check == 'y'){ anal_in(f1,f2,df);
     analysis(a_width,b_h,i_th,N,f1,f2,df,nf);
   }
return 0;
}

/*********************************************************************
                    File nf.cc
*********************************************************************/

int n;
void filter_in(int &nf)
{
float t,alpha,epsilon,temp1,temp2,y,Y[15],f1,f2,f3,J;
int r;
cout << "Enter the value of the number
         of resonators" << endl;
 cin >> nf;
```

```
 n = nf;
cout << "\n Required filter order = "<<nf <<"\n";
}


void rect_in(float &a_width,float b_h[],float &bc,int &law,
float &i_th, int &N)
{
 float b,alpha,bm;
 int i,k;
 char c;
 cout << "\nEnter the width of the waveguide a= ";
 cin >> a_width;

 k = (n+1)/2;

 cout << "\nEnter the  height of the  waveguide b= ";
 cin >> b ;
 cout << "\nEnter the  height of the central
         section bc= ";
 cin >> bc ;

 b_h[0] = b_h[n+1] = b;

 cout << "Enter the Height Distribution law" << endl;
 cout << "1 for Square Law" << endl;
 cout << "2 for Cosine Law" << endl;
 cout << "3 for Exponential Law" << endl;
 cout << "4 for Linear Law" << endl;
 cout << "5 for Uniform Law" << endl;
 cout << "6 for Own data " << endl;
 cin >> law;
 switch(law){
 case 1:
// square law
 alpha = (b-bc)/(k*k);
 for(i=1;i<=k;i++){
  bm = alpha*(i-k)*(i-k)+bc;
  b_h[i] = b_h[n-i+1] = bm;
 }
  break;
 case 2:
```

```
// cosine law
 for(i=1;i<=k;i++){
  bm = b - (b-bc)*sin(i*M_PI/(n+1));
  b_h[i] = b_h[n-i+1] = bm;
 }
  break;
  case 3:
// exponential law
 alpha = -log(b/bc)/(n+1);
 for(i=1;i<=k;i++){
  bm = b * exp(2.0*alpha*i);
  b_h[i] = b_h[n-i+1] = bm;
 }
  break;
  case 4:
// Linear law
 alpha = (b-bc)/n;
 for(i=1;i<=k;i++){
  bm = b -alpha*i;
  b_h[i] = b_h[n-i+1] = bm;
}
   break;
   case 5:
// Uniform law
  bm = b ;
 for(i=1;i<=k;i++)
  b_h[i] = b_h[n-i+1] = bm;
  break;
  default:
  cout << "Enter a number 1-5 please,
          BYE" << endl;
   exit(0);
  case 6:
//Own Data
    for(i=1;i<=n;i++){
     cout << endl<<"b_h["<<i<<"]=";
     cin >> b_h[i] ;}
     break;
 }

if (n % 2 == 0) k = n/2+1;
 k = n/2;
```

```
 for(i=1;i<=n/2+1;i++)
  {
   z[i] = b_h[i]/b_h[i-1];
   z[n-i+1] = z[i];
  }
  z[0] = z[n+1] = 1;
for(i=0;i<=n;i++)
  K[i] /= sqrt(z[i]*z[i+1]);
for(i=0;i<=n+1;i++)
cout << "b["<<i<<"]="<<b_h[i]<< "\t" <<endl;
 cout << "\nEnter the  Iris thickness of the waveguide i_th= ";
  cin >>i_th;
 cout <<"\nEnter the value of N the no of modes\n";
 cout << "N= "<<"\n";
 cin >> N ;
}

void anal_in(float &f1,float &f2,float &df)
{
cout << "\n Enter the Lower Frequency bound in Ghz";
cin >> f1;
cout << "\n Enter the Upper Frequency bound in Ghz";
cin >> f2;
cout << "\n Enter the frequency step  in Ghz";
cin >> df;
}

/*****************************************************************
                  File  iris.cc
*****************************************************************/
void iris(float a_width,float b_h,float d_h,float b_h1, float i_th,
float freq, int N,array *S11T,array *S12T,array *S21T, array *S22T)
 {
        int M;
        Complex en;
        M  = (int)(floor(d_h/b_h))*N;
        if(M < 5) M = 5;
        array L(M,M),*I,*Y2,*U1;
        array *S22R,*S21R,*S12R,*S11R,*S11F,*S12F,*S21F,*S22F;
        Y2 = new array(M,M);
        U1 = new array(M,M);
        S22R = new array(M,M);
```

```
        S21R = new array(N,M);
        S12R = new array(M,N);
        S11R = new array(M,M);
        S11F = new array(N,N);
        S12F = new array(N,M);
        S21F = new array(M,N);
        S22F = new array(M,M);

        step(a_width,b_h,d_h,i_th,freq,N,M,S11F,S12F,S21F,S22F);
        step(a_width,b_h1,d_h,i_th,freq,N,M,S22R,S21R,S12R,S11R);

        *Y2 = Y(a_width,d_h,freq,M);
        I = new array(M,M);
        for(int i=0;i<M;i++) (*I)(i,i) = Complex(1,0);
        en = Complex(0,1.0);
        for(int i=0;i<M;i++)
           {
            if(imag((*Y2)(i,i)) == 0 )
           L(i,i) = exp(-en*(*Y2)(i,i)*i_th);
            else
           L(i,i) = exp(imag((*Y2)(i,i))*i_th);
            }

        *U1 = ~(*I - L*(*S22F)*L*(*S11R));
        *S11T = *S11F + (*S12F)*L*(*S11R)*(*U1)*L*(*S21F);
        *S21T = *S21R*(*U1)*L*(*S21F);
        *S12T = *S12F*L*(*I + (*S11R)*(*U1)*L*(*S22F)*L)*(*S12R);
        *S22T = *S22R + *S21R*(*U1)*L*(*S22F)*L*(*S12R);

        delete I;
        delete Y2;
        delete S22R;
        delete S21R;
        delete S12R;
        delete S11R;
        delete S11F;
        delete S12F;
        delete S21F; delete S22F; delete U1;
}

void step(float a_width,float b_h, float d_h, float i_th,float freq,
int N, int M,array *S11,array *S12,array *S21, array *S22)
```

```
{
        array H(N,M),*I,*temp;
        int i,j;
        H = Hmn(a_width,b_h,d_h,N,M,freq);

        temp = new array(N,N);
        I = new array(N,N);
        for(i=0;i<N;i++) (*I)(i,i) = Complex(1,0);
        *temp = ~(H*(!H)+(*I));
        *S11 = (*temp)*(H*(!H)-(*I));
        *S12 = (*temp)*H;
        for(i=0;i<N;i++)
                for(j=0;j<M;j++)
                        (*S12)(i,j) *= Complex(2,0);
        *S21 = (!H)*(*I-(*S11));
        delete I;
        I = new array(M,M);
        for(i=0;i<M;i++) (*I)(i,i) = Complex(1,0);
        *S22 = (*I) - (!H)*(*S12);
        delete temp;
        delete I;
}



array Hmn(float a_width,float b,float d,int N, int M,float freq)
{
        array h(N,M),Y1(N,N),Y2(M,M); int i,j; float u,v;


        Y1 = Y(a_width,b,freq,N);
        Y2 = Y(a_width,d,freq,M);


    h(0,0) = Complex(sqrt(Y2(0,0)/Y1(0,0)*(d/b)));


        for(i=1;i<N;i++)
        {
           for(j=1;j<M;j++)
             {
```

```
          u = 2*M_PI*i/b;
          v = 2*M_PI*j/d;
      h(0,j) = 0;
      h(i,0) = Complex(2*sqrt(2)*sqrt(Y2(0,0)/Y1(i,i))
               *sin(u*d/2)/(u*sqrt(b*d)));
      if (u == v ) h(i,j) = Complex(2*sqrt(d/b)
                            *sqrt(Y2(j,j)/Y1(i,i)));
      else
      h(i,j) = Complex(sqrt(Y2(j,j)/Y1(i,i))*4*u*cos(M_PI*j)
               *sin(u*d/2)/((sqrt(b*d)*(u*u - v*v))));
         }}

         return(h);
}


array Y(float a, float b,float freq,int M)
{
         array y(M,M);
         double k0;
         double gamma;
         int i,j;

         k0 = 2*M_PI*freq/VEL;

         for(i=0;i<M;i++)
         {
           gamma = (pow(k0,2)-pow(M_PI/a,2) - pow(2*i*M_PI/b,2));
           if(gamma > 0)
           y(i,i) = Complex(sqrt(gamma),0);
           else
           y(i,i) = Complex(0,-sqrt(-gamma));
         }
         return(y);
}


void check( array *S11, array *S12, array *S21, array *S22)
{
   Complex S11I, S12I, S21I, S22I;
   S11I = (*S11)(0,0);
   S12I = (*S12)(0,0);
```

```
   S21I = (*S21)(0,0);
   S22I = (*S22)(0,0);

   cout << "CHECKING FOR UNITARY S MATRIX" << endl;
   cout << S11I*conj(S11I)+S21I*conj(S21I)<<endl;
   cout << S11I*conj(S21I)+S21I*conj(S22I)<<endl;
   cout << S21I*conj(S11I)+S22I*conj(S12I)<<endl;
   cout << S21I*conj(S21I)+S22I*conj(S22I)<<endl;
}

/*****************************************************************
                    File analyse.cc
*****************************************************************/

#include <iostream.h>
#include <iomanip.h>
#include <fstream.h>

const f_size = 10;
char outfile[f_size];


void analysis(float a_width,float b_h[],float i_th, int N,float f1,
float f2,float df,int nf)
{
    array *SO11, *SO12, *SO21, *SO22, *O11, *O12, *O21, *O22;
    array *T11, *T12, *T21, *T22, *S11, *S12, *S21, *S22;

        S11 = new array(N,N);
        S12 = new array(N,N);
        S21 = new array(N,N);
        S22 = new array(N,N);
        O11 = new array(N,N);
        O21 = new array(N,N);
        O12 = new array(N,N);
        O22 = new array(N,N);
        T11 = new array(N,N);
        T21 = new array(N,N);
        T12 = new array(N,N);
        T22 = new array(N,N);

int i,j,k=0;
```

```
float ww,bl,b1;
double il,rl,F[100],IL[100],RL[100];

   cout << "Enter the file to save the results" << endl;
   cin  >> outfile;
   ofstream  oFile(outfile,ios::app);
       if(!oFile){
         cerr << "Could not open the file " << endl;
         cout.write(outfile,f_size);
         exit(-1);
        }

    oFile <<endl;
    oFile <<"**********************************"<<endl;
    oFile << setiosflags(ios::left) << setw(10) << "FREQ"
          << setw(20)<<"IL "<<setw(10)<<"RL "<<endl;
    oFile <<"**********************************"<<endl;
    for(;f1<=f2;f1+=df) {
        SO22 = new array(N,N);
        SO12 = new array(N,N);
        SO21 = new array(N,N);
        SO11 = new array(N,N);
for(j=0;j<N;j++) {
                    (*SO12)(j,j) = Complex(1.0,0.0);
   (*SO21)(j,j) = Complex(1.0,0.0);
}
        for(i=0;i<=(nf-1)/2;i++){
ww = w[i];
bl = L[i];

iris(a_width,b_h[i],ww,b_h[i+1],i_th,f1,N,
             S11,S12,S21,S22);
overall(SO11,SO12,SO21,SO22,S11,S12,S21,S22,
               T11,T12,T21,T22,N);

        copy(SO11,SO12,SO21,SO22,T11,T12,T21,T22);
length(a_width,b_h[i+1],bl,f1,N,SO12,SO21,SO22);
        }
       if (nf %2 == 0){
       iris(a_width,b_h[(nf-1)/2],w[nf/2],b_h[nf-1],
            i_th,f1,N,S11,S12,S21,S22);
overall(SO11,SO12,SO21,SO22,S11,S12,S21,S22,
```

```
                T11,T12,T21,T22,N);
        overall(T11,T12,T21,T22,SO22,SO21,SO12,SO11,
                S11,S12,S21,S22,N);

        }
        else
         overall(SO11,SO12,SO21,SO22,T22,T21,T12,T11,
                 S11,S12,S21,S22,N);

il = 20 * log10(abs((*S21)(0,0)));
rl = 20 * log10(abs((*S11)(0,0)));
        IL[k]  = il;
        RL[k]  = rl;
        F[k]  = f1;

        oFile << setiosflags(ios::left) << setw(10) << f1
              << setw(20)<<il<<setw(10)<<rl<<endl;
        oFile << flush;
        cout << setiosflags(ios::left) << setw(10) << f1
            << setw(20)<<il<<setw(10)<<rl<<endl;

        k++;
        delete SO22;
        delete SO12;
        delete SO21;
        delete SO11;

}
        delete S11;
        delete S12;
        delete S21;
        delete S22;
        delete O11;
        delete O21;
        delete O12;
        delete O22;
        delete T11;
        delete T21;
        delete T12;
        delete T22;
 oFile.close();
}
```

```
void overall(const array *S11A,const array *S12A,const array *S21A,
const array *S22A,const  array *S11B,const  array *S12B,const
 array *S21B,const  array *S22B,array *T11,array *T12,array *T21,
array *T22,int N)
{
        int i;
        array *I, temp(N,N);
        I = new array(N,N);
        for(i=0;i<N;i++) (*I)(i,i) =Complex(1.0,0.0);

        temp = ~(*I-(*S22A)*(*S11B));
        *T21 = *S21B*temp*(*S21A);
        *T11 = *S11A + *S12A*(*S11B)*temp*(*S21A);
        *T12 = *S12A*(*I+(*S11B)*temp*(*S22A))*(*S12B);
        *T22 = *S22B + *S21B*temp*(*S22A)*(*S12B);
        delete I;

}


void length(float a,float b,float bl,float fc,int N,array *ST12,
array *ST21, array *ST22)
{
double k0,gam;
        Complex en;
        array L(N,N);

        en = Complex(0,1);

k0 = 2*M_PI*fc/VEL;
for(int i=0;i<N;i++)
{
          gam = (pow(k0,2)-pow(M_PI/a,2) - pow(2*i*M_PI/b,2));
          if (gam > 0)
  L(i,i) = exp(-en*sqrt(gam)*bl);
          else
          L(i,i) = exp(-sqrt(-gam)*bl);
}

       *ST12 = (*ST12) * L;
       *ST21 = L * (*ST21) ;
```

```
        *ST22 = L * (*ST22) * L;
}


void copy(array *S11A,array *S12A,array *S21A, array *S22A,array
const *S11B,array  const *S12B,array const *S21B,array const *S22B)
{
  *S11A = *S11B;
  *S12A = *S12B;
  *S21A = *S21B;
  *S22A = *S22B;
}
```